Fakultät für Medizin

Institut für Allgemeine Pathologie und Pathologische Anatomie

The role of Aldehyde dehydrogenase 1 A3 in chemoresistance regulation in human glioblastoma

Wei Wu

Vollständiger Abdruck der von der Fakultät für Medizin der Technischen Universität München zur Erlangung des akademischen Grades eines

Doctor of Philosophy (Ph.D.)

genehmigten Dissertation.

Vorsitzende/r: Prof. Dr. Claus Zimmer

Betreuer: Prof. Dr. Jürgen Schlegel

Prüfer der Dissertation:

1. Prof. Dr. Wilko Weichert

2. Priv.-Doz. Dr. Frauke Neff

Die Dissertation wurde am 23.10.2018 bei der Fakultät für Medizin der Technischen Universität München eingereicht und durch die Fakultät für Medizin am 10.12.2018 angenommen.

TABLE OF CONTENTS

A. Summary

Glioblastoma (GBM) is the most aggressive primary intracranial neoplasm, displaying high heterogeneity that renders this tumor class difficult to treat. The standard therapy is surgical resection combined with radio-chemotherapy. Despite of progresses in multiple treatments, the prognosis of GBM patients remains poor. About 90% of malignant gliomas recur at the original site after treatment. Strong intrinsic resistance to adjuvant therapy promotes tumor cells growth, and this is the primary reason for tumor relapse. The DNA repair factor O6-methylguanine methyltransferase (MGMT) has been recognized as the most prominent mechanism for the resistance to alkylating chemotherapeutic agents. However, some GBM patients with favorable MGMT status don´t respond to chemotherapy or even those who respond to therapy unavoidable relapse. Thus, there must exist subpopulations of cells that featured with additional mechanisms of Temozolomide (TMZ) resistance.

Aldehyde dehydrogenases (ALDHs) are characterized as markers for cancer stem cells, and are responsible for oxidizing aldehydes to carboxylic acids. Members of the ALDH family are also indicators of worse prognosis in various kinds of cancers, including sarcoma, non-small cell lung cancer, gastric cancer and malignant glioma. Our group previously showed that GBM cells with ALDH1 low expression are more susceptible to TMZ treatment and those GBM patients with high ALDH1 expression have poor outcomes. However, the reason for ALDH-mediated chemoresistance is still elusive. Additional mechanisms are suggested other than DNA repair pathways since ALDHs are mainly located in the cytoplasm instead of the nucleus. It has been suggested that ALDHs are involved in the reaction to reactive oxygen species (ROS) in the drug-tolerant subpopulations. ROS have been detected in multiple malignant tumors and due to the detrimental modifications of the DNA, lipid, and protein macromolecules, they are involved in numerous drug-induced toxicities.

The present data demonstrated the pivotal role of ALDH1A3 in regulating chemoresistance in GBM. ALDH1A3 knockout (KO) cells showed more sensitivity to TMZ treatment than ALDH1A3

wild-type (WT) cells and oxidative stress is an important and clinical relevant component of TMZ induced therapeutic effects, where ALDH1A3 exerts its effect on the resistance against TMZ. ROS react with the polyunsaturated fatty acids of lipid membranes and induce lipid peroxidation, yielding the bioactive aldehydes, including malondialdehyde (MDA) and 4-hydroxynonenal, that are detoxified by ALDH enzymatic activity. Furthermore, the data also showed that TMZ caused a significant dose-dependent reduction of ALDH1A3. The decrement of ALDH1A3 was apparently not transcriptionally modulated since the mRNA levels of ALDH1A3 were not affected. Interestingly, ALDH1A3 was confirmed to physically bind with autophagy adaptor p62, indicating that the elimination of ALDH1A3 is possibly owing to autophagy.

These results are corroborated by clinical data that ALDH1A3 expression in specimens from patients suffering from recurrent GBMs were significantly higher than primary tumor of the same patients and patients with high ALDH1A3 expression showed a shorter median survival time (16 months vs. 21 months, $P<0.05$). The present study presents a molecular interpretation of the role of ALDH1A3 in therapeutic resistance of human glioblastoma. ALDH1A3 enzymatically reduces the number of toxic aldehydes, which identifies ALDH1A3 as a target for inhibitor therapy.

B. Introduction

1. Malignant gliomas

According to the World Health Organization (WHO) classification, gliomas are graded into grade I to IV. Grade I gliomas are benign tumors that can be healed by surgical resection, while grade II to IV gliomas are malignant and more aggressive. According to genetic concept, malignant gliomas can be classified to IDH-mutant and IDH-wildtype tumors (Louis et al., 2016).

2. Glioblastoma

2. 1 Epidemiology and etiology

Glioblastoma multiforme (GBM) is the most aggressive type of tumor and has been designated as grade IV glioma. GBM is the most common malignant glioma. The incidence of GBM increases with age and shows the highest incidence in the 75 to 84 years old group in the United States (Wick *et al.*, 2018). The incidence is higher in men than in women and is higher in Caucasians, when comparing to other ethnicities (Davis, 2016).

The etiology of GBM has not been fully elucidated. Glioblastoma is believed to be a spontaneous tumor. By far, the only unequivocal factor related to increased glioma risk is therapeutic ionizing irradiation, and receiving prophylactic CNS irradiation may result in malignant glioma (Braganza et al., 2012). Intake of N-Nitroso compounds does not have a definite association with malignant glioma (Dubrow et al., 2010). However, some researchers proved that increased generation of oxygen radicals may influence initial tumorigenic event (neoplasia of the brain), since the oxygen species may cause chemical modifications of DNA bases, inducing spontaneous mutation of oncogenes or tumor suppressor genes (Salazar-Ramiro et al., 2016, Rinaldi et al., 2016).

2. 2 Genome-, epigenome-, and transcriptome-based classification

In view of the profiles of genetic and epigenetic aberrations, GBMs were previously classified into four clusters: mesenchymal, classical, proneural, and neural (Ilkanizadeh et al., 2014). Mesenchymal GBMs are the most aggressive subtype and characterized by neurofibromin 1 (NF1) tumor suppressor gene mutation. Frequent mutations in the PTEN and TP53 tumor suppressor genes also appeared in this group. The classical subtype is characterized by EGFR amplification and reveals high-level proliferative ability but no TP53 mutation is found in classical GBM tumors. Unlike in classical tumors, TP53 is frequently mutated in proneural subtype. Besides that, IDH1 gene and PDGFRA mutation are found in proneural subtype but not in any other subgroups. Neural subtype is characterized by many genes which also exist in the brain´s normal noncancerous neurons. (Sturm et al., 2014, Verhaak et al., 2010). A recent study, which based on a comprehensive longitudinal analysis of the GBM tumor transcriptome, reveals that GBMs only have three subtypes: proneural, classical, mesenchymal. The neural subtype initiates from contamination of the original samples with non-tumor cells (Wang et al., 2017).

The mesenchymal and classical subtypes typically represent more aggressive behavior, while the proneural subtype is associated with less aggressive tumors. Patients with proneural GBMs are younger than the patients with mesenchymal and classical subtypes and associate with better prognosis (Zong et al., 2012). Proneural-to-Mesenchymal switching has been indicated in treatment resistance in GBM relapse (Bhat et al., 2013; Ozawa et al., 2014; Phillips et al.). Longitudinal transcriptome analysis showed that expression subtype is retained in 55% of cases (Wang et al., 2017).

It is evident that the subtypes of GBM not only differ from patient to patient but also differ from spatial zones within the same tumor. Recently, according to the CpG island methylator phenotype, a new cluster of tumors has been identified as G-CIMP tumors. These tumors are

characterized by distinct DNA methylation patterns, copy number alterations and transcriptomic profiles when compared to other subsets of GBMs. The patients with G-CIMP tumors are normally associated with a more favorable outcome (Malta et al., 2018).

2. 3 Treatment of glioblastoma

GBM is the most aggressive primary malignant brain neoplasm. Although great progress has been made in radiation and chemotherapy, malignant gliomas remain one of the most challenging cancers. Universal mortality is observed in almost all patients. The 2-year survival is only 26–33% (Stupp et al., 2005).

The standard therapeutic treatment for GBM is resection followed by concurrent radiation (RT, 60 Gy in 30 fractions) and TMZ (75 mg/m^2/day for 6 weeks) and again six cycles of TMZ (150–200 mg/m^2/day for the first 5 days of a 28-day cycle—TMZ) (Malmstrom et al., 2017). After surgery, treatment regimens with RT and adjuvant TMZ help patients to achieve longest survival (Yabroff et al., 2012, Li et al., 2016). Stupp et al. presented that patients receiving combination therapy survive longer than RT alone (median OS 14.6 vs. 12.1 months; $P < 0.001$) (Stupp et al., 2005). There are also angiogenesis inhibitors applied in clinical trials, such as bevacizumab, blocking angiogenesis via inhibiting VEGF (Wenger et al., 2017); Cilengitide, functioning by suppressing the FAK/SRC/AKT pathway (Weller et al., 2016).

2. 4 Mechanisms of resistance

Despite of advances in therapy, prognosis for GBM patients is still devastating, with a median survival of approximately 12-15 months (Pearson and Regad, 2017). The unfavorable prognosis mainly results from inevitable tumor relapse (Ringel et al., 2016). Strong intrinsic resistance to adjuvant therapy facilitates tumor cell survival, which is the main reason for

regular tumor recurrence (Osuka and Van Meir, 2017). TMZ, an alkylating agent used in standard therapy, induces tumor cytotoxicity by transferring methyl groups to DNA (70% at N7-guanine sites, 10% at N3-adenine sites and 5% at O6-guanine sites). The O^6 site alkylation on guanine causes the connection with a thymine rather than a cytosine during DNA replication process, which results in cell death (Zhang et al., 2012, Johannessen and Bjerkvig, 2012).

The most well-known mechanism of TMZ resistance is mediated by the DNA repair protein MGMT (O^6-methylguanine DNA methyltransferase), which is able to remove O^6-MG adducts and thus eliminates the cytotoxicity of TMZ (Zhang et al., 2013, Weller, 2013, Thon et al., 2013). DNA mismatch repair (MMR) is also associated with the resistance. Loss of MMR renders the cells tolerant to O^6-MG lesions, thus the cells are not able to process the mismatch, DNA replication process, and no cell cycle arrest or apoptosis occurs (Munoz et al., 2014, McFaline-Figueroa et al., 2015). In addition, other resistance mechanisms seem to be active, since some GBMs are resistant to TMZ instead of a favorable MGMT status, and this has also been shown experimentally (Gaspar et al., 2010). Thus, a subpopulation of cells in GBM is speculated to possess additional mechanisms inducing tumor re-growth.

Potential mechanisms have been discussed including the concept of GBM cancer stem cells (CSCs), which could escape the standard therapy, enhance infiltration of hypoxic cells, and initiate substitutive angiogenic pathways (Ramirez et al., 2013, Maugeri-Sacca et al., 2013).

3. Aldehyde dehydrogenase

It is commonly accepted that a small subpopulation of cells within malignant tumors is defined as cancer stem cells (CSCs). CSCs are normally characterized by quiescence, decreased ROS

and enhanced DNA repair. The current available therapies mainly target the undifferentiated, fast-proliferative cells and leave the quiescent and chemoresistant CSCs behind. (Batlle and Clevers, 2017, Rich, 2016). Once treatment has terminated, CSCs become active and produce resistant tumor cells, which lead to recurrence of the tumor (Batlle and Clevers, 2017). The aldehyde dehydrogenases (ALDHs), especially ALDH1, have been regarded as cancer stem cell markers.

To date, nineteen ALDH genes have been identified in humans with different expression levels and anatomical distributions. The enzyme family is not only responsible for converting small aldehydes to carboxylic acids but also the large aldehyde retinal to retinoic acid. (Hong et al., 2016). ALDHs are mediated by potentially oncogenic signaling pathways like MUC1-C/ERK and WNT/β-catenin (Alam et al., 2013, Cojoc et al., 2015). The oxidizing effect of ALDHs could in turn influence ROS production and regulate retinoid acid (RA) signaling cascades (Pors and Moreb, 2014, Singh et al., 2013). These regulatory mechanisms determine that ALDH activity is vital to cell differentiation, detoxification and drug resistance (Fig. 1) .

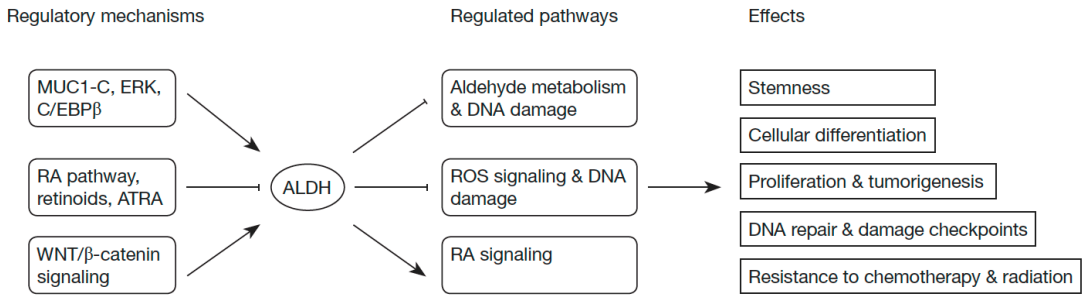

Figure 1. Pathways mediated by ALDHs that manipulate carcinogenesis. (Clark and Palle, 2016)

It has been shown that ALDH1 expression appears to be directly involved in the resistant subpopulation of tumor cells, including breast cancer (Qiu et al., 2016), non-small cell lung cancer (Shao et al., 2014) and malignant glioma (Xu et al., 2015, Cheng et al., 2016). The cells with ALDH1 high expression exhibit stronger resistance to chemotherapy than the cells with

ALDH1 low expression. However, it is still unclear that how ALDHs regulate chemoresistance in tumors.

4. Oxidative stress in cancer

Experimental and clinical data confirmed the crucial role of oxidative stress in cancer development. Gene mutations might be raised or intracellular signal transduction could be affected when the oxidative stress is overloaded (Di Meo et al., 2016, Cobley et al., 2018).

Hanahan and Weinberg demonstrated in the 2000s that the so-called hallmarks of cancers embrace essential features of almost all malignant cells, which allow them to escape endogenous protective system and proceed to rapid proliferation (Hanahan and Weinberg, 2000). Oxidative stress exerts a crucial influence on signal transduction controlling cell proliferation (Fig. 2). It has been confirmed that ROS are imperative in the process of ligand-independent RTK transactivation, p53 activation and expression of telomerase which enable the cells to rapid proliferation (Cattaneo et al., 2014, Gambino et al., 2013, Correia-Melo et al., 2014). The important role of ROS in improving the invasion and metastasis of cancer cells is mediated by matrix metalloproteinase secretion, plasticity in cell motility and EMT (Fiaschi and Chiarugi, 2012, Giannoni et al., 2012, Lee and Kang, 2013). Additionally, ROS are also crucial for activating endothelial progenitor, releasing VEGF and maintaining continuous angiogenesis (Zhou et al., 2013, Lee and Kang, 2013). ROS have also been reported involved in signaling of apoptosis (Kamogashira et al., 2015, Holze et al., 2018), metabolism (Liemburg-Apers et al., 2015, Panieri and Santoro, 2016) and immune destruction (Zhang and Zehnder, 2013, Belikov et al., 2015).

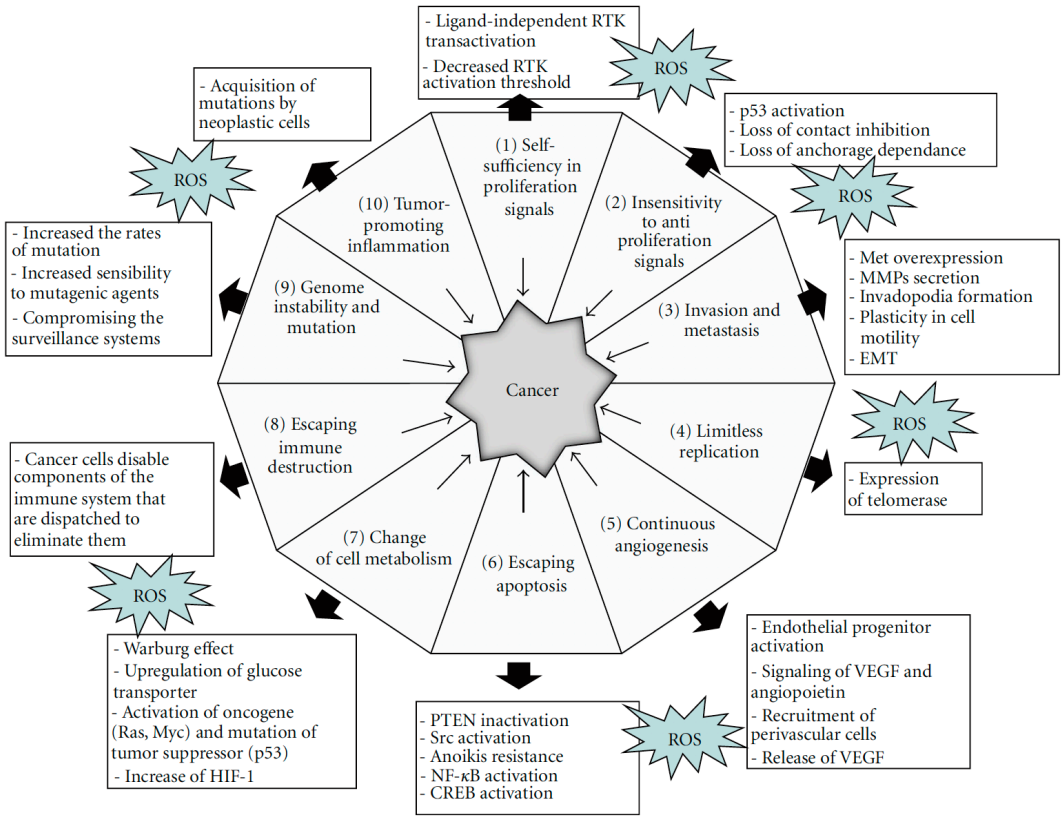

Figure 2. The role of ROS in the hallmarks of cancers. (Fiaschi and Chiarugi, 2012)

Furthermore, the generation of ROS can be applied as a therapeutic approach in the treatment of cancer (Fig. 3). Many dysregulating signaling modulators are able to elevate the ROS production. The cytotoxicity of ROS has been applied to inactive cancer cells. A unique therapeutic strategy, called as “oxidation therapy”, has been applied by delivering cytotoxic ROS directly to solid tumors, or inactivate the antioxidative enzyme system (Rinaldi et al., 2016).

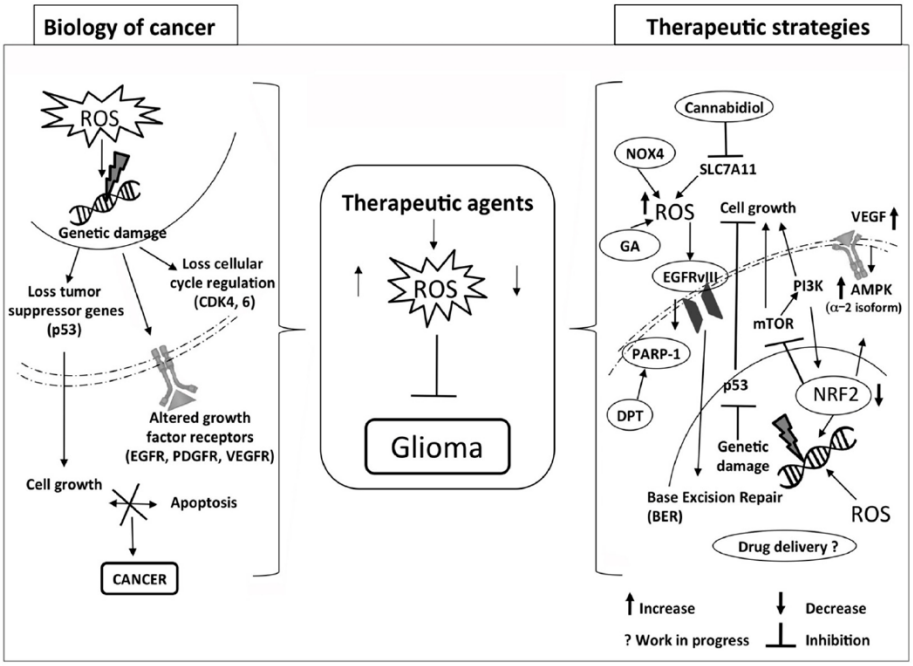

Figure 3. Modulation of ROS pathways acts as therapeutic approaches in glioma. (Rinaldi et al., 2016)

5. Autophagy

Accumulating evidence has defined the survival-promoting role of autophagy, since autophagy contributes to maintain homeostatic cellular environment and genomic stability by eliminating damaged organelles and proteins (Mathew et al., 2007a). There are at least three types of autophagy: macroautophagy, microautophagy and chaperone-mediated autophagy, all of which promote proteolytic degradation of cytosolic components. In macroautophagy, defective organelles or proteins are delivered to lysosomes through a double membrane-bound vesicles, the autophagosome, while the damaged components are directly taken by lysosomes in microautophagy. Chaperone-mediated autophagy requires the targeted protein to translocate to the lysosome in a chaperone protein complex. The present study focuses on macroautophagy (Glick et al., 2010).

Macroautophagy is universally categorized into five stages: initiation, autophagosome nucleation, autophagosome membrane expansion and elongation, closure and fusion with the lysosome, and finally, intravesicular products degradation (Fig.4) . Under cellular stress, such as starvation, the decrease of glucose releases the inhibition effect of mTOR on ULK1 complex , which activates class III PI3K complex. The tumor suppressor Beclin 1, an overall scaffold for the PI3K complex, promoting the localization of autophagic proteins to the phagophore. The formation of double-membrane of autophagosome is mediated by two ubiquitin-like conjugation systems. The first system is mediated by the E1-like enzyme ATG7 and E2-like enzyme ATG10, resulting in an ATG5-ATG12 conjugation. The second system starts from the conjugation of cytoplasmic LC3I to phosphatidylethanolamine (PE). Then, ATG4B and ATG7 facilitate LC3I to generate the lipidated form, LC3II, which is incorporated into the growing membrane. This formation of LC3II is commonly recognized as the marker of autophagy. Subsequently, the autophagolysosome is formed by the fusion of autophagosome and the lysosome, which is facilitated by the SNARE protein syntaxin 17 (STX17). Ultimately, the low pH of lysosome leads to the degradation of the contents of autophagosome. The adaptor protein p62, which targets specific substrates to autophagosomes, is degraded and can be used as another marker of autophagic flux (Levy et al., 2017).

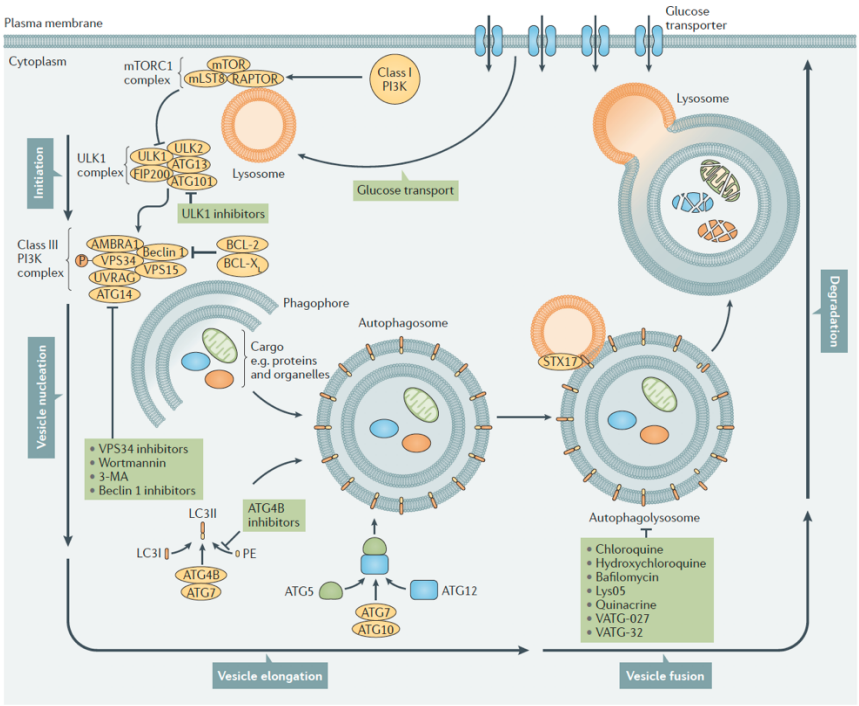

Figure 4. Molecular process of autophagy (Levy et al., 2017).

Recently, enormous scientific interest has been attracted to the investigation of the role of autophagy in tumor biology. Autophagy has been reported as a double-edge sword in cancer progression. Some research show that the blockage of autophagy enhances cancer cells growth (White, 2015, Takamura et al., 2011, Marino et al., 2007). Conversely, autophagy can be induced by metabolic stress and serves as a back-up energy to reinforce adaptation of cancer cells (Guo et al., 2013, Katheder et al., 2017). Multiple reasons have been proposed for either the suppression or promotion role of autophagy for tumorigenesis (Fig. 5). Autophagy deficiency may induce p62 accumulation, DNA damage and cell death, leading to chronic tissue damage and genome instability thereby promoting cancer (Strohecker et al., 2013, Mathew et al., 2007b). In another way, initiation of autophagy helps to eliminate the oxidative stress, support metabolism and thus improve the survival of tumor cells (Guo et al., 2011, Lock et al., 2011, Yang et al., 2011).

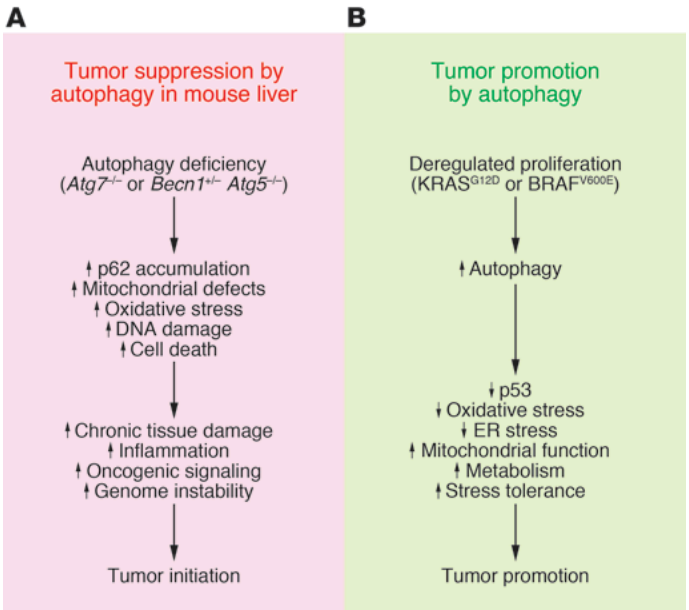

Figure 5. The role of autophagy as a tumor suppressor or tumor promoter (White, 2015).

6. Objective

Despite aggressive therapies, including surgical resection and combined radio- and chemotherapy the overall prognosis of patients with GBM remains poor since 90% of malignant gliomas recur due to strong intrinsic resistance against adjuvant therapies. Cancer Stem Cells (CSCs) in GBM have been discussed as a potential reason for tumor recurrence since CSCs escape the standard therapy. The aldehyde dehydrogenases (ALDHs), especially ALDH1, have been identified as biomarkers of CSCs and indicators of worse prognosis in multiple types of cancers. It has been shown that ALDH1 not only acts as a biomarker for this resistant cell population but is directly involved in the biological process leading to chemoresistance. The exact molecular and functional mechanism by which ALDH1 exerts these effects, however, have not been clarified in detail so far.

The aim of the present study and of my thesis was therefore the investigation of the molecular tumor biology of ALDH in GBM cells in vitro. ALDHs are primarily located in the cytoplasm and have no direct relation to DNA repair. Therefore, it has been hypothesized that ALDH1A3 plays a major role in regulating chemoresistance by detoxifying aldehydes resulting from lipid peroxidation due to therapy induced oxidative stress. In the resent study I aimed to

1. show the effect of variants of GBM cell lines by recombinant techniques including CRISPR-Cas9 gene editing and chemical inhibition of ALDH1A3 on ALDH enzyme activity and response to chemotherapeutic treatment with temozolomide.

2. investigate the role of oxidative stress on chemotherapy by direct measure of reactive oxygen species (ROS) and scavengers of ROS in variant ALDH1A3 GBM cells.

3. investigate the induction of lipid peroxidation by ROS by direct measure of end products of lipid peroxidation (LPO) including malondialdehyde (MDA) and 4-hydroxynonenal (4-HNE) in variant GBM cells with and without scavenging oxidative stress products.

4. investigate the functional modulation of ALDH1A3 activity under treatment conditions. Here, by excluding transcriptional regulation alterations of autophagy were expected as a consequence of ROS and LPO. Therefore, the regulation of ALDH1A3 by autophagy was investigated by biochemical and immunofluorescence techniques.

5. investigate ALDH1A3 expression in vivo in patient samples from operation of primary and recurrent GBM to show the clinical relevance of ALDH1A3 expression in human tumors in situ.

C . Materials and methods

1. Technical devices

Device	Model	Producer
60℃ incubator	INB 200	Memmert GmbH + Co. KG, Schwabach, Germany
96-well plates cooler	Z606634-1EA	Eppendorf AG, Hamburg, Germany
Aqualine water bath	AL12	LAUDA-Brinkmann, Lauda-Königshofen, Germany
Autoclave	VX-120	Memmert GmbH + Co. KG, Schwabach, Germany
Centrifuge	5417R/5425	Eppendorf AG, Hamburg, Germany
CO_2 incubator	HERAcells 150i	Thermo Fisher Scientific Inc, Waltham, MA, USA
Digital sonifier	250-D	Branson, Darmstadt, Germany
Flow cytometer	FACS Calibur™	Becton Dickinson, Heidelberg, Germany
Fluorescence microscope	HBO 100	Carl Zeiss AG, Jena, Germany
Freezing containers	CoolCell®LX	Biocision, Hannover, Germany
Gel imaging system	E-Box CX5	Peqlab, Erlangen, Germany
Heater mixer	53355	Eppendorf AG, Hamburg, Germany
Inverted Routine Microscope	TS100	Sigma, Deisenhofen, Germany
Microcentrifuge	063089(1R)	Eppendorf AG, Hamburg, Germany
Mini cooler	C12R	A. Hartenstein GmbH, Würzburg, Germany
pH-meter	EL-20	Mettler Toledo, Gießen, Germany

Power supply	PowerPac 300	Bio-Rad Laboratories, Inc., Munich, Germany
Real-time PCR system	Lightcycler® 480 II	Roche Diagnostics GmbH, Mannheim, Germany
Rotary microtome	RM2255	Leike, Leipzig, Germany
Shaker	Minishaker MS1	IKA-Werke GmbH & Co. KG, Staufen, Germany
Shaker bacteria	Ecotron	INFORS HT, Einsbach, Germany
Spectrophotometers	NanoDrop 2000c	Thermo Fisher Scientific Inc, Waltham, MA, USA
Thermal cycler	22331	Eppendorf AG, Hamburg, Germany
Tissue cooling plate	TES Valida	Medite GmbH, Burgdorf, Germany
X-ray film processor	Konica SRX-101A	Konica Minolta GmbH, Langenhagen, Germany

2. Chemicals and reagents

Substances	Catalogue Number	Producer
ABC kit	3579	INARIS Biologische Produkte GmbH, Dossenheim, Germany
Acetic acid	7332.1	Carl Roth GmbH + Co. KG, Karlsruhe, Germany
Acrylamide	3029.1	Carl Roth GmbH + Co. KG, Karlsruhe, Germany
Aldefluor assay kit	01700	STEMCELL Technologies, Cologne, Germany

Ammoniumperoxosulphate(APS)	9592.2	Carl Roth GmbH + Co. KG, Karlsruhe, Germany
Aqua Poly/Mount	18606	Polysciences Europe GmbH, Hirschberg an der Bergstraße, Germany
Avidin Biotin Blocking Kit	SP-2001	BioZol, Eching, Germany
BbsI restriction enzyme	R0539S	New England BioLabs GmbH, Frankfurt am Main, Germany
Biozyme LE agarose	840004	Biozym Scientific GmbH, Hessisch Oldendorf, Germany
Bromphenol-blue	B0126	Sigma Aldrich, Munich, Germany
BSA albumin fraktion V (BSA)	8076.4	Carl Roth GmbH + Co. KG, Karlsruhe, Germany
Citrate buffer	K91345644718	Merck, Darmstadt, Germany
Crystal violet	C0775	Sigma Aldrich, Munich, Germany
Diamidino-phenylindole (DAPI)	D1306	Thermo Fisher Scientific, Karlsruhe, Germany
Dimethylsulfoxide(DMSO)	A994.2	Carl Roth GmbH + Co. KG, Karlsruhe, Germany
Dithiothreitol (DTT)	ab141390	Abcam, Cambridge, UK
DNase I	LK003172	CellSystems Biotechnologie Vertrieb GmbH, Troisdorf, Germany
Donkey serum	D9663	Sigma Aldrich, Munich, Germany

Duolink® In Situ Red Starter Kit Mouse/Rabbit	DUO92101	Sigma Aldrich, Munich, Germany
Ethanol	T171.1	Carl Roth GmbH + Co. KG, Karlsruhe, Germany
Ethylenediaminetetraacetic acid (EDTA)	CN06.3	Carl Roth GmbH + Co. KG, Karlsruhe, Germany
Formaldehyde solution	252549	Carl Roth GmbH + Co. KG, Karlsruhe, Germany
Glycerol	G5516	Carl Roth GmbH + Co. KG, Karlsruhe, Germany
Glycine	3790.3	Carl Roth GmbH + Co. KG, Karlsruhe, Germany
Hoechst 33342 solution	62249	Thermo Fisher Scientific, Karlsruhe, Germany
Hydrogen peroxide solution (H_2O_2)	H1009	Sigma Aldrich, Munich, Germany
ImmPACT DAB	SK-4 105	BioZol, Eching, Germany
Isopropanol	9866.1	Carl Roth GmbH + Co. KG, Karlsruhe, Germany
LB medium powder	12795027	Thermo Fisher Scientific, Karlsruhe, Germany
Lipid Peroxidation (MDA) Assay Kit	MAK-085	Sigma Aldrich, Munich, Germany
Lipofectamine™ 3000 Transfection Reagent	L3000008	Thermo Fisher Scientific, Karlsruhe, Germany
N-Acetyl-L-cysteine(NAC)	A7250	Sigma Aldrich, Munich, Germany

NEB® 5-alpha competent E.coli	C2987H	New England BioLabs GmbH, Frankfurt am Main, Germany
NEBuffer™ 2	B7002S	New England BioLabs GmbH, Frankfurt am Main, Germany
Nonidet P40 Substitute (P40)	11332473001	Sigma Aldrich, Munich, Germany
Normal horse serum	VEC-S-2000	BioZol, Eching, Germany
OxiSelect™ In Vitro ROS/RNS Assay Kit (Green Fluorescence)	STA-347	Cell Biolabs, Heidelberg, Germany
Page Ruler Plus	26619	Thermo Fisher Scientific, Karlsruhe, Germany
Ponceau S	5938.1	Carl Roth GmbH + Co. KG, Karlsruhe, Germany
Primescript™ RT Reagent Kit	RR037A	TAKARA Clontech, Av du Pdt Kennedy St-Germain-en-Laye, France
Propidium iodide solution	P4864	Carl Roth GmbH + Co. KG, Karlsruhe, Germany
Protease/Phosphatase inhibitor cocktail (100X)	5872	Cell Signaling Technology, Frankfurt am Main, Germany
Protein G sepharose 4 fast flow	10246735	GE Healthcare, Munich, Germany
RNeasy mini kit	74104	Qiagen, Hilden, Germany
Skimmed milk powder	T145.3	Carl Roth GmbH + Co. KG, Karlsruhe, Germany
Sodium azide	S2002	Sigma Aldrich, Munich, Germany

Sodium chloride (NaCl)	9265.3	Carl Roth GmbH + Co. KG, Karlsruhe, Germany
Sodium dodecyl sulfate (SDS)	2326.2	Carl Roth GmbH + Co. KG, Karlsruhe, Germany
Sodium hydroxide (NaOH)	0993.1 45% T135.1 2N	Carl Roth GmbH + Co. KG, Karlsruhe, Germany
Solution I	6022	TAKARA Clontech, Av du Pdt Kennedy St-Germain-en-Laye, France
T4 DNA ligase buffer (10X)	B69	Thermo Fisher Scientific, Karlsruhe, Germany
T4 Polynucleotide kinase	EK0031	Thermo Fisher Scientific, Karlsruhe, Germany
TAQ all inclusive	PEQL01-1000	VWR International GmbH, Ismaning, Germany
Temed	2367.3	Carl Roth GmbH + Co. KG, Karlsruhe, Germany
Temozolomide	PHR1437	Sigma Aldrich, Munich, Germany
Thiazolyblue(MTT)	4022.1	Carl Roth GmbH + Co. KG, Karlsruhe, Germany
Tris	0188.3	Carl Roth GmbH + Co. KG, Karlsruhe, Germany
Triton-X-100	3051.3	Carl Roth GmbH + Co. KG, Karlsruhe, Germany
Tween-20	9127.2	Carl Roth GmbH + Co. KG, Karlsruhe, Germany

Xylol	CN80.2	Carl Roth GmbH + Co. KG, Karlsruhe, Germany

3. Material

Substances	Catalogue Number	Producer
21G/26G needle	3043 174/228	Dispomed Witt oHG, Gelnhausen, Germany
40µM/70µM Cell strainer	08-771-1/2	Fisher Scientific, Schwerte, Germany
Blotting paper sheets	FT-2-519-580600N	Sartorius Stedim Biotech GmbH, Göttingen, Germany
Bottle top filter	431118	Greiner Bio-One GmbH, Frickenhausen, Germany
Cell culture flasks (250mL)	58170	Greiner Bio-One GmbH, Frickenhausen, Germany
Counting chamber	Profondeur	Paul Marienfeld GmbH & Co. KG, Lauda-Königshofen, Germany
Glass pipette	M4150N0250SP4	Kimble-Chase, Meiningen, Germany
ImmEdge Hydrophobic Barrier PAP Pen	H-4000	LINARIS Biologische Produkte GmbH, Dossenheim, Germany
Nitrocellulose membrane	GE10600002	GE Healthcare, Munich, Germany
Parafilm	PF10	A. Hartenstein GmbH, Würzburg, Germany

Plastic pipette(5,10,25mL)	606180/607180/760180	Greiner Bio-One GmbH, Frickenhausen, Germany
Scalpel	0268878	Fisher Scientific, Schwerte, Germany
Sterilization tape	STKD	A. Hartenstein GmbH, Würzburg, Germany
Storage bottle	8323	Greiner Bio-One GmbH, Frickenhausen, Germany
Syringe filter	FI02	A. Hartenstein GmbH, Würzburg, Germany
Thermanox plastic coverslip	174969	Thermo Fisher Scientific, Karlsruhe, Germany
Ultra-low attachment plate	CLS3471-24EA	Sigma, Munich, Germany
WesternSure® Pen	926-91000	LI-COR Biosciences GmbH, Bad Homburg vor der Höhe, Germany

4. Software

Software	Software Producer
Adobe. Photoshop. CS5	Adobe Systems incorporated, San Jose, CA, USA
Axiovision Rel. 4.8.	Carl Zeiss Microscopy, LLC, Thornwood, NY, USA
FlowJo	Tree Star, Inc., Ashland, OR, USA
GraphPad Prism	GraphPad Software, La Jolla, CA, USA
NIS Elements F 3.2	Nikon Instruments Inc., Melville, NY, USA

SPSS Statistics	IBM Deutschland GmbH, Ehningen, Germany

5. Cell culture

5. 1 Consumables and additives

Substances	Catalogue Number	Producer
Accutase	A1110501	Thermo Fisher Scientific, Karlsruhe, Germany
BIT-100 admixture	PB-SH-033-0000	PeloBiotech GmbH, Planegg, Germany
Dulbecco's Modified Eagle Medium GlutaMAX-I, high Glucose (DMEM)	41966052	Thermo Fisher Scientific, Karlsruhe, Germany
Earle's Balanced Salts solution (EBSS)	E2888	Sigma-Aldrich, Munich, Germany
Fetal Bovine Serum (FBS)	S0415	Biochrom AG, Berlin, Germany
Geltrex™ LDEV-Free, hESC-Qualified, Reduced Growth Factor Basement Membrane Matrix	A1413201	Thermo Fisher Scientific, Karlsruhe, Germany
Hanks' Balanced Salt solution (HBSS)	H6648	Sigma-Aldrich, Munich, Germany
L-15 Medium (Leibovitz)	L5520	Sigma-Aldrich, Munich, Germany
L-glutamine	G7513	Sigma-Aldrich, Munich, Germany

MEM Non-Essential-Amino Acid Solution (NEAA)	M7145	Sigma-Aldrich, Munich, Germany
Minimum Essential Medium Eagle (MEM)	M2279	Sigma-Aldrich, Munich, Germany
N1 Supplement	N6530	Sigma-Aldrich, Munich, Germany
Ovomucoid inhibitor	AS9035	Biomol GmbH, Hamburg, Germany
Papain, Suspension	LK003178	CellSystems Biotechnologie Vertrieb GmbH, Troisdorf, Germany
Penicillin-Streptomycin	P4333	Sigma-Aldrich, Munich, Germany
Phosphate Buffered Saline(PBS)	14190250	Thermo Fisher Scientific, Karlsruhe, Germany
Primocin	ant-pm-1	InvivoGen, Germany
Recombinant human EGF	C029-A	PeloBiotech GmbH, Planegg, Germany
Recombinant human FGF Basic (bFGF)	C046-A	PeloBiotech GmbH, Planegg, Germany
Recombinant human TGF-ß1	100-21-A	PeloBiotech GmbH, Planegg, Germany
RPMI-1640 Medium	R7638	Sigma-Aldrich, Munich, Germany
Trypsin-EDTA	T4049	Sigma-Aldrich, Munich, Germany

5. 2 Cultivation and cryopreservation of GBM cell lines

LN229, U87MG, T98G human glioblastoma cell lines were obtained from American Type Culture Collection (ATCC). LN229 cell lines were cultivated in Dulbecco's modified eagle's medium (DMEM), which was supplemented with 4mM glutamine, 5% (v/v) FBS, 100U/mL penicillin and 100µg/mL streptomycin. U87MG and T98G cell lines were maintained in minimum essential medium (MEM) supplemented with 10% (v/v) FBS, 2mM glutamine, 100 U/mL penicillin and 100µg/mL streptomycin. GBM cell lines were passaged twice every week with 2mL trypsin applied per T75 flask for cell detachment.

For cell cryopreservation, GBM cells were collected at 80% confluence. Gradual freezing process was applied using an alcohol-free cell freezing container. The cells were stored in freezing medium (90% FBS, 10% DMSO) in the container at -80℃ overnight and stored in liquid nitrogen.

5. 3 Primary cell culture

The specimens from patients with GBM were obtained with patients' consent based on the tissue preservation guidelines from TUM medical faculty. After resection, tumor tissue was preserved in serum free medium at 4℃ and was isolated for primary cells within 24 hours.

Isolation of human primary glioblastoma tumor cells T84: Tumor tissue was transferred into a 10cm dish and cut with two sterile scalpels for 2–3 minutes into small pieces. Then, 10mL pre-warmed HBSS containing 500U/mL penicillin and 500µg/mL streptomycin was added onto the tissue and then the mix was transferred into a 50mL falcon tube. After washed twice for removing the debris and red blood cells, the mix was spun down for 5 minutes at 300g and

resuspended in fresh pre-warmed Papain – DNaseI digestion solutions. Then the tube was incubated for 10 – 30 minutes in a water bath (+37°C) with inversion every 2 minutes until the tissue solution became viscous. A 70µm cell strainer was used to filter out the remaining tissue clumps. Subsequently, red blood cell lysis buffer was used to lyse erythrocytes, 4mL Ovomucoid Inhibitor (0.71mg/mL in EBSS) and 250µL DNase were added and spun down at 250g for 5 minutes at room temperature (RT). Finally, the cells were resuspended in glioma stem cell medium (GSCM, RPMI-1640, 20% BIT-100 Add Mixture, 1% N1 Supplement, 1% NEAA-MEM, 2% L-Glutamine, 20ng/mL bFGF, 300pg/mL TGF- ß1, 500pg - 2ng/mL EGF, 0.2% Primocin), passed through a 40µm cell strainer (Greiner) and seeded on a cell culture flask. For adherent cell culture, flasks were pre-coated with Geltrex.

Splitting human primary glioblastoma tumor cells T84: The cells need to be splitted when the confluence reaches 80% or the sphere size is between 200 - 400µm. The spheres were harvested and centrifuged at 250g for 5 minutes at RT and dissociated to single cells with 800 µL pre-warmed accutase which supplemented with 50µL DNaseI solution (15 minutes incubation at +37°C/150g in Thermocycler). If large spheres remain after accutase treatment, dissociation can be performed again mechanically by pipetting or passing through a 21G and then a 26G needle. Finally, the cells were resuspended in fresh GSCM after going through a pre-wetted 40µm cell strainer.

*For coating, geltrex was placed on ice for 2 hours to thaw. Then the geltrex was diluted in cold serum-free medium (1:100) to avoid pre-gelling. Then the dishes/flasks were coated at least 1 hour at +37°C. Coated dishes/flasks were kept in DPBS at 4°C for at most 14 days, and dishes/flasks should be pre-warmed for 1 hour at +37°C before use.

5. 4 Mycoplasma test

Mycoplasma test was conducted using PlasmoTest™ mycoplasma Detection Kit every 2-3 months. Briefly, 500µL cell culture supernatant has been taken and transferred into a microtube. The supernatant was heated at 100℃ for 15 minutes. A total of 50µL of each heated sample was transferred to a 96-well plate. And, 50µL of positive or negative control (provided by the kit) was added as well. Subsequently, HEK-Blue™-2 cell suspension was prepared using pre-warmed HEK-Blue™ Detection medium. Finally, 200µL (~50,000 cells) cell suspension was added to each well containing the samples or controls and incubated at 37℃ in a CO_2 incubator overnight (16-24 hours) for detection.

6. CRISPR-Cas9 knockout

6. 1 Single guide RNAs (sgRNA) were designed using an online tool (http://crispr.mit.edu/).

Table 1. sgRNA Oligonucleotides for CRISPR/Cas 9 knockout

Oligos	Sequences (5'→3')
ALDH1A3_gRNA_01_Forward	CACCTTCCACGGCCCCGTTAGCGG
ALDH1A3_gRNA_01_Reverse	AAACCCGCTAACGGGGCCGTGGAA
ALDH1A3_gRNA_02_Forward	CACCGTTTTCCACGGCCCCGTTAG
ALDH1A3_gRNA_02_Reverse	AAACCTAACGGGGCCGTGGAAAAC
ALDH1A3_gRNA_03_Forward	CACCGTCCGGCTGCCCGTTTTCCA
ALDH1A3_gRNA_03_Reverse	AAACTGGAAAACGGGCAGCCGGAC

6. 2 Preparation of the sgRNA oligos inserts.

The oligos were resuspended to a final concentration of 100µM and annealed as indicated.

Table 2. Annealing mix for sgRNA oligos

Component	Amount(µL)

T4 PNK	1
T4 ligation buffer	1
sgRNA top (100µM)	1
sgRNA bottom (100µM)	1
ddH_2O	6
Total	10

The oligos were phosphorylated and annealed by using the following parameters:

37℃ 30 minutes

95℃ 5 minutes and then ramp down to 25℃ at 5℃/min

After annealing, the oligos were diluted at a 1:200 dilution in sterile water.

6. 3 pSpCas9 plasmid was cut into linearized DNA.

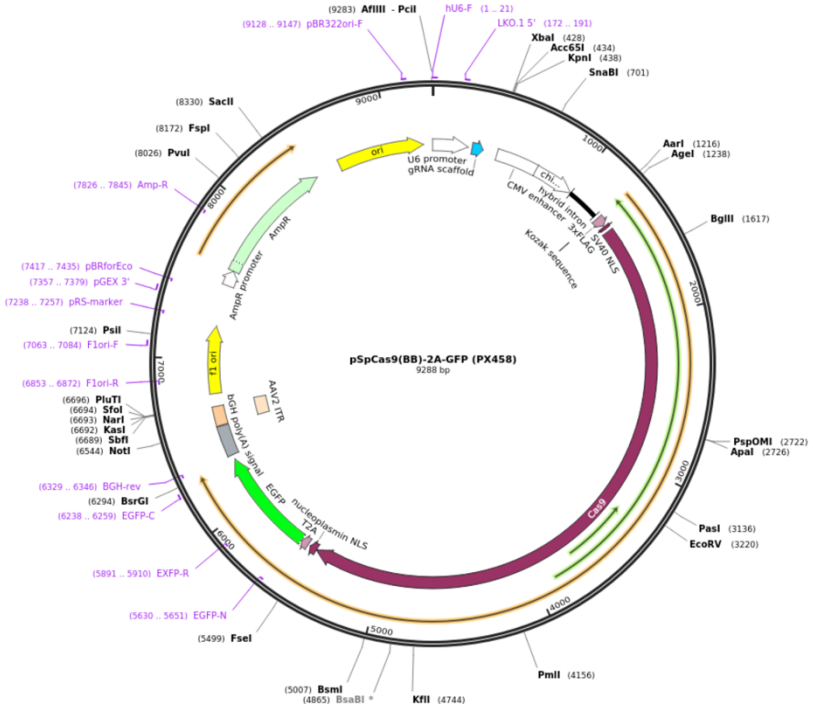

Figure 6. Scheme of pSpCas9-2A-GFP (PX458) plasmid

Table 3. Digestion mix

Component	Amount
DNA	8μg
Restriction Enzyme	2.5μL
NEBuffer	5μL
ddH2O	40.5μL
Total	50μL

The mixture was incubated at 37℃ for 4 hours.

6. 4 Linear DNA purification

0.6% agar gel was made to separate the Linear plasmid. pSpCas9 circular DNA plasmid was used as the control, and 80V was used for running the gel (about 2 hours). Subsequently, the positive band was cut for gel extraction with a QIAquick® Gel Extraction Kit. Briefly, The gel slice was weighed and dissolved in Buffer QG. After mixed with isopropanol, the gel solution went through a QIAquick spin column. And 50μL RNase-free water was used to dissolve the purified DNA and then the concentration was measured with the spectrophotometer NanoDrop™ 2000c.

6. 5 Ligation of sgRNA oligos inserts and pSpCas9 linear DNA.

Table 4. Ligation mix

Component	Amount(μL)
linearized DNA	0.5(at least 50ng)
gRNA oligos	2
Solution 1	2.5

Total	5

The mixture was incubated for 30 minutes at 16℃ for ligation.

6. 6 Transformation

Transformation was conducted using NEB 5-alpha Competent E. coli cells. The mixture above was added to the E.coli. After mixed carefully, the cells were incubated on ice for 30 minutes. Subsequently, the cells were activated by heat shock at 42℃ for 30 seconds, followed by 5 minutes incubation on ice again before incubating with 950µL SOC medium in a shaker at 37℃ for 60 minutes. After centrifuged, 950µL medium was discarded and rest medium with pellet was applied to a selective agar plate and incubated at 37℃ overnight in a shaker.

6. 7 PCR

8 colonies from each gel plate were tested by PCR.

Table 5. PCR program

Step	Temp	Time
Initial Denature	95℃	30s
30 cycles	95℃	30s
	58℃	1min
	68℃	30s
Final Extension	68℃	5min
Hold	10℃	

U6 promoter and reverse oligos of gRNA were used as primers for PCR.

U6 forward primer: GAGGGCCTATTTCCCATGATTCC

The bacteria colony with successful ligation plasmid was shook at 37℃ in 6mL LB medium (100 μg/mL ampicillin) overnight for plasmid isolation.

6. 8 Plasmid isolation and sequencing

QIAprep spin miniprep kit was used to perform DNA isolation. Then the CRISPR plasmid was sent for sequencing with the U6 forward primer.

6. 9 Cell transfection and cell sorting

U87 MG, LN229, T98G cells, respectively, were plated in 6-well plates at a density of 500,000 cells / well and transfected with ALDH1A3 sgRNA plasmids using lipofectamine 3000.

For 1 well of a 6-well plate:

Tube 1. Opti-MEM Medium	125μL
Lipofectamine 3000	7.5μL
Tube 2. Opti-MEM Medium	125μL
DNA	1.5μg
P3000TM Reagent	5μL

A total of 125μL solution was taken from each tube and mixed. Afterwards, the mixture was kept at RT for 5 minutes and added to the cells. After transfected for 48 hours, the cells were harvested in the sorting buffer (3% FCS and 1mM EDTA in PBS). Subsequently, the single cell solution was forwarded to fluorescence-activated cell sorting to collect green fluorescence protein (GFP) labeled cells. Then the GFP-labelled cells were cultured for 2 weeks before the validation of ALDH1A3 expression.

7. Cell viability assay

3-(4,5-dimethylthiazol-2-yl)-2,5-diphenyltetrazolium bromide (MTT) was used to investigate the viability of cells after TMZ treatment. Metabolic active cells possess cellular reductase, which can reduce MTT to formazan crystals. The crystals can be dissolved in DMSO to a purple dye and evaluated with a microplate reader at 595nm.

U87MG (2000 cells / well), LN229 (1500 cells / well) and T98G (1500 cells /well) cells, respectively, were plated in 96-well plates, and treated with different doses of TMZ (100-500µM) for 5 consecutive days. Subsequently, MTT was applied to the cells (final concentration: 0. 5mg/mL) and then the cells were incubated at 37°C for 4 hours. Finally the formazan was dissolved in 200µL DMSO and quantitative evaluated with a microplate absorbance reader.

8. Clonogenic assay

The cells received the treatment of TMZ with/without DEAB for 24 hours and were re-seeded in six-well plates (500 cells/well). After culturing for 7-10 days, the cells were fixed with 4% formaldehyde and stained with 0.05% crystal violet. The cell colonies consisting of ≥ 50 cells were counted.

9. Sphere forming assay

X01 and T84 cells were treated with TMZ in the presence or absence of DEAB for 24 hours and replated in ultra-low attachment plates (1000 cells/well). After growing for 5 days, cell clusters of diameters >100µm were counted with a Nikon eclipse TS100 microscope.

10. EGFP-LC3 transfection

U87MG, LN229 and T98G cell lines were grown in 6-well plates (500,000 cells / well) overnight before transfected with EGFP-LC3 plasmid. 24 hours post transfection, the cells were treated with 300µM TMZ for 5 consecutive days. Bafilomycin (50nM) was used as a positive control. After the treatment, the cells were fixed and checked under a Zeiss LSM780 confocal microscope.

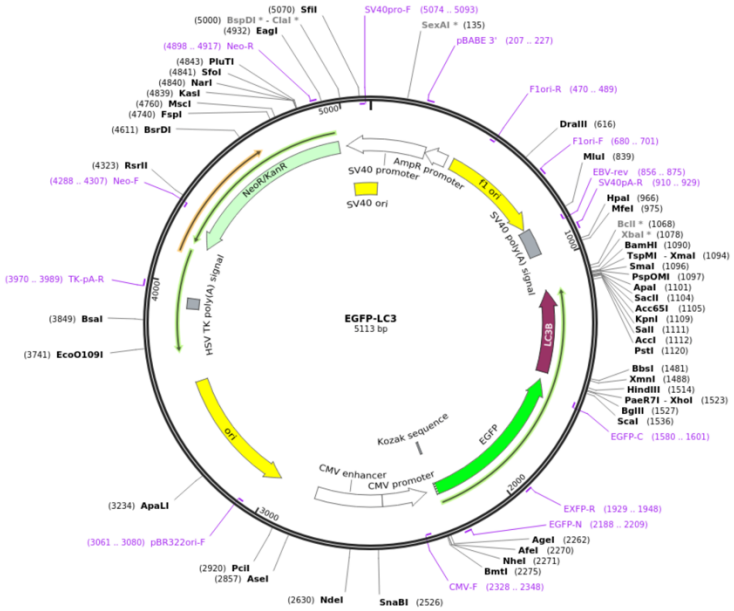

Figure 7. Scheme of EGFP–LC3 plasmid

11. Western Blot analysis

11. 1 Buffers and solutions

Table 6. 1X RIPA Buffer

Reagent	Final concentration
SDS	0.1%
Tris-Cl	10mM

EDTA	0.5mM
Triton X -100	1 %
NaCl	140mM
Sodium deoxycholate	0.1%

After mixed, buffer was aliquoted (1mL for each) and stored at -20℃.

Protease/phosphatase inhibitor was added before use.

Table. 7 5 x Laemmli buffer (10mL)

Reagent	volumn	Final concentration
SDS	1g	2%
1.5M Tris-Cl pH 6,8	2.1mL	63mM
Glycerol	5mL	10%
1% Bromophenol blue	0.2mL	0.004%
H_2O	2.7mL	

Table. 8 10 x Running buffer (1L)

Reagent	volumn	Final concentration
Tris	30.3g	0.25M
Glycine	144.1g	2M
SDS	10g	1%

Table 9. 10 x Transfer buffer (1L)

Reagent	volumn	Final concentration
Tris	30.3g	0. 25M
Glycine	144.1g	2M

Transfer Buffer(1X):

100 mL Transfer Buffer (10X)

200 mL ethanol

Add ddH_2O to 1L.

Large proteins (>100 kD): ethanol concentration at 10%. SDS concentration at 0.1%.

Small proteins (<100 kD): ethanol concentration at 20%. SDS is not essential.

Table.10 10 x TBS buffer (1L)

Reagent	volumn	Final concentration
Tris	24.2g	0.2M
NaCl	87.66g	1.5M

adjust pH to 7.5 with HCl.

1x TBS-T: 1 x TBS, 0.05% Tween-20

Blocking Buffer: 1 x TBS-T, 5% Slim Milk Powder or 5% BSA

Stripping Buffer: 12.5mL 0.5M Tris HCl (pH 6.8), 67.5mL ultrapure water, 20mL 10% SDS, 0.8 mL 2-mercaptoethanol

Table 11. SDS-PAGE gel preparation

For 2 Gels

Separation Gel

Gel Percentage	6%	8%	10%	12%	15%
H_2O	7.9mL	6.9mL	5.9mL	4.9mL	3.4mL
30% Acrylamid	3.0mL	4.0mL	5.0mL	6.0mL	7.5mL
1.5M Tris pH 8.8	3.8mL	3.8mL	3.8mL	3.8mL	3.8mL
10% SDS	150µL	150µL	150µL	150µL	150µL
10% APS	150µL	150µL	150µL	150µL	150µL
Temed	9µL	9µL	6µL	6µL	6µL

Stacking Gels

For 2 Gels

Gel Percentage	5%

H_2O	5.5mL
1.5 M Tris pH 6.8	1.0mL
10% SDS	80µL
30% Acrylamid	1.3mL
10% APS	80µL
Temed	8.0µL

Table 12. Gel percentage according to protein size

Protein size (kDa)	Gel acrylamide percentage (%)
4-40	20
12-45	15
10-70	12
15-100	10
25-200	8

11. 2 Antibodies

Antibody	Company
ALDH1A3 rabbit mAb SQSTM1/p62 rabbit mAb	Thermo Fisher Scientific, Karlsruhe, Germany
4-Hydroxynonenal rabbit mAb	Abcam, Cambridge, UK
Vinculin HRP-conjugated secondary antibody	Cell Signaling Technology, Frankfurt, Germany
LC3B rabbit mAb ALDH1A3 mouse mAb	Novus Biologicals, Wiesbaden Nordenstadt, Germany
Normal Rabbit IgG	Millipore, Darmstadt, Germany

11. 3 Protein isolation and denaturation

Protein isolation: Cells were washed in PBS and collected with cell scrapers. The pellet from centrifugation was suspended in RIPA buffer (1x 10^6 cells/80µL). Then the lysis was handed to sonicator to smash the nucleus and incubated on ice for 15 minutes. Following centrifuging at 13,000rpm for 10 minutes at 4℃, the supernatant was collected for denaturation. The concentration of the protein was determined by Bradford assay. The Coomassie blue binds to aromatic amino acid residue (especially arginine), which can be detected by a microplate absorbance reader at 465nm-595nm.

Protein denaturation: The Laemmli buffer has been used for protein denaturation. The buffer contains SDS, an anionic detergent, which is able to break up the secondary and tertiary structure and coat proteins with negative charges. Another reagent, DTT, is able to reduce the disulfide bonds of the proteins. Briefly, the supernatant from above procedures were mixed with Laemmli buffer and incubated in heater at 95℃ for 5 minutes. After cooling down, the protein lysate was stored at -20℃.

11. 4 Procedures

After sample preparation, Sodium Dodecyl Sulfate-Polacrylamide Gel Electrophoresis (SDS-PAGE) was used to separate the protein by molecular weight. 25µg lysate of each treated group was loaded into each well of the gel. Voltage starts with 50V for 15 minutes, and then to 150–200V until finishing the running.

Afterwards, proteins in SDS-PAGE can be visualized with Coomassie Blue. Separated proteins were gently transferred to nitrocellulose membranes with a wet blot system at 110V for 60 minutes, or 30V overnight. Ponceau Red stain can be applied to visualize the protein from membranes. Subsequently, 5% non-fat milk or 5% BSA blocking was conducted to prevent non-specific binding of antibody (1 hour at RT). Following the incubation, the membranes were kept in primary antibodies with gently shaking at 4℃ overnight. On the 2nd day, the membranes were washed in TBST (3x10 minutes) and incubated with secondary

immunoglobulins for 1 hour at RT. Subsequently, immunoreactivity was visualized by adding of HRP substrate and exposing to chemiluminescence detection film.

Antibody reprobing: The membrane can be reprobed with another primary antibody if the original primary antibody has been removed by the stripping buffer. Briefly, the membranes from exposure were washed with TBST (3x10 minutes) and gently shook in stripping buffer for 10 minutes. After washed in TBST and blocked with milk/BSA, the membranes were incubated with other primary antibodies.

12. Aldefluor assay

Aldefluor assay was conducted to investigate ALDH activity. The ALDEFLUOR™ kit (StemCell Technologies, Cologne, Germany) contains BODIPY labelled aminoacetaldehyde (BAAA), which is a fluorescent substrate for ALDH. BAAA can be oxidized by ALDH to BAA. These ALDH-bright cells can be counted by flow cytometer.

U87 MG, LN229 and T98G cell lines were plated in 6-well plates (100,000 cells / well) and treated with 300µM TMZ for 5 consecutive days. After treatment, 500,000 cells from each treated group were harvested and washed with PBS. Then the cells were resuspended in 1mL plain medium (DMEM or RPMI-1640), which supplemented with verapamil (50µM) and fumitromorgin C (5µM) to inhibit the ABC/PgG Transporters. A total of 5µL Aldefluor assay substrate (AAS, greenish/yellow color, hold in the dark until use) was added into the single cell suspension and mixed properly. 500µl of the cell suspension with the AAS was transferred immediately into the tube with DEAB (the inhibitor of ALDH). After incubated at 37°C for 45 minutes, the cells were resuspended in aldefluor assay buffer for flow cytometric analysis.

13. Analysis of mRNA: RT-PCR and qPCR

13. 1 RNA extraction and reverse transcription

RNA extraction: RNeasy® Mini Kit was used to isolate total RNA. 1x10^6 cells were harvested, washed with ice-cold PBS and centrifuged at 500g for 5 minutes. Subsequently, the cells pellet was suspended in 350µL RLT buffer, containing 10µL ß-mercaptoethanol/mL RLT buffer. After vortex, the lysate passed through a 21G needle 5–10 times to Homogenize cells. 350µL 70% ethanol were added to the homogenized lysate and subsequently the sample was applied to an RNeasy midi column. After washed with the buffer provided, the RNA was eluted with RNase free water and stored at -80°C. The concentration of RNA was measured by Nanodrop (A260 = 1 = 40µg/mL).

Reverse transcription: PrimeScript™ RT reagent Kit (Perfect Real Time) was used to conduct reverse transcription.

Table 13. Mixture for Reverse Transcription

Reagent	Amount (µL)	Final concentration
5X PrimeScript Buffer	2	1x
Oligo dT Primer (50µM)	0.5	
Random 6 mers (100µM)	0.5	25pmol
PrimeScript RT Enzyme Mix I	0.5	50pmol
total RNA	N (500ng)	
RNase Free dH_2O	=10-N-3.5	
total	10	

37°C 15 minutes

85°C 5 seconds

4°C

13. 2 PCR process

Table 14. PCR-mix for RT-PCR

Reagent	Amount (µL)

10x buffer (15mM Mg^{2+})	2.5
Taq Polymerase (5/µl)	0.25
dNTPS (each 1.25mM)	4
Forward primer (20µM)	0.5
Reverse Primer (20µM)	0.5
cDNA (from 500ng RNA)	2
H_2O	15.25

Table 15. PCR program for RT-PCR

Process	Temp. [℃]	Duration	Cycles
Initial Denature	95	5min	single
Denaturation	95	30s	35 cycles
Primer annealing	55-62	30s	
Elongation	72	30s	
Final extension	72	7min	single
Hold	4	∞	single

10µL PCR product was mixed with 2µL 6x DNA loading buffer and separated on a 1% agarose gel.

13. 3 Gradient PCR

Gradient PCR was performed to investigate the suitable annealing temperatures for quantitative real-time PCR. LN229 cDNA (from 1µg RNA) was diluted 1:50 and served as a template. Each master-mix consists of 10µL SYBR Green I Master®, 2µL primers, 5µL cDNA and 3µL H_2O. Gradually increasing temperatures were used for gradient PCR. Finally, the PCR products were separated on an agarose gel to check the specificity. The temperature of the group with less unspecific bands and maximum product was defined as the optimum annealing temperature.

Table 16: PCR-program for gradient PCR (*Gradient 8)

Process	Temp. [℃]	Duration	
Initial Denature	94	5min	single
Denaturation	94	30s	35 cycles
Primer annealing	G=8*	30s	
Elongation	72	30s	
Final Extension	72	7min	single
Hold	4	∞	single

13. 4 Quantification of ALDH1A3 mRNA by qPCR

LightCycler 480 SYBR green I Master was used to conduct real-time PCR. SYBR green I is an asymmetrical cyanine dye specific to DNA double-strand. During amplification process of PCR, the SYBR green I binds to the PCR product. Increasing fluorescence of the dye will be measured to monitor the newly synthesized DNA. GAPDH was used as the housekeeping gene. GAPDH forward primer: CATGAGAAGTATGACAACAGCCT. GAPDH reverse primer: AGTCCTTCCACGATACCAAAGT. Human ALDH1A3 primers were designed and synthesized in QIAGEN company. The quality of primers was verified by the PCR efficiency and melting curve. A serial dilutions of the cDNA were used to make the standard curve to investigate the PCR efficiency (sequence doubled in each cycle was defined as an efficiency of 2.0).

Table 17: PCR-mix for qPCR

Reagent	Amount (µL)
SYBR Green Master (ROX)	25
Forward Primer (30µM)	0.5
Reverse Primer (30µM)	0.5
RNase Free dH_2O	=50-26-N
Template DNA	N(250ng)
Total Volume	50

Table 18: PCR-program for qPCR

Process	**Temp. [℃]**	**Duration**	
Initial Denature	95	15min	single
Denaturation	95	5s	40 cycles
Annealing/Extension	60	30s	
Melting curve analysis	According to instrument guidelines		

Optimal: PCR primers final concentration: 0.2-1µM

cDNA final concentration: 25-50ng/10µL

14. Cell cycle analysis

Cell cycle analysis using propidium iodide (PI) was conducted to investigate the effect of TMZ on different phases of the cell cycle. The cells are normally permeabilized and stained with fluorescent dye PI. Different amount of DNA synthesized during each phase (G_0/G_1 versus S versus G_2/M) will be reflected by fluorescence intensity.

U87MG, LN229 and T98G cells, respectively, were plated in 10 cm^2 dishes at a density of 500,000 cells per dish. After settled down, the cells received 300µM TMZ treatment with/without 2mM NAC for 5 consecutive days. Then the fixation was performed with 70% ethanol and RNase was used to remove RNA. Finally, the cells were incubated with PI solution (50µg/mL) for 10 minutes at RT and analyzed by flow cytometry.

15. Proximity ligation assay

Proximity ligation assay (in situ PLA) is a technique that enables direct detection of protein modifications and protein interactions in various samples including protein suspensions (e.g.

cell lysates), or fixed tissues (e.g. cell culture slides, cytospin preparations or tissue sections). In a typical PLA, two antibodies are used to recognize two proteins of interest. Each antibody is conjugated with a short sequence of oligonucleotides. These two oligonucleotides are complementary to each other, denoted as a PLUS and a MINUS probe. When distance of these probes is less than 40nm, the addition of two connector oligonucleotides that hybridize with the probes will lead to the formation of a closed circle template in the presence of a ligase. The subsequent addition of a polymerase and fluorescent-labelled oligonucleotides then result in a rolling circle amplification of the closed circle template, which can be visualized as a distinct fluorescent spot that can be detected and quantified by epifluorescence or confocal microscopy.

PLA was conducted using Duolink® In Situ Red Starter Kit Mouse/Rabbit to investigate the interaction between ALDH1A3 and p62, ALDH1A3 and p62 with HNE-modified proteins, separately. LN229, U87MG and T98G, respectively, were seeded on glass coverslips. After blocking in the buffer provided, cells were incubated with rabbit-anti-ALDH1A3 (1:500) and mouse-anti-p62 (1:500) antibodies at 4°C overnight. The cells were subsequently incubated with PLUS and MINUS probes against rabbit and mouse IgG at 37° C for 1 hour, followed by ligation for 30 minutes and amplification for 100 minutes at 37° C. In the end, the coverslips were mounted and forwarded to fluorescence imaging (Zeiss HBO 100 Upright Fluorescence Microscope).

16. Co-Immunoprecipitation (Co-IP)

U87MG, LN229 and T98G, respectively, were treated with 50µM chloroquine for 2 hours and harvested in lysis buffer (10% glycerol, 1mM dithiothreitol, 50mM HEPES pH7.5, 150mM NaCl, 0.1% Triton x-100, 2mM $MgCl_2$, Protease Inhibitor cocktail). Protein G Sepharose was washed 3 times (1000g, 1 minute) in PBS (twice amount of beads were needed from the bead slurry) and added to the lysate for further 2 hours incubation. Then the mixture was centrifuged and

the supernatant was taken out to exclude sepharose for the unspecific binding. 50µL of the lysate was transferred to a new tube as input. The rest was incubated with antibody against p62 at 4℃ overnight (500µg lysate/2µg antibody). Anti-IgG was taken as a control. On the next day, the Protein G Sepharose was washed 3 times in PBS and added to the lysate for further incubation for 1 hour. Subsequently, the protein-sepharose complex was washed 5 times with lysis buffer (10 minutes for each time) to avoid the unspecific binding. Then the complex was boiled in 2x laemmli buffer for 5 minutes to detach the proteins from beads. Finally, the samples were centrifuged and the supernatants were taken for immunoblotting.

17. Reactive oxygen species assay

Reactive oxygen species (ROS) were detected by the OxiSelect™ *In Vitro* ROS/RNS Assay Kit (Cell Biolabs, Heidelberg, Germany). The assay employs a proprietary quenched fluorogenic probe, dichlorodihydrofluorescin DiOxyQ (DCFH-DiOxyQ), which is widely used as a specific ROS/RNS probe based on similar chemistry to 2', 7'-dichlorodihydrofluorescein diacetate. The DCFH-DiOxyQ probe is primarily connected with a quench removal reagent, afterwards the complex stabilizes in a highly reactive DCFH form. ROS and RNS are capable to directly react with DCFH, which leads to rapid oxidation of DCFH to the highly fluorescent reagent 2', 7'-dichlorodihydrofluorescein (DCF). The fluorescence can be detected at 480 nm/530 nm. The ROS and RNS include nitric oxide (NO), hydrogen peroxide (H_2O_2), peroxynitrite anion (ONOO-) and peroxyl radical ($ROO^{\cdot}$), which are the representative of both ROS and RNS.

Briefly, U87MG, LN229 and T98G cells, respectively, were plated on black 96-well plates (2000 cells/well) and treated with TMZ (100-500µM) either alone or with 2mM NAC for 4 consecutive days. Subsequently, cells were treated with DCFH-DA at 37℃ for 30 minutes and followed again with TMZ (100-500µM) with/without NAC treatment for 30 minutes. The fluorescence intensity was evaluated with a fluorometric plate reader at 480 nm/530 nm.

18. lipid peroxidation detection

Lipid peroxidation was investigated by measuring malondialdehyde (MDA) levels using Lipid Peroxidation (MDA) Assay Kit (Sigma, Munich, Germany). The end products of lipid peroxidation are bioactive aldehyde compounds such as Malondialdehyde (MDA) and 4-hydroxynonenal (4-HNE). The detection of these bioactive aldehydes has been widely accepted for the investigation of oxidative stress. Thiobarbituric Acid Reactive Substances (TBARS) is used to screen and monitor lipid peroxidation. MDA is able to generate stable adducts with TBARS, which can be measured colorimetrically or fluorometrically.

Briefly, all three cell lines were seeded in 10 cm^2 dishes, treated with TMZ (100-500µM) either alone or with 2mM NAC for 5 consecutive days, cells of each group of identical quantities were collected 30 minutes after last treatment. Subsequently, the cells were mixed with 300µL MDA Lysis Buffer (1% BHT) and incubated on ice. After centrifugation, 200µL supernatant from each sample was mixed with 600 µL TBA solution and incubated at 95 ℃ for 60 minutes. Finally, 200µL solution was taken from each reaction mixture for colorimetric detection (532 nm).

19. Immunofluorescence

Glioblastoma cell lines LN229, U87MG, T98G, respectively, were seeded on glass coverslips and treated with 300µM TMZ for 5 consecutive days, the cells were fixed with 4% formaldehyde at 30 minutes after last TMZ treatment or 1 hour after 30µM HNE treatment. After washing, the cells were blocked in blocking buffer (PBS, 1% BSA, 0.1% Triton X-100, 0.01% Tween, 0.02% sodium azide, 2.5% donkey serum) at RT for 30 minutes. Subsequently, the coverslips were covered with primary antibodies (anti-p62 and anti-HNE 1:500) overnight at 4℃, followed by second antibody incubation (1:500). Finally, the cells were stained with Hoechst dye (dilute 1:10,000 in PBS) and mounted with Aqua Poly/Mount, ready for fluorescence imaging (Zeiss HBO 100 Upright Fluorescence Microscope).

20. Immunohistochemistry (IHC) of patient tissue samples

112 specimens from 56 patients with GBM (WHO grade IV) were collected with patients´ consent (according to tissue preservation guidelines of the TUM medical faculty). All patients underwent primary and secondary surgical resection (alkylating agent based chemotherapy and radiation therapy were applied after primary surgery).

20. 1 Buffers and solutions

Table 19. 10x PBS (1L)

Reagent	Amount (g)	Final concentration (mM)
NaCl	81.8	140
KCl	2	2.7
Na_2HPO_4	17.5	10
KH_2PO_4	2.4	1.8

The pH was adjusted to 7.4 by HCl.

Table 20. Blocking Buffer (500 mL)

Reagent	Amount	Final concentration
PBS	500mL	1x
BSA	5g	1%
Gold Fish Gelatine	1g	0.1%
Triton X -100	0.5mL	0.2%
10% NA Azid	1mL	0.02%
Normal Horse Serum	Add freshly	2.5%

20.2 Procedures

The tissue was sectioned (5µm) and deparaffinized in Xylol and ethanol. Then the slides were incubated in citric acid buffer (10mM pH 6.0) for epitope unmasking. After a cooling down step in aqua water (pH 7.6), endogenous peroxidase was quenched in 1.5% H_2O_2 at RT for 10 minutes. Subsequently, tissues were blocked in Blocking buffer (NHS 2.5%, 25µL NHS/1mL Buffer) with Avidin (1 Tpf Avidin/mL Buffer) for 15 minutes to reduce unspecific staining from endogenous avidin-biotin activity. Primary antibody is diluted in blocking buffer with Biotin (1 Trp Biotin/mL Buffer) (1:600) and added on each tissue section. Then the slides were stored at 4°C overnight. On the next day, following the incubation with the 2nd antibody (1:400) at RT for 30 minutes, the slides were incubated with reagent from ABC kit for 30 minutes at RT. At last, each tissue slide was incubated with DAB chromogen solution for 30 s – 2 min until the brownness is visible and then the slides were counterstained with hematoxylin. Expression score of each slide was evaluated using a modified Immunoreactivity Score (IRS) system: Negative (0), ≤10% (1), 11%-25% (2), 26%-50% (3), ≥51% (4).

21. Statistical analysis

Three independent experiments of each assay were conducted to validate the results. t-test was used for analysis of normally distributed, unpaired groups. Kaplan-Meier models were applied to examine survival curves of patients. Differences between the groups were analyzed using the log-rank (Mantel-Cox) test. SPSS 23 (IBM, Chicago, Illinois, USA) was used for the analysis. p values <0.05 were regarded as statistically significant (* $p < 0.05$, ** $p < 0.01$, ***$p < 0.001$).

D. Results

1. ALDH enzyme activity is primarily regulated by ALDH1A3 in human GBM cells

To investigate the critical role of ALDH1A3 in regulating TMZ resistance, CRISPR/Cas9 system was applied in LN229, U87MG and T98G cell lines to establish ALDH1A3 knockout (KO) cells. As showed in Fig. 8, ALDH1A3 single-guide RNA 2 (sgRNA 2) worked the best in all three cell lines, the protein levels of ALDH1A3 reduced dramatically to virtually undetectable levels.

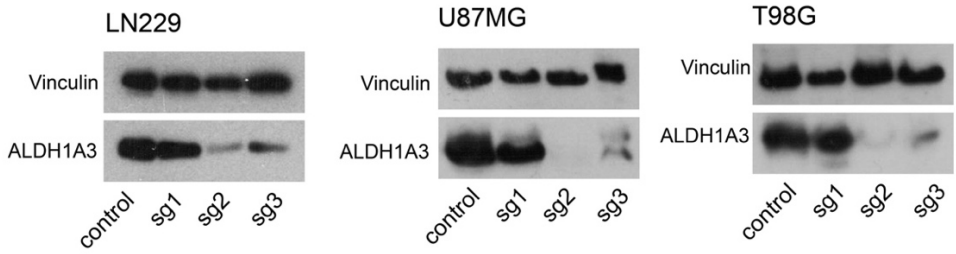

Figure 8. Western blot analysis of ALDH1A3 levels in sgRNA-transfected cells

ALDH1A3 protein levels of LN229, U87MG and T98G cell lines in all three sgRNA-transfected groups. sgRNA 2 worked the best.

Subsequently, ALDH enzyme activity was investigated by Aldefluor assay to check the effect of ALDH1A3 knockout. As expected, ALDH enzyme activities all decreased dramatically in sgRNA 2-transfected groups, which eliminated from 24.7%, 8.57%, 3.05% to 2.36%, 1.88%, 1.72% in LN229, U87MG and T98G, respectively (Fig. 9).

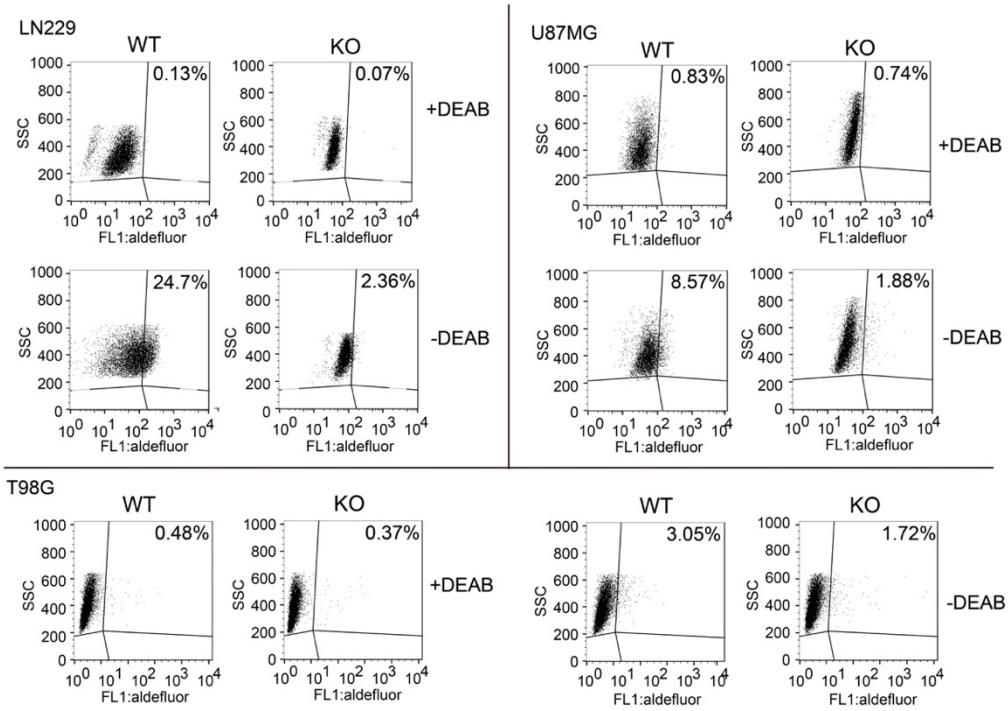

Figure 9. ALDH enzyme activity analysis of sgRNA-transfected cells

ALDH enzyme activities in 3 sgRNA-transfected LN229, U87MG and T98G cell lines. ALDH1A3 knockout leads to a significant decrease in ALDH enzyme activity.

2. ALDH1A3 knockout sensitizes glioblastoma cell lines to TMZ treatment

MTT assay was performed to explore the cytotoxicity of TMZ in ALDH1A3 wildtype (WT) and knockout (KO) cells, ALDH1A3 WT and KO cells received different dosages of TMZ treatment (100µM-500µM) for 5 consecutive days, and the metabolic activities were evaluated by MTT assay (Fig. 10). The data reveal that ALDH1A3 KO rendered GBM cells more sensitive to TMZ treatment than ALDH1A3 WT cells, and this difference was significant primarily at low dosages ≤ 300µM. The inhibition of ALDH either by KO or by DEAB caused an additional 15% - 20% reduction of cell viabilities than in WT cells at 100µM and 200µM TMZ treated groups in LN229 and U87 cells. T98G cells were not as sensitive as the other two cell lines to TMZ treatment, and ALDH1A3 KO was less effective than ALDH inhibition by DEAB, which indicated that other ALDH isoforms might play a role in TMZ response of T98G cells and the function is independent

of the enzyme function measured by Aldefluor. Surprisingly, the difference was diminished between WT and KO or DEAB with high concentration TMZ treatment in every cell line.

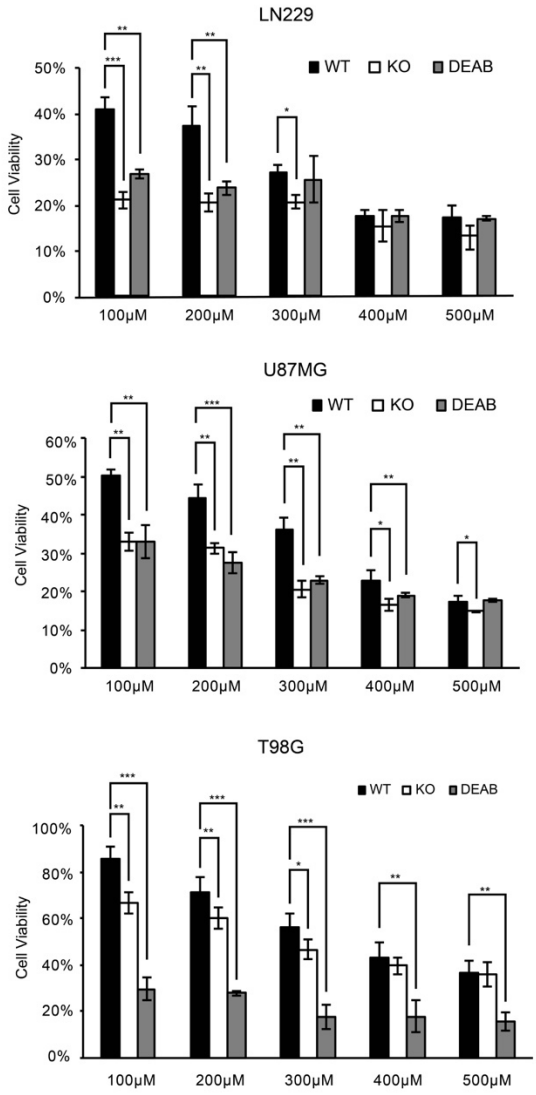

Figure 10. MTT analysis of ALDH1A3 inhibited or depleted GBM cell lines after TMZ treatment

Glioblastoma cells received TMZ treatment for 5 days. ALDH1 inhibited or ALDH1A3 depleted cells were more fragile to TMZ treatment than ALDH1A3 WT cells. Three independent experiments were conducted. Each bar indicates the mean ± SD. *, $P < 0.05$; **, $P < 0.01$;***, $P < 0.001$. (WT– wild-type, KO- knockout, WT DEAB – chemical inhibition by DEAB)

These results were in line with the results of the clonogenic assay. There were no colonies visible of LN229 ALDH1A3 KO cells even in 10μM TMZ treated-group . For U87 cells, ALDH1A3

blockage led to a dramatical decrease of colonies at 10µM TMZ. In T98G cells, ALDH1A3 inhibition resulted in less colony formation with 300µM TMZ treatment (Fig. 11).

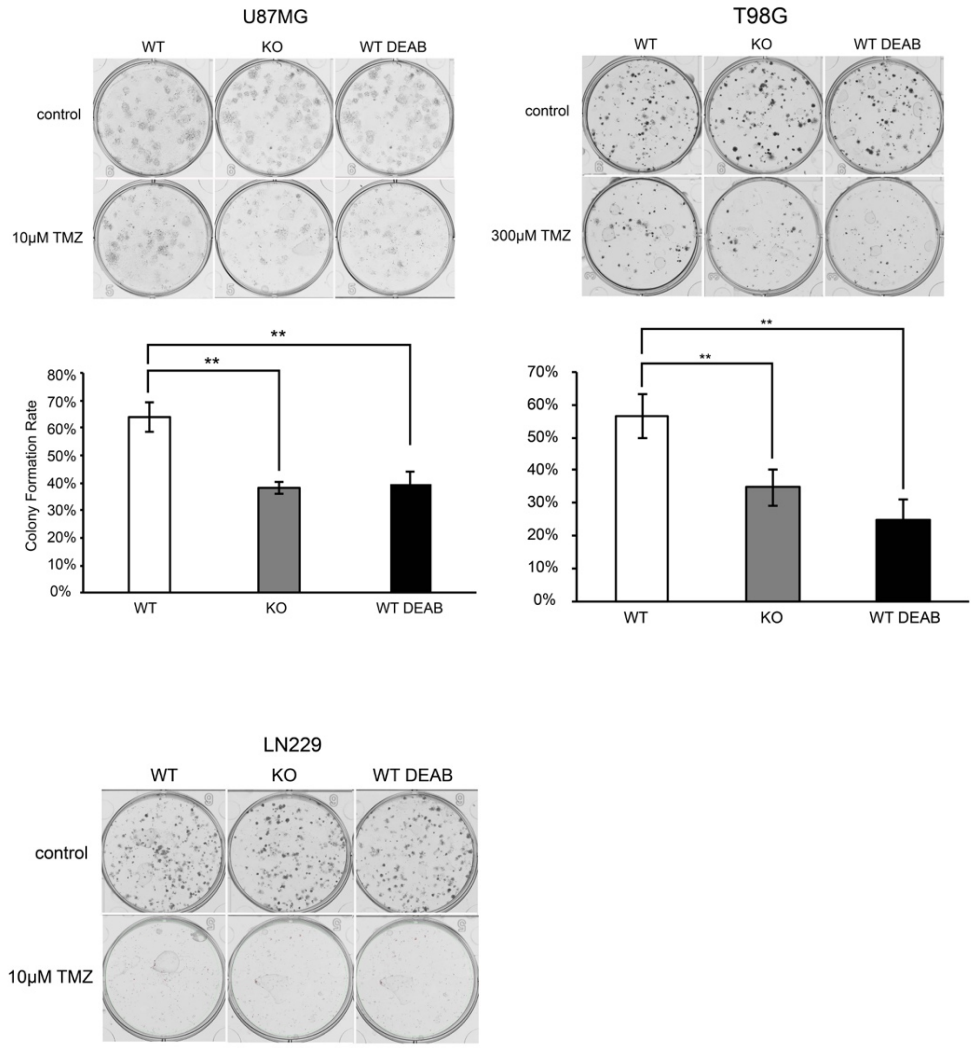

Figure 11. Colony formation assay of LN229, U87MG and T98G cell lines

Colony formation assays demonstrated a more significant reduction of clonogenic ability in DEAB treated and ALDH1A3 KO groups after TMZ treatment, at 10µM TMZ in U87 and at 300µM in T98G cell lines. There were no colonies visible of LN229 cell lines even in 10µM TMZ treated-group.

Additionally, we treated two stem-like glioma cell lines X01 and T84 with the same condition as described above. Similarly, the inhibition with DEAB resulted in a more dramatic reduction of cell viabilities at 100µM (59% to 40% in X01, 47% to 27% in T84) and 200µM (46% to 35% in X01, 32% to 22% in T84) (Fig. 12A). Sphere forming assay also showed a more significant

decrease of spheres when ALDH was inhibited by DEAB in both stem-like glioma cells (Fig. 12B).

These results illustrate that the blockage of ALDH1A3 renders the cells more sensitive to TMZ, especially at low dosages.

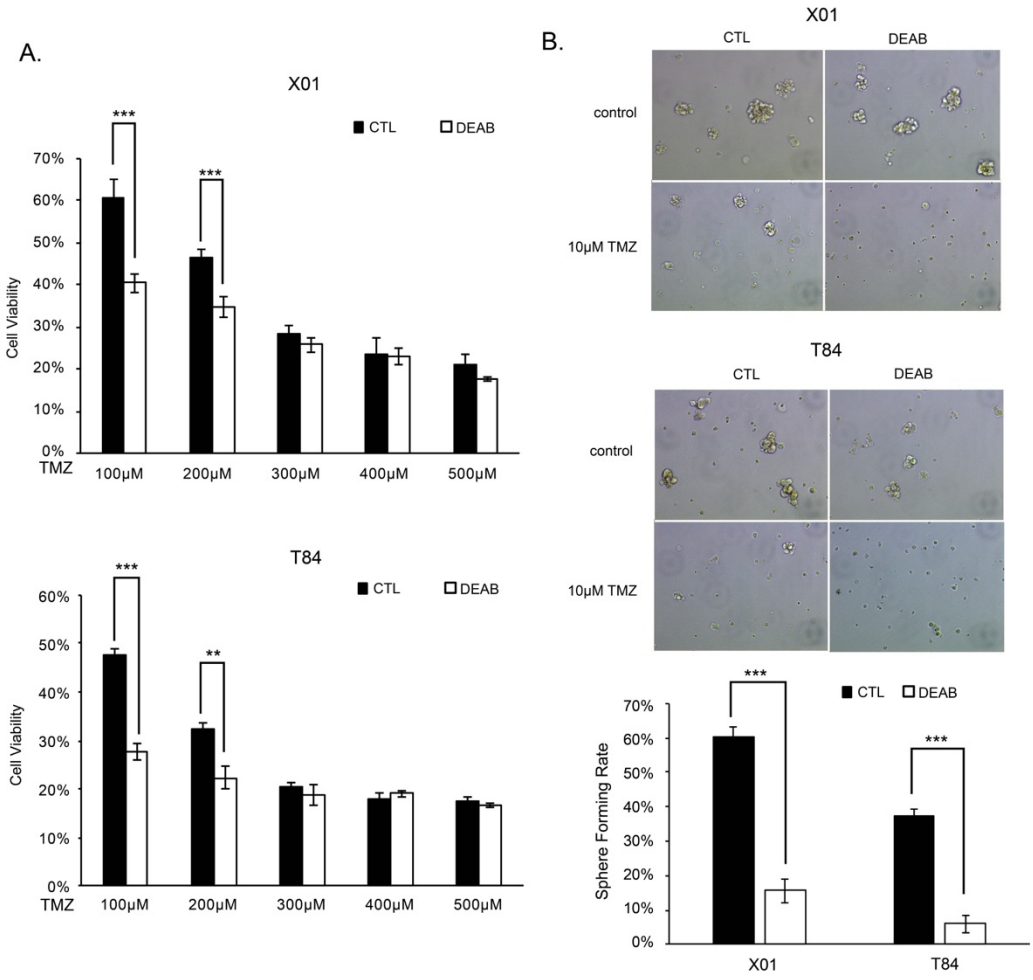

Figure 12. Clonogenic assay of X01 and T84 cells

A. MTT assay analysis of XO1 and T84 cells. ALDH1 inhibition by DEAB resulted in a more dramatic decline of survival rates at low dosages (100-200μM TMZ). B. Sphere formation assay illustrated a significant decrease of sphere formation ability in TMZ treated group, the effects were more dramatic when received combine treatment with DEAB.

3. TMZ treatment results in a significant decline of ALDH1A3 and an increase of autophagy

ALDH1A3 KO GBM cell lines are more sensitive than WT cells to TMZ treatment, and this difference is significant especially at dosages ≤ 300µM, but the effects mostly abrogates when the cells receive 500µM TMZ treatment. Thus immunoblotting was performed to explore ALDH1A3 protein expression in each glioblastoma cell line. After 5 days treatment with TMZ, the cells were collected for protein lysis. Interestingly, protein expression of ALDH1A3 reduced dose-dependently after TMZ treatment (Fig. 13). This could explain that why ALDH1A3 WT cells didn´t show more resistance than KO cells at 500µM TMZ. Furthermore, the markers of autophagy LC3 and SQSTM1/p62 have been investigated (Mizushima et al., 2010, Klionsky et al., 2016). LC3-II was up-regulated and p62 protein was down-regulated in all three cell lines (Fig. 13), which indicates that autophagy has been activated after TMZ treatment. Besides, LC3-II expressed higher levels in ALDH1A3 KO cells, which indicates autophagy can be induced by TMZ treatment, especially in ALDH1A3 depletion cells.

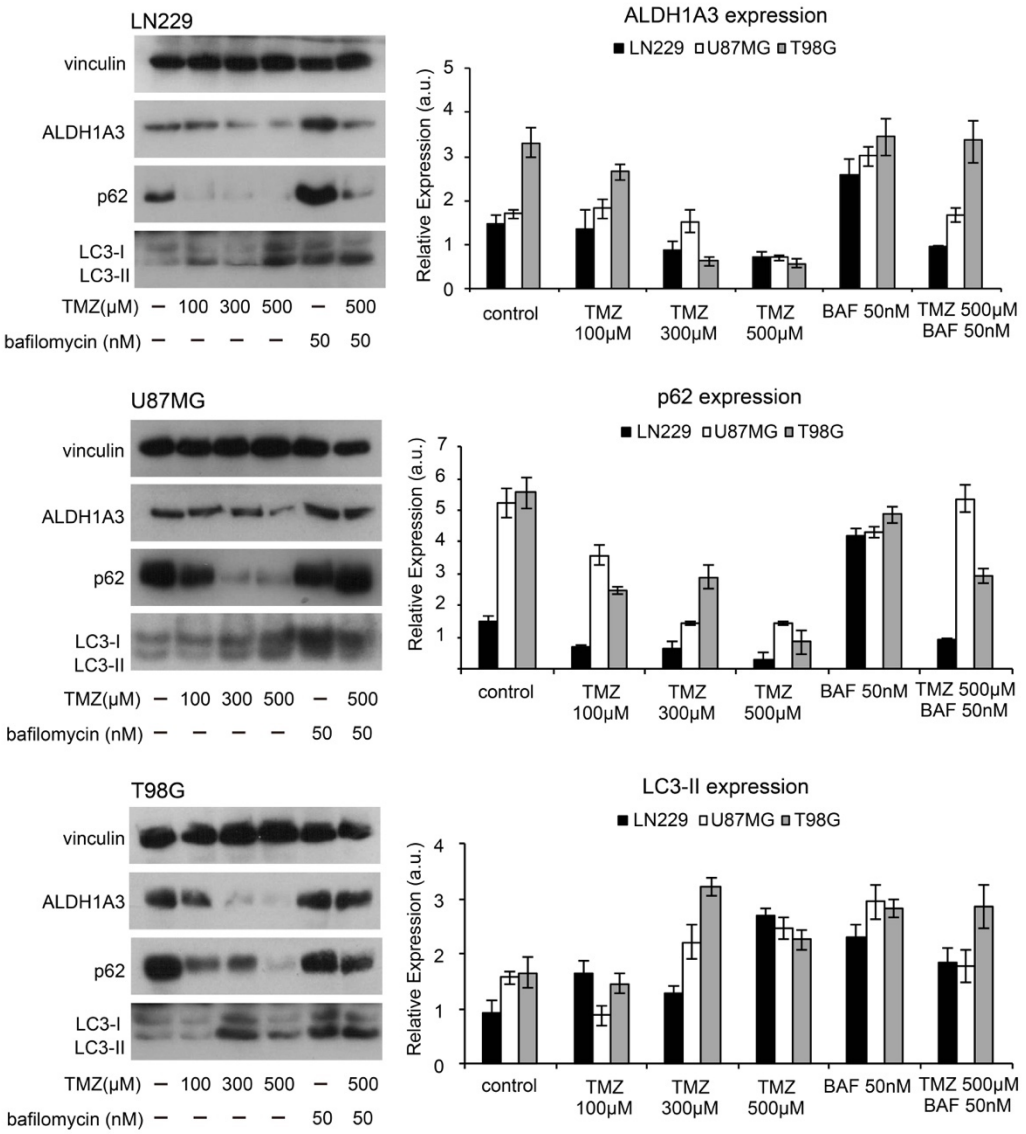

Figure 13. Immunoblotting of ALDH1A3, LC3 and SQSTM1/p62 in established cell lines

U87MG, LN229 and T98G cell lines were treated with or without TMZ and /or bafilomycin. The results showed that p62 was greatly downregulated while LC3-II increased generally. Density analysis results from each concentration in Immunoblotting. a.u. stands for arbitrary units.

In order to investigate whether the phenomenon is only applicable to established cells lines, stem-like primary glioma cells were also checked for ALDH1A3 expression under serum-free circumstances (Fig. 14). As in established cell lines, ALDH1A3 and p62 were greatly downregulated while LC3-II increased generally. Besides, ALDH1A3 KO cells have higher LC3-II expression than WT cells, which indicates that TMZ treatment induced autophagy and

reduced the protein expression of ALDH1A3. The autophagy inhibitor bafilomycin was also used to validate the involvement of ALDH1A3 in autophagy after TMZ treatment. Interestingly, the co-treatment of TMZ with bafilomycin enables the recovery of protein expressions of both ALDH1A3 and p62 from established cell lines and stem-like primary glioma cells, which demonstrates the possible involvement of ALDH1A3 in autophagy.

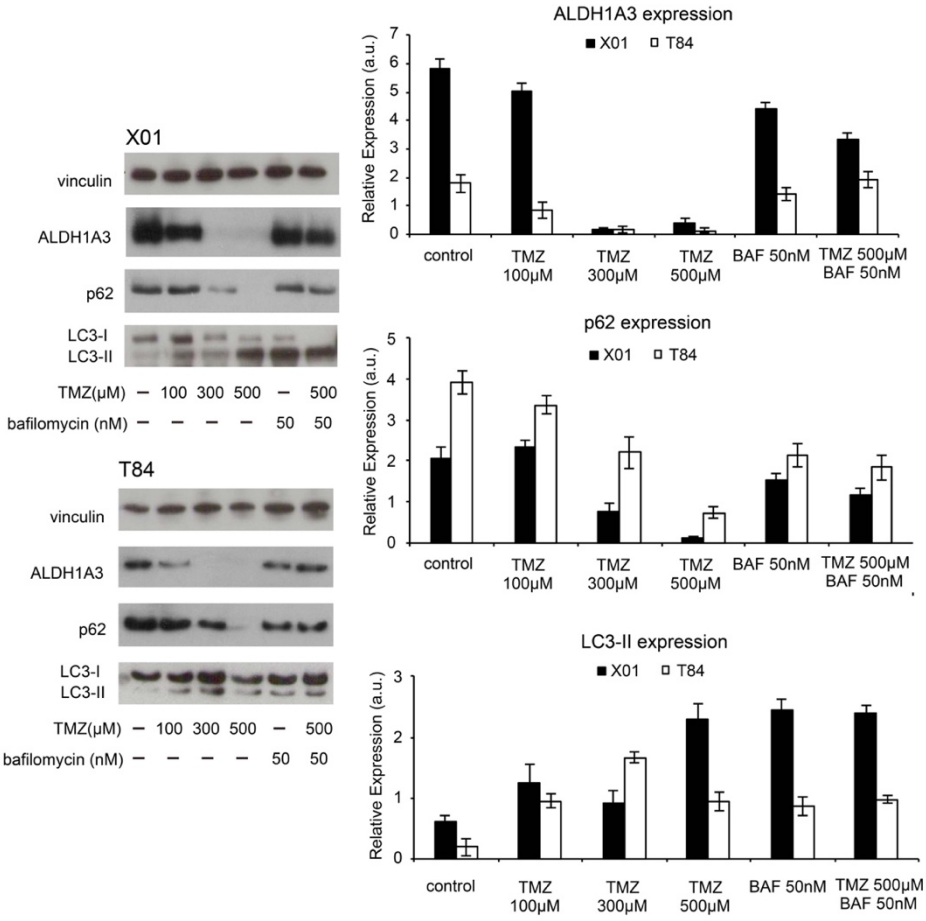

Figure 14. Immunoblotting of ALDH1A3, LC3 and SQSTM1/p62 in stem-like primary glioma cells

The stem-like primary glioma cells X01 and T84 cells were treated with or without TMZ and /or bafilomycin. The results showed that p62 was greatly downregulated while LC3-II increased generally. Density analysis results from each concentration in Immunoblotting. a.u. stands for arbitrary units.

In order to explore the involvement of ALDH1A3 in the process of autophagy, GFP-LC3 has been transfected into the established cell lines to enable LC3 protein expression visible (Fig. 15). A significant increase of GFP-positive puncta was observed in both ALDH1A3 WT and KO

cells at TMZ treated groups, which indicates that TMZ treatment induced more autophagic flux.

Furthermore, more puncta were observed in ALDH1A3 KO glioblastoma cells than WT cells (Fig. 15), which is consistent with the results of western blot, LC3-II protein expression in ALDH1A3 KO cells was higher than WT cells (Fig. 16).

The western blot analysis and GFP-LC3 transfection indicate that TMZ treatment induces autophagy and diminishes ALDH1A3.

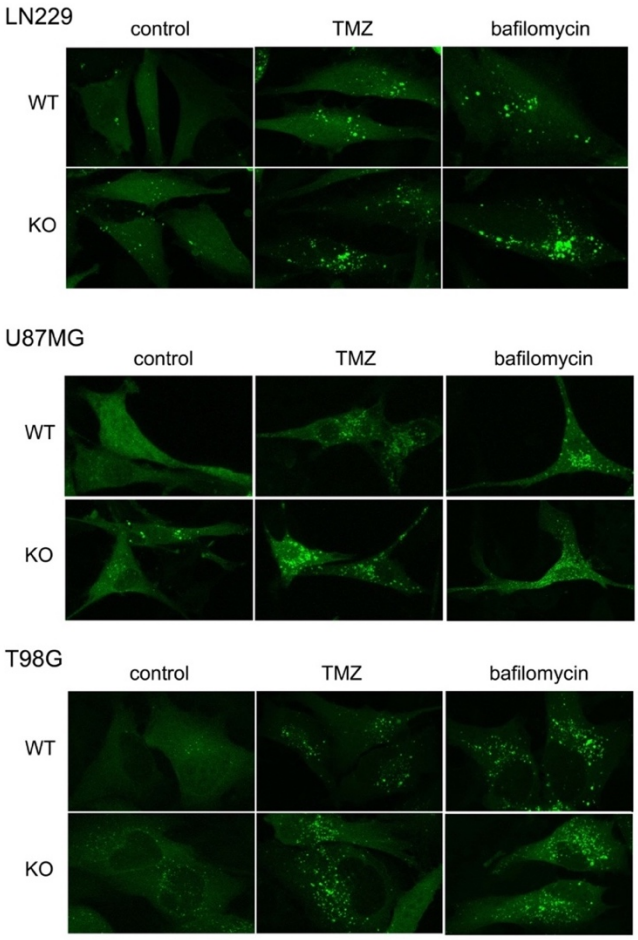

Figure 15. GFP-LC3 transfection in glioblastoma cell lines.

All three cell lines were transfected with EGFP-LC3 vector and received treatment of 300μM TMZ for 5 consecutive days or 50nM bafilomycin for 6 hours. The number of LC3 puncta increased in all TMZ treated groups, implying the enhancement of autophagy after TMZ treatment.

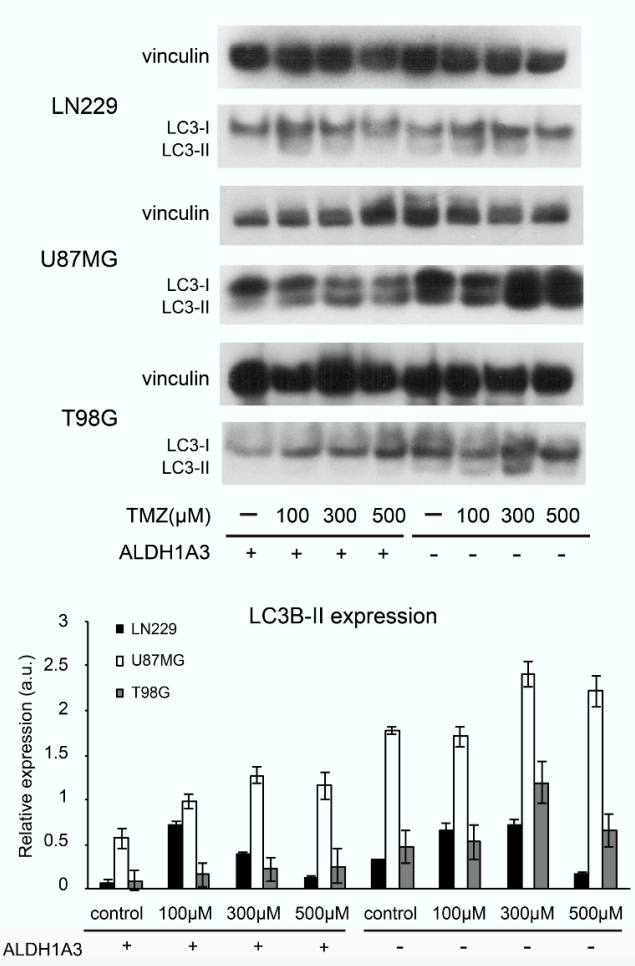

Figure 16. Immunoblotting of LC3 in GBM ALDH1A3 WT and KO cell lines.

LC3-II protein expression in ALDH1A3 KO cells was higher than WT cells.

Aldefluor assay was used to explore the ALDH enzyme activity, a down-regulation of ALDH enzyme activity was observed when cells received TMZ treats alone, and this reduction can be restored with the addition of bafilomycin (Fig. 17).

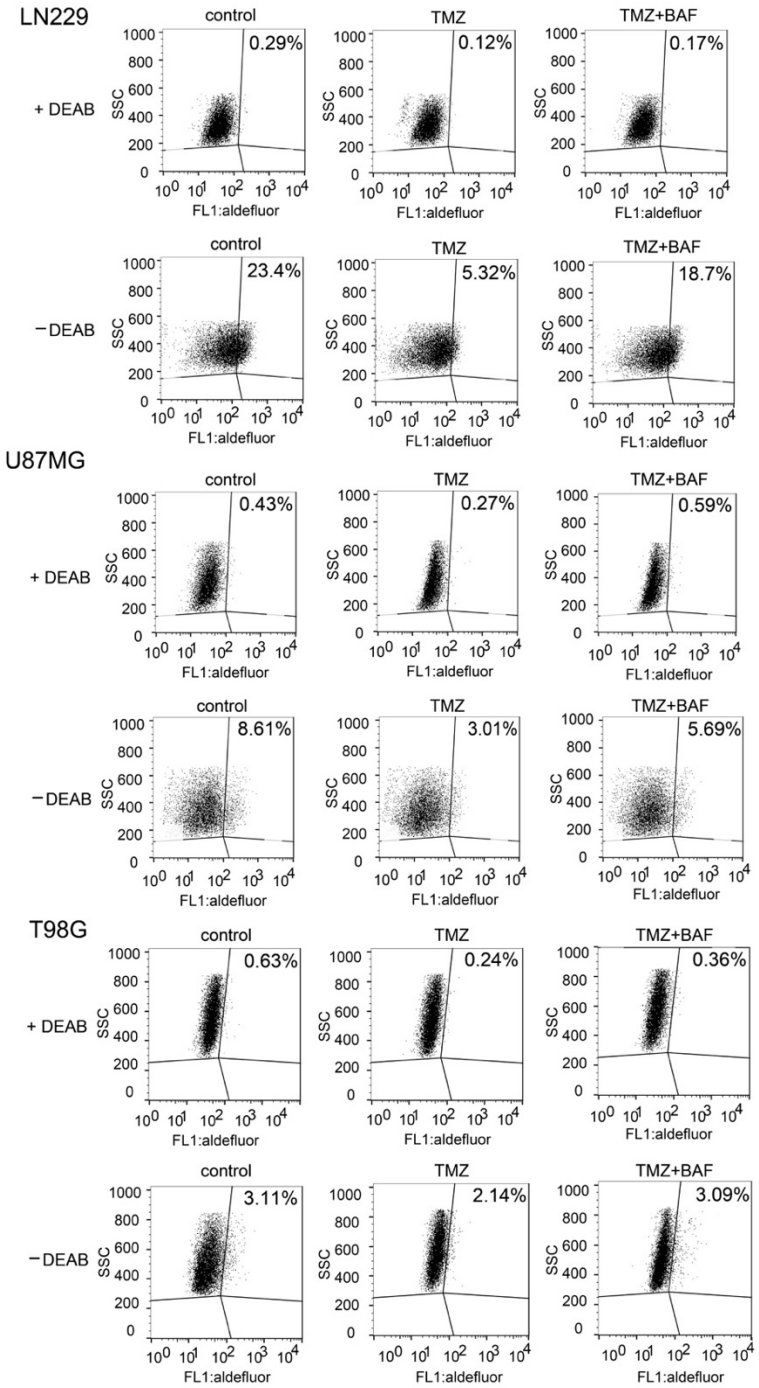

Figure 17. ALDH enzyme activity analysis after TMZ and bafilomycin treatment.

LN229, U87MG and T98G cells received 500µM TMZ treatment with/without 10nM bafilomycin for 5 consecutive days. ALDH activity decreased dramatically after TMZ treatment but partially recovered after co-treatment with bafilomycin.

4. The decline of ALDH1A3 is regulated by autophagy under TMZ treatment

As showed in the data above, both protein levels and enzyme activities of ALDH1A3 were dramatically down-regulated after TMZ treatment in all three GBM cell lines. Next, it is important to investigate that whether the down-regulation of ALDH1A3 is transcriptionally regulated. Quantitative RT-PCR was employed to explore mRNA expression of ALDH1A3, however, the change of ALDH1A3 mRNA expression was undetectable even at 500μM TMZ (Fig. 18).

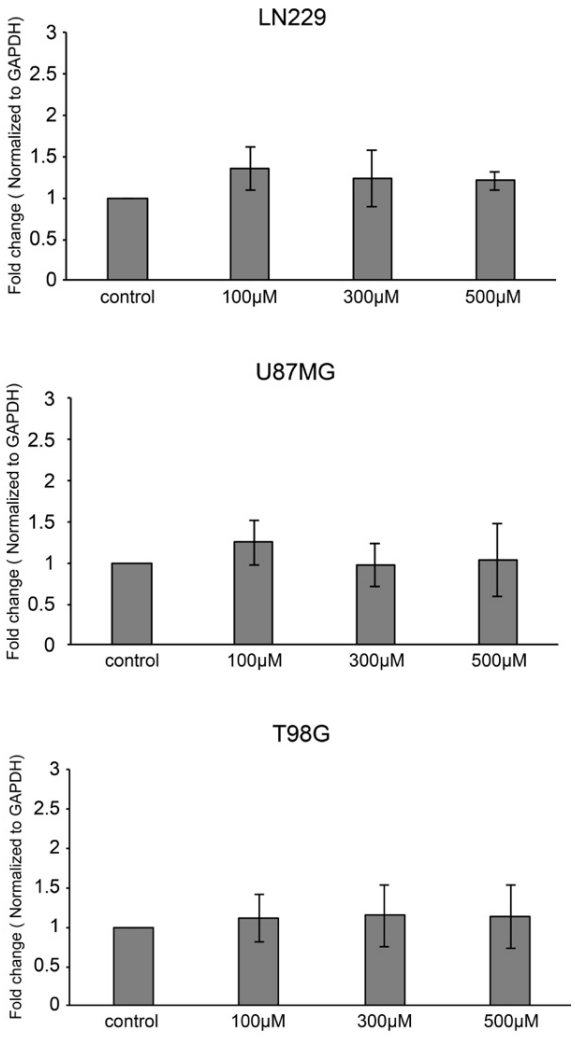

Figure 18. Quantitative RT-PCR analysis of ALDH1A3 in GBM cell lines

No significant change was observed in all three cell lines after TMZ treatment.

Since the downregulation of ALDH1A3 seems to be post-transcriptional, autophagy could be responsible for the decrease of ALDH1A3. Thus, the cells were treated with an autophagy activator (rapamycin) and an autophagy inhibitor (bafilomycin) (Fig. 19). The accumulation of LC3-II and p62 has been observed after inhibiting the fusion of autophagosomes and lysosomes by bafilomycin. The autophagy activator rapamycin simulated autophagy, which reflected by the degradation of p62. As expected, autophagy inhibitor bafilomycin treatment led to ALDH1A3 accumulation while autophagy activator rapamycin decreased ALDH1A3 expression. Co-treatment of bafilomycin and rapamycin reflected a counteractant effect in ALDH1A3 expression.

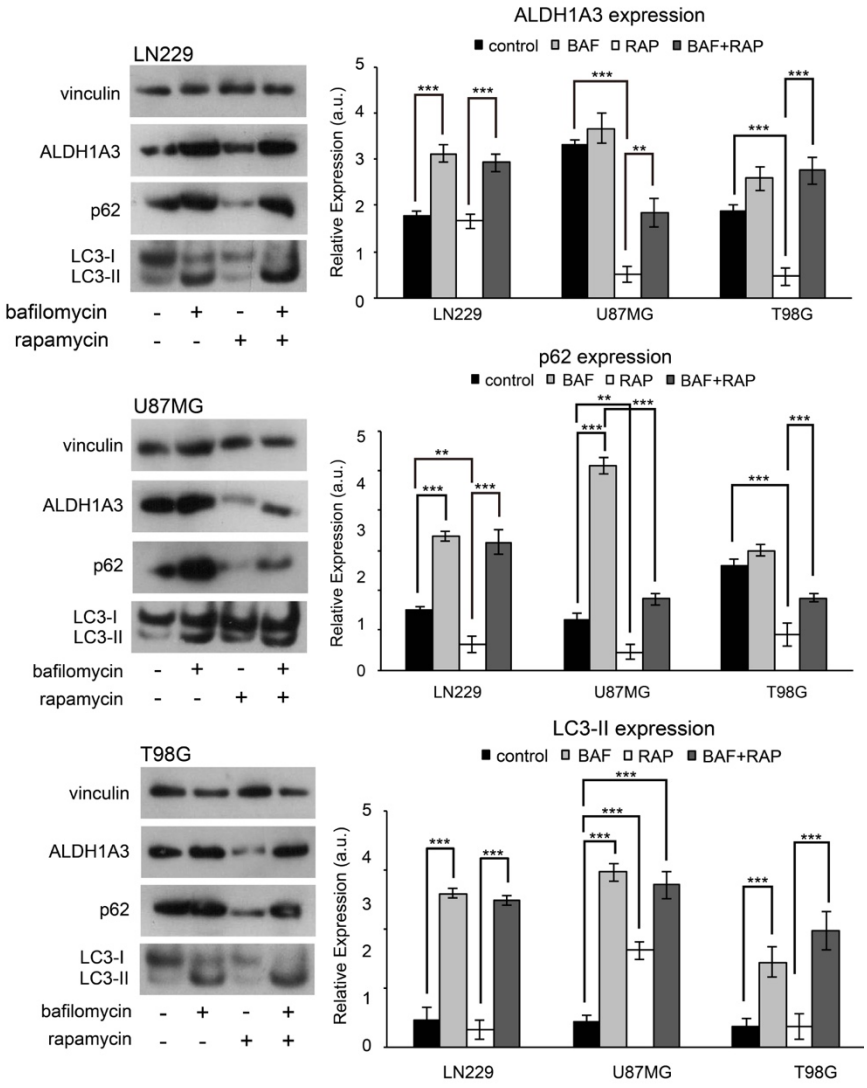

Figure 19. Immunoblotting of ALDH1A3, LC3 and SQSTM1/p62 in GBM cell lines

The cells received 100nM rapamycin treatment for 3 hours or 50nM Bafilomycin treatment for 6 hours.

Bafilomycin up-regulated ALDH1A3 expression while rapamycin down-regulated ALDH1A3 expression.

The same phenomenon was also detected with chloroquine (Fig. 20). Overall, these data suggest that ALDH1A3 seems to be recruited to the membranes of autophagosomes and involved in the process of autophagy.

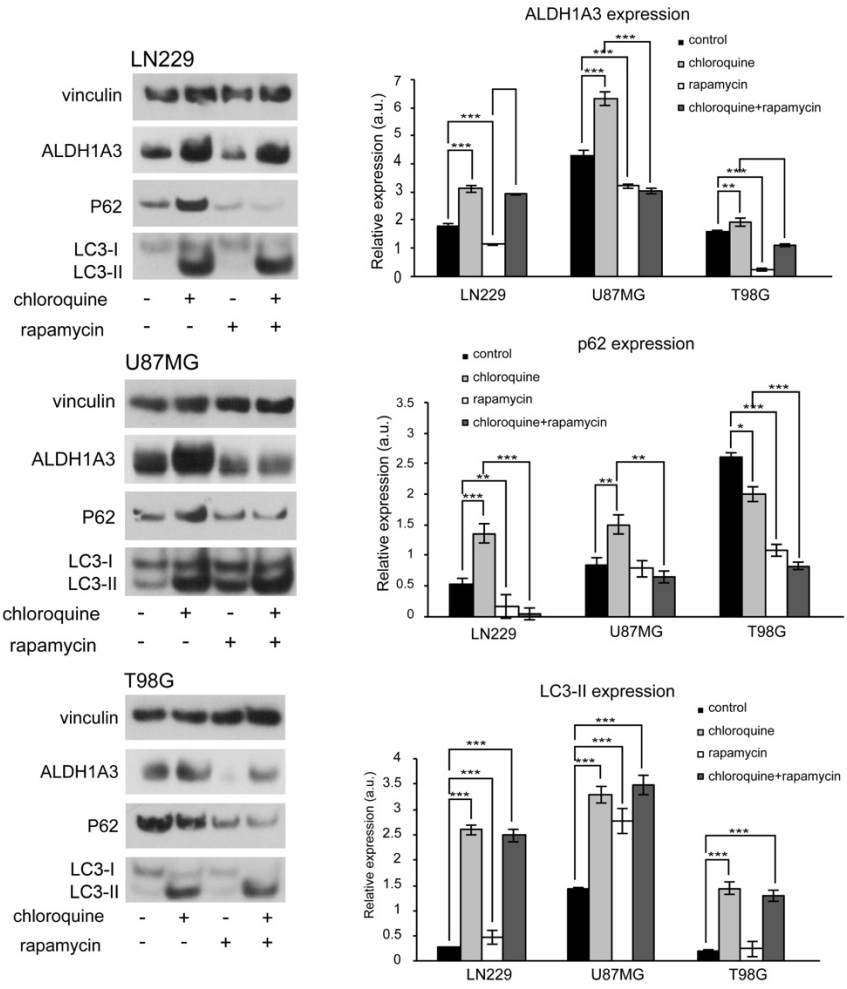

Figure 20. Immunoblotting of ALDH1A3, LC3 and SQSTM1/p62 in GBM cells lines

Chloroquine induced the accumulation of ALDH1A3, rapamycin stimulated ALDH1A3 degradation.

Subsequently, proximity ligation assay was performed to investigate the physical interaction between ALDH1A3 and p62 (Fig. 21). The red dots represent the direct interaction between these two proteins. More red dots were observed in bafilomycin treated groups, which

indicates that ALDH1A3 might accumulate in autophagosomes, since bafilomycin inhibits the fusion with lysosomes.

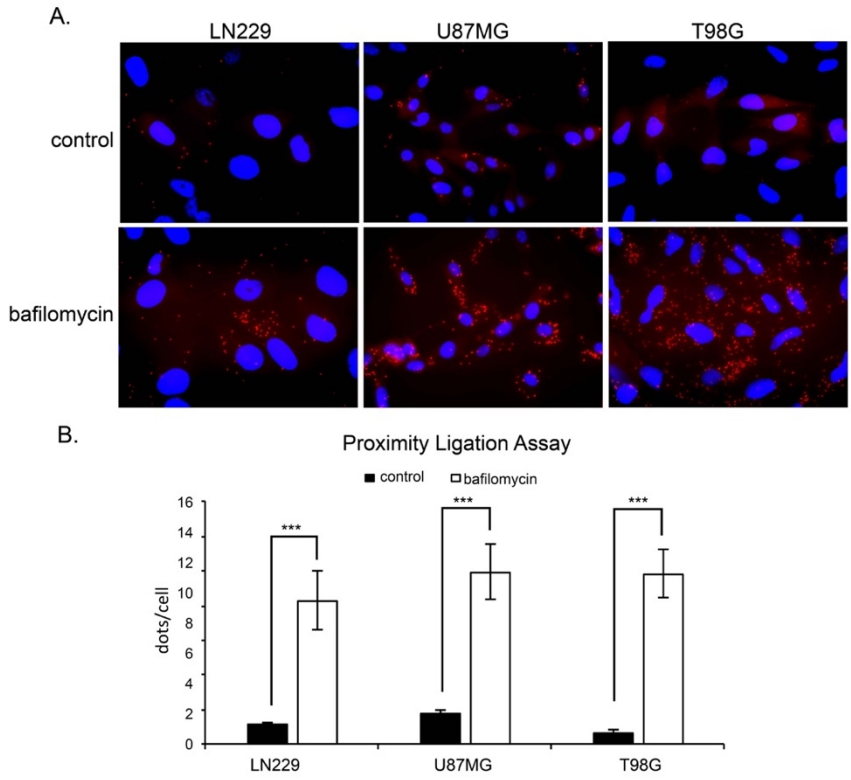

Figure 21. PLA of ALDH1A3 and p62 in GBM cell lines

The cells were incubated with 50nM Bafilomycin for 6 hours. ALDH1A3 and p62 interaction were observed in all three cell lines, especially in bafilomycin-treated groups.

These results were consistent with the results of Co-IP (Fig. 22). p62 protein has been pulled down with anti-p62 antibody. Normal IgG was applied as a negative control. Then, ALDH1A3 antibody was used to detect the physical interaction of two proteins. The presence of ALDH1A3 was observed in p62 protein fraction, and an up-regulation of p62 and ALDH1A3 proteins was observed after the inhibition of autophagy by chloroquine. These results suggest a direct physical interaction between p62 and ALDH1A3, which could explain the ALDH1A3 elimination after chemotherapy with TMZ.

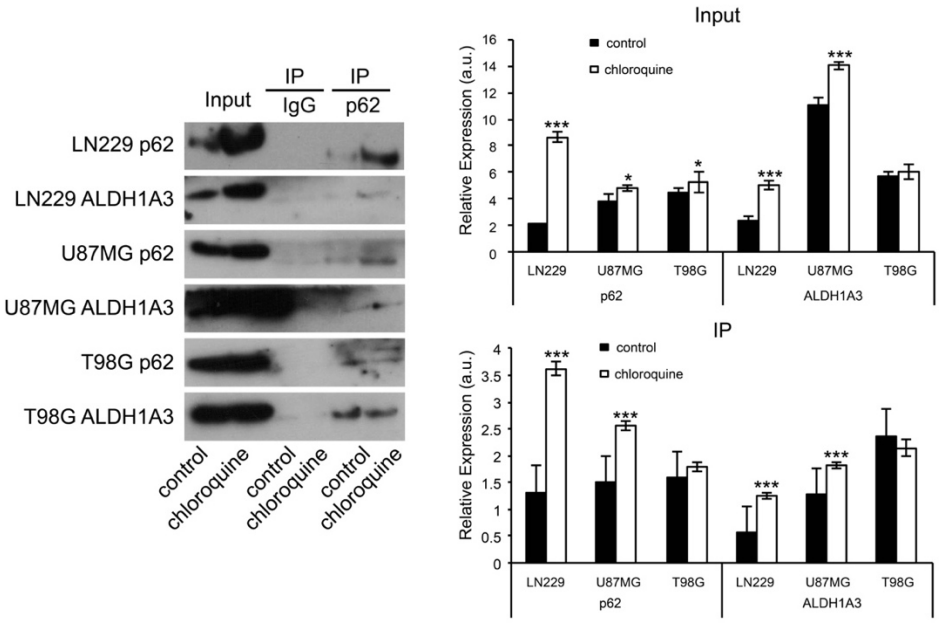

Figure 22. Co-IP of ALDH1A3 and p62.

The cells were treated with 50μM Chloroquine for 3 hours. ALDH1A3 was detected in p62 protein fractions, especially when autophagy has been inhibited by chloroquine.

5. ALDH1A3 KO renders the glioblastoma cell lines more sensitive to TMZ but the difference can be eliminated by scavenging oxidative stress products

TMZ, an alkylating chemotherapeutic agent, causes the double-strand breaks (DSBs) of DNA, decreases the survival rate of the tumor cells and thus prolongs the overall survival of patients with GBM. However, some other mechanisms also have been suggested. TMZ administration results in an imbalance of reactive oxygen species. Oxidative stress could also be one of the most critical mechanisms which leads to cell death. So oxidative scavenger NAC was applied together with TMZ to investigate the cell survival rate. Following treatment with different dosages of TMZ (100μM-500μM) either alone or with NAC for 5 consecutive days, the survival rates of ALDH1A3 WT and KO cells were measured by MTT assay (Fig.23).

ALDH1A3 depletion resulted in a more significant reduction of cell survival in the 100μM and 300μM TMZ treated groups in all three cell lines. The addition of NAC neutralized the effect

of TMZ and eliminated the difference between ALDH1A3 WT and KO cells (100µM TMZ, approx. 50% WT vs 30% KO to 80% in both LN229 WT and KO cells, approx. 55% WT vs 40% KO to 80% in both U87MG WT and KO cells. 300µM TMZ, approx. 40% WT vs 30% KO to 60% in both LN229 WT and KO cells, approx. 35% vs 20% to 70% in both U87MG WT and KO cells). T98G cells were more robust against TMZ treatment. The addition of NAC enhanced the survival rate to approx. 80%-90% with ≤ 300µM and approx. 70% with 500µM TMZ treatment. These data illustrate that ALDH1A3 depletion renders the glioblastoma cells more sensitive to TMZ, but the difference can be abolished with the addition of NAC and at high TMZ concentrations.

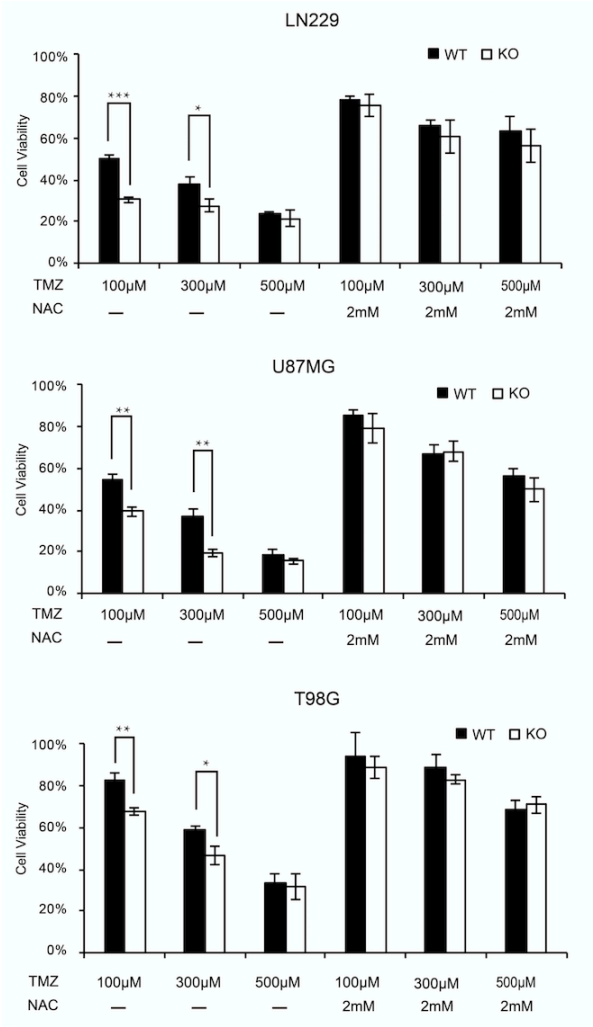

Figure 23. MTT assay of GBM cell lines after either TMZ treatment alone or with NAC.

Survival rate was significantly reduced in ALDH1A3 KO groups compared with ALDH1A3 WT groups , which can be neutralized by the addition of NAC.

The results were consistent with the results of cell cycle analysis (Fig.24). More pronounced G_2/M arrest was observed in ALDH1A3 KO cells compared with WT cells in all three cell lines. The addition of NAC was able to neutralize the difference between ALDH1A3 WT and KO cells (LN229: 36.6% WT vs 47.5% KO to approx. 27% both in WT and KO cells. U87MG: 38.8% WT vs 49% KO to approx.30% in both WT and KO cells. T98G: 12% WT vs 13.9% KO to approx. 10% in both WT and KO cells).

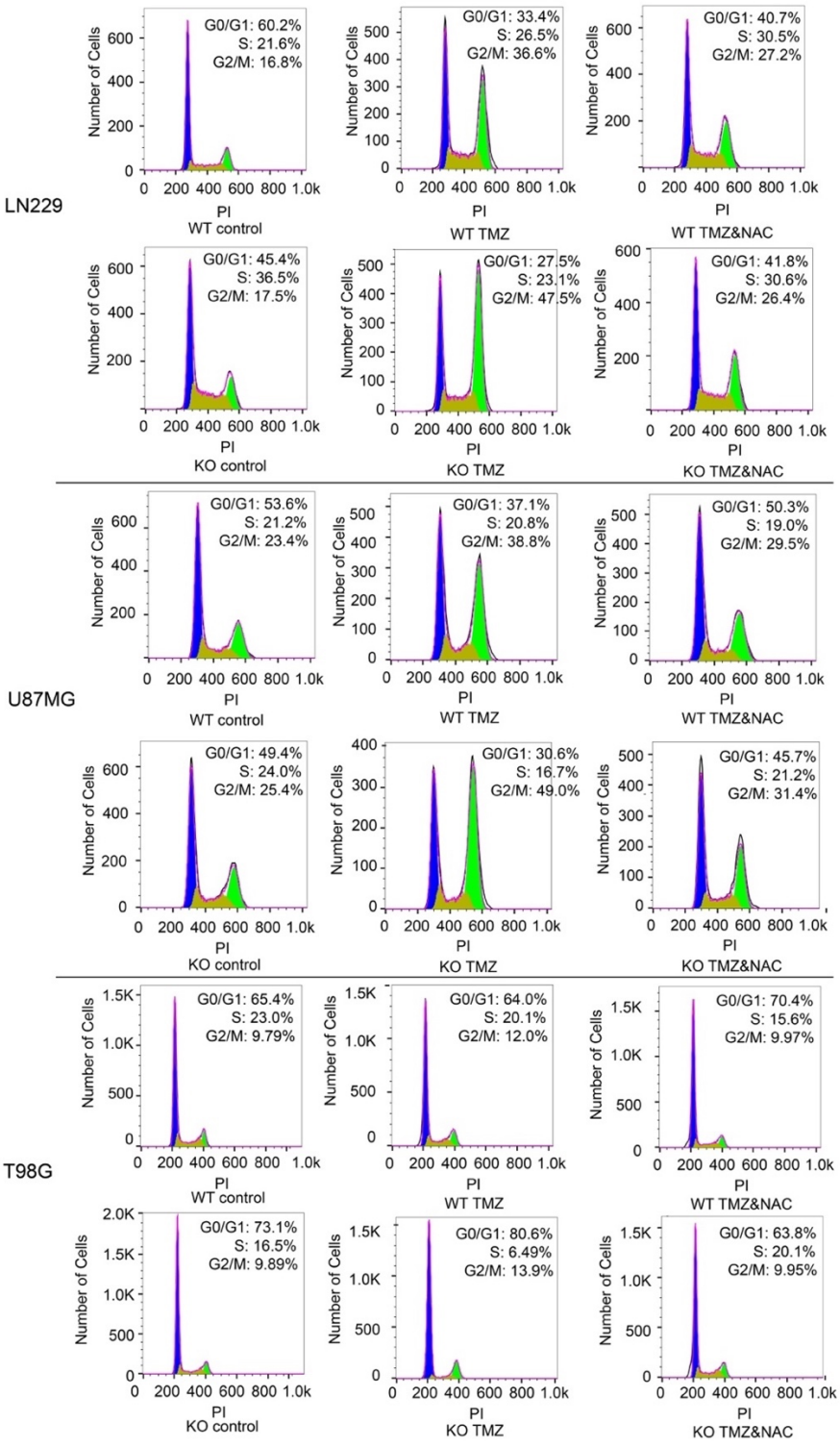

Figure 24. Cell cycle analysis of GBM cell lines after either TMZ treatment alone or with NAC

Flow cytometry histograms of LN229, U87MG and T98G cell lines, respectively. 300μM TMZ treatment caused dramatic G_2/M cell cycle arrest in both ALDH1A3 WT cells and KO cells, and the effect was more

pronounced in KO cells. The addition of NAC rescued the cell cycle arrest and diminished the difference between ALDH1A3 WT and KO cells.

6. ALDH1A3 KO cells are more sensitive to TMZ due to higher levels of toxic aldehydes but the difference can be eliminated by scavenging oxidative stress products

OxiSelect™ ROS/RNS Assay and Lipid Peroxidation (MDA) Assay were used to detect the amount of free radical molecules and MDA production in cells, separately. DCFH-oxidation increased under TMZ treatment in a dose-dependent manner, but no differences between ALDH1A3 WT and KO cells were visible (Fig. 25). TMZ induced an increase in the levels of the cytotoxic aldehyde MDA, which produced by lipid peroxidation. Interestingly, MDA levels were significantly higher in ALDH1A3 KO cells than WT cells, which indicates that ALDH1A3 might be effective in detoxifying of the end products of lipid peroxidation. The effect abrogated at 500µM TMZ. NAC co-treatment dramatically reduced the production of MDA to control levels in both WT and KO cells.

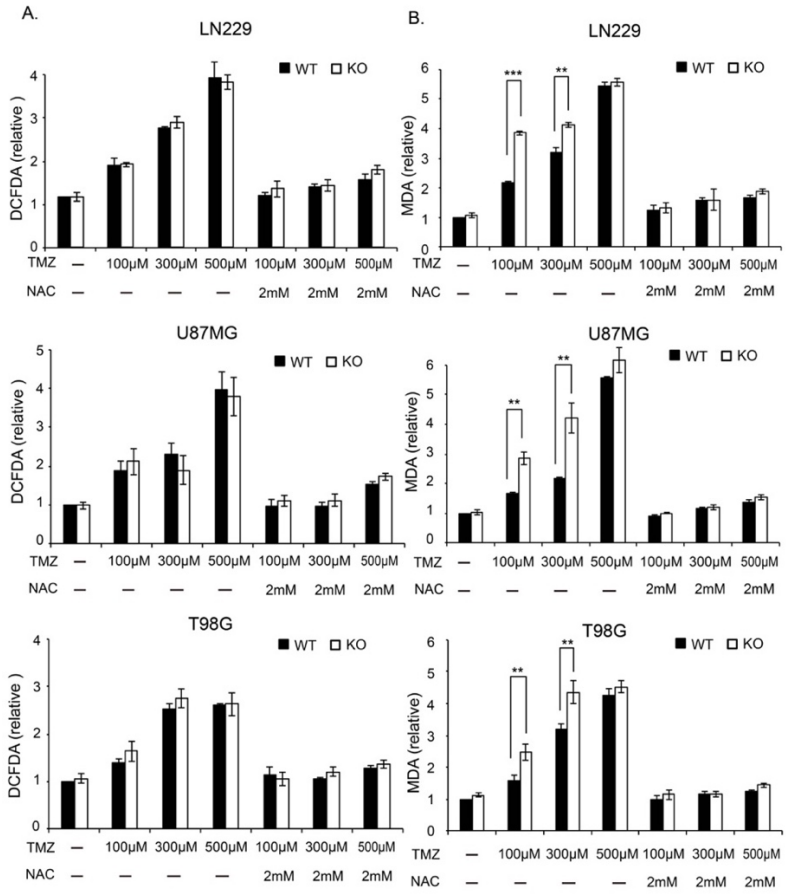

Figure 25. Oxidative stress and lipid peroxidation investigation after TMZ treatment

Quantitative results of ROS/RNS Assay and Lipid Peroxidation (MDA) Assay in LN229, U87MG and T98G cells, respectively. Significant increase of ROS production and MDA content was observed in all three cell lines. No difference of ROS (A) and significant difference of MDA (B) were observed between ALDH1A3 WT and KO cells, which can be eliminated by the addition of NAC.

HNE (4-hydroxynonenal) is a stable product of lipid peroxidation and contributes to the cytotoxic effects of oxidative stress. By Western blot analysis using an anti-HNE antibody, which is able to specifically bind to HNE modified proteins, the presence of HNE has been investigated after TMZ treatment. In line with Lipid Peroxidation (MDA) Assay, the amount of HNE-modified proteins in ALDH1A3 KO cells is much higher than in WT cells, which further verifies the detoxifying role of ALDH1A3 (Fig. 26).

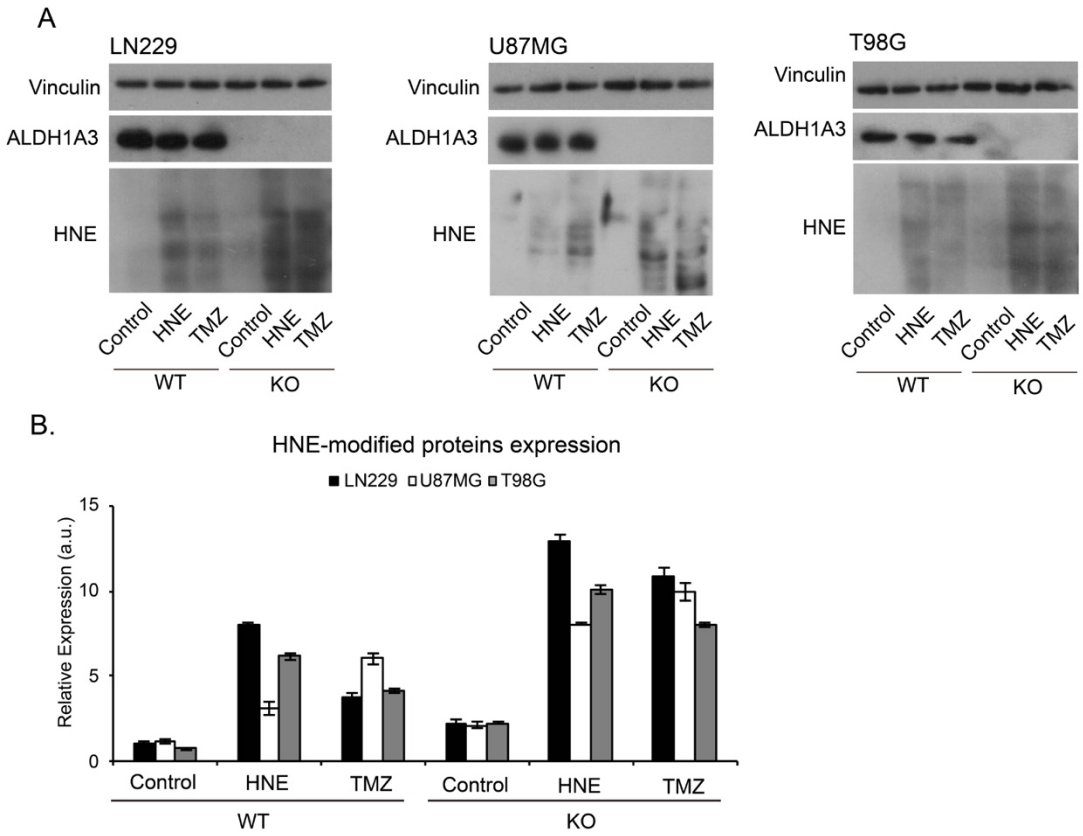

Figure 26. Western blot analysis of HNE-modified proteins after TMZ treatment

A. The cells were treated with 100μM TMZ for 5 days. The protein was isolated at 30 minutes after the last day treatment. 30μM HNE treatment for 1 hour was served as a positive control. More HNE-modified protein was observed in ALDH1A3 KO groups than WT groups. B. Quantitative results of western blot analysis.

These results indicate that the cytotoxicity of TMZ may partly due to oxidative stress. ALDH1A3 plays a key role in detoxifying active aldehydes derived from lipid peroxidation which induced by oxidative stress. This could be the reason for the resistance of ALDH1A3 WT cells to TMZ treatment.

7. Oxidative stress might be the reason for TMZ-induced autophagy and ALDH1A3 degradation

ALDH1A3 decreases in a dose-dependent manner when received TMZ treatment, and autophagy is responsible for the degradation of ALDH1A3. However, it is still unknown why ALDH1A3 recruits to autophagosome after TMZ treatment. Since oxidative stress scavenger NAC is able to increase the survival rate of GBM cells and eliminate the difference between ALDH1A3 WT and KO cells, autophagy and ALDH1A3 expression have been investigated after the addition of NAC. Interestingly, p62 levels increased while LC3-II decreased after the co-treatment with NAC, which indicates the switch off of the process of autophagy. Moreover, ALDH1A3 levels significantly recovered by NAC treatment (Fig. 27).

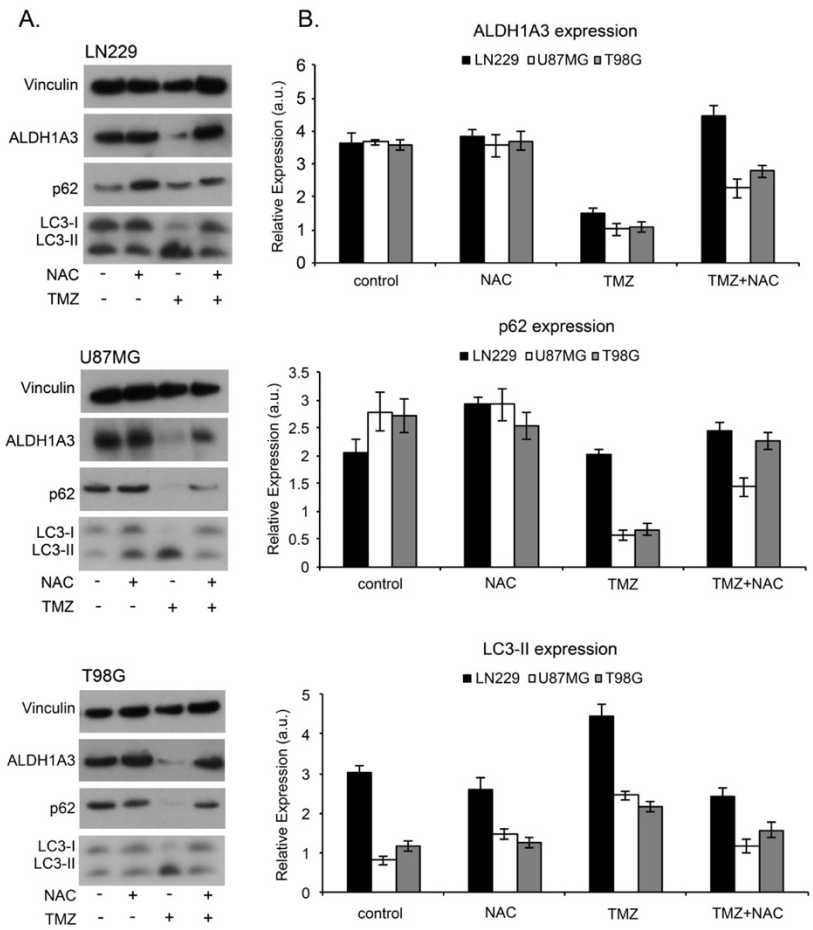

Figure 27. Western blot analysis of ALDH1A3 and autophagy markers after TMZ and/or NAC treatment

The cells were treated with either 500µM TMZ or 2mM NAC or in combination for 5 days. Down-regulation of ALDH1A3 protein expression, up-regulation of LC3-II and down-regulation of p62 were observed in all 3 cell lines after TMZ treatment, but can be recovered by the co-treatment of NAC.

Aldefluor assay was conducted to investigate ALDH1 enzyme activities after the scavenging of oxidative stress. ALDH enzyme activity dramatically decreased after TMZ treatment alone, but the effect can be recovered by the addition of NAC (Fig. 28).

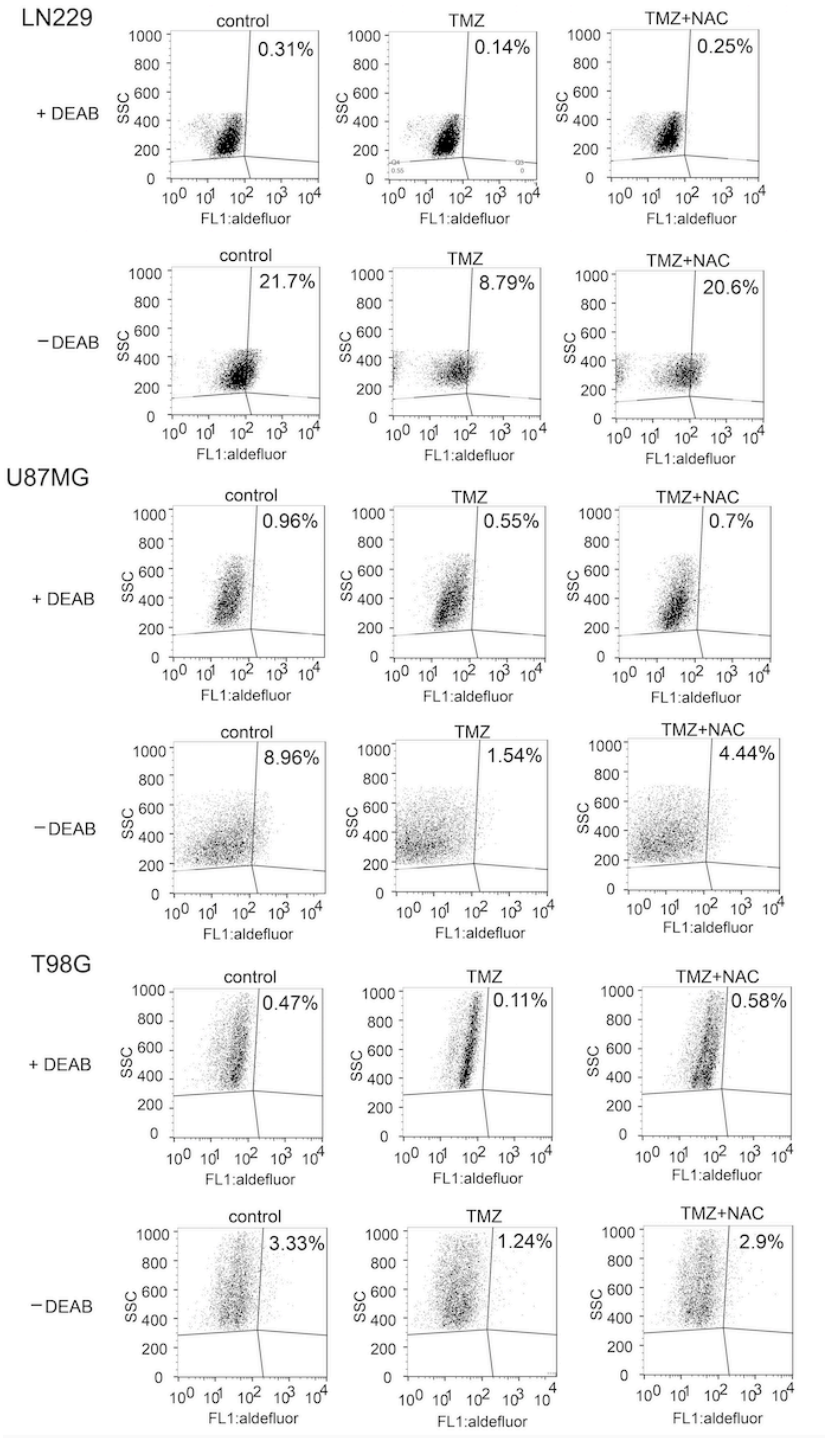

Figure 28. Aldefluor analysis of GBM cell lines after either TMZ treatment alone or with NAC

The cells were treated with either 300µM TMZ or 2mM NAC or in combination for 5 days. ALDH enzyme activities reduced after TMZ treatment but can get recover with the addition of NAC.

8. TMZ-induced lipid peroxidation leads to autophagy and ALDH1A3 degradation

Next, it is interesting to know how oxidative stress induces autophagy and ALDH1A3 degradation. As there is no difference of DCFH-oxidation between ALDH1A3 WT and KO cells, but MDA levels are significantly higher in ALDH1A3 KO cells than WT cells, which indicates that ALDH1A3 may be effective in dealing with end products of lipid peroxidation. To further confirm our hypothesis, the cells were treated with 300µM TMZ for 5 days or 30µM HNE for 2 hours, and detected the physical interaction between HNE-modified protein and ALDH1A3, p62 separately. The proximity between HNE-modified proteins and both p62 and ALDH1A3 dramatically increased after HNE and TMZ treatment, which indicated by a significant increase of red dots in the TMZ and HNE treated groups (Fig. 29).

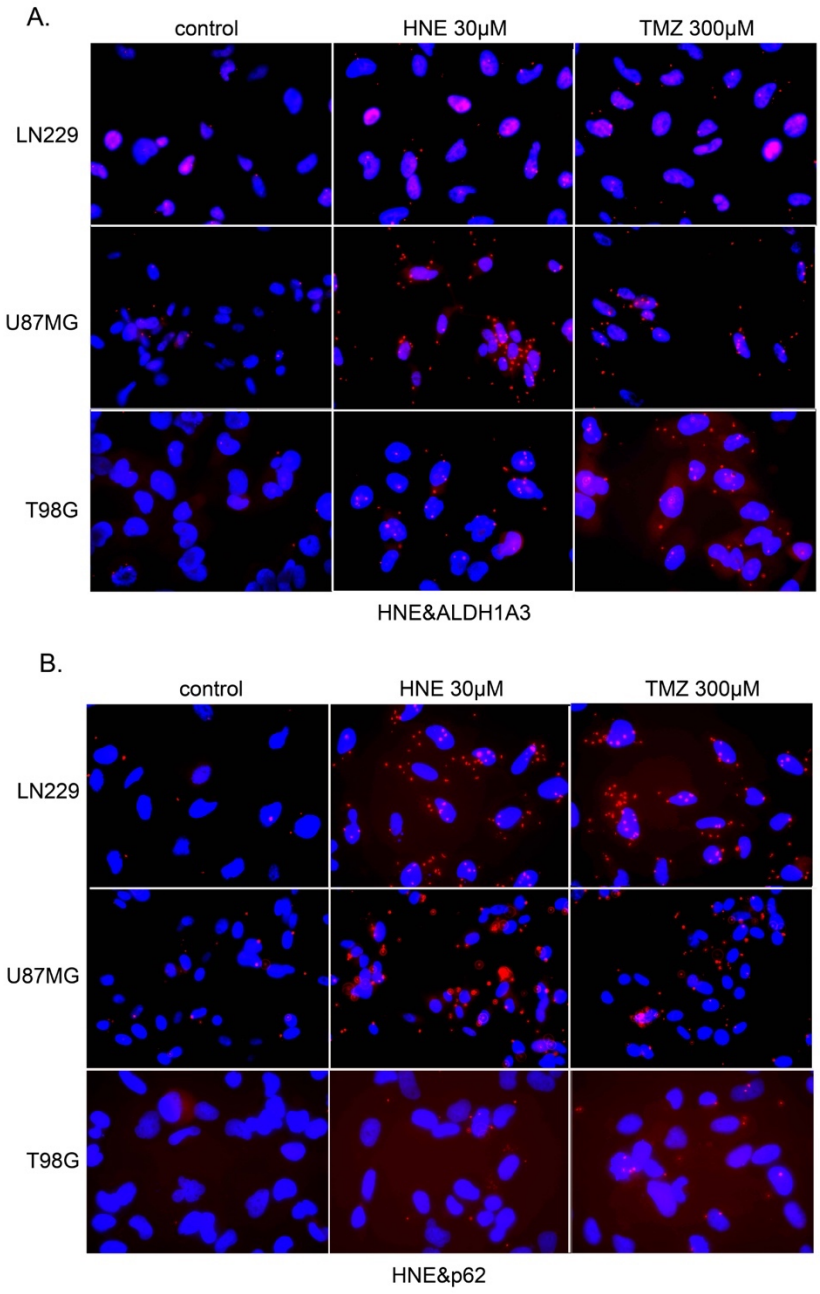

Figure 29. PLA of HNE-modified protein and ALDH1A3 and p62, respectively, in GBM cell lines

The cells were treated with 300μM TMZ for 5 days or 30μM HNE for 2 hours. The proximity between HNE-modified proteins and both p62 and ALDH1A3 were observed in all three cell lines, especially in bafilomycin-and TMZ-treated groups.

What is more, the co-localization has been found between HNE-modified protein and p62 after HNE and TMZ treatment, which indicates that the defected proteins might switch on the process of autophagy (Fig. 30).

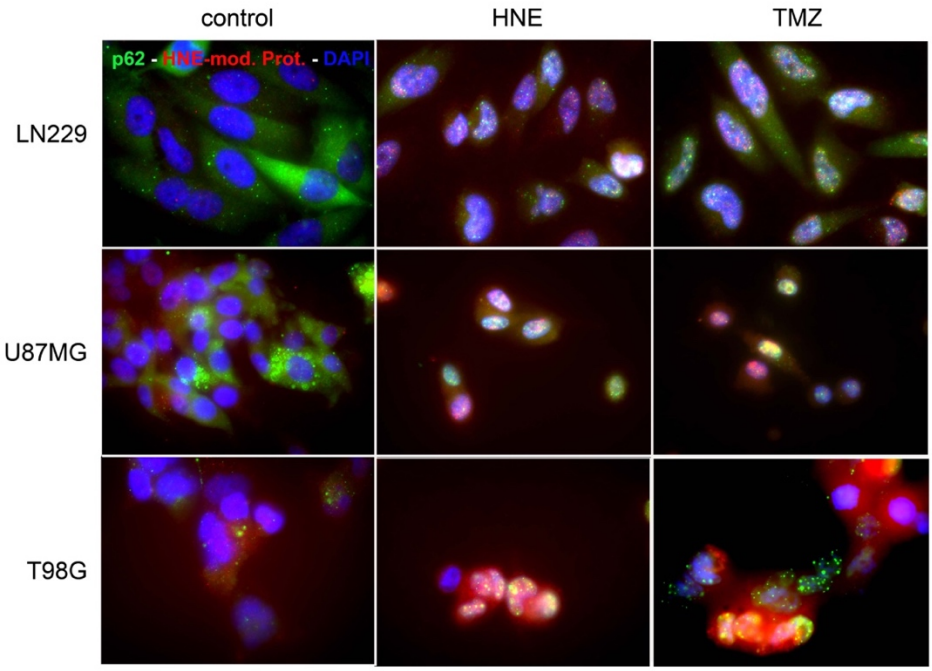

Figure 30. Co-immunofluorescence of p62 and HNE in LN229, U87MG and T98G cell lines.

The cells were treated with 300µM TMZ for 5 days or 30µM HNE for 2 hours, co-localization between HNE-modified protein and p62 were observed in all 3 cell lines.

9. ALDH1A3 positive cells are enriched in tumor relapse and after TMZ treatment *in vitro*

In order to investigate the function of ALDH1A3 in GBM *in vivo*, immunohistochemistry has been conducted in the primary and recurrent tumors of 56 GBM patients. The percentages and intensities of ALDH1A3 positive cells were evaluated (Fig. 31). Significantly higher ALDH1A3 expression levels were observed in specimens of recurrent GBM than the respective samples from the primary tumor in the same patient (Fig. 31B). I presume that ALDH1A3 positive cells are more robust to the TMZ chemotherapy after first surgery. It is most likely that ALDH1A3 positive cells survive the adjuvant therapy and form the resistant subpopulation in the tumor regrowth and are therefore responsible for tumor relapse. There are 41 patients whose survival times are available, the data show that patients with ALDH1A3 low expression have much longer survival times compared with the patients with ALDH1A3 high expression based on the analysis of the specimens of the recurrent GBMs (16 months vs.

21 months, *P*<0.05). These findings indicate that high ALDH1A3 expression correlates with a worse prognosis (Fig. 31C).

A.

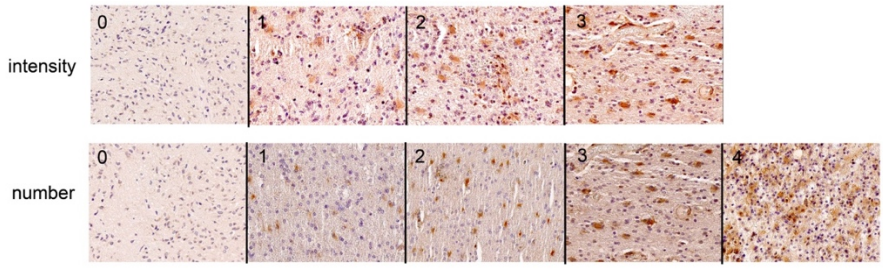

B.

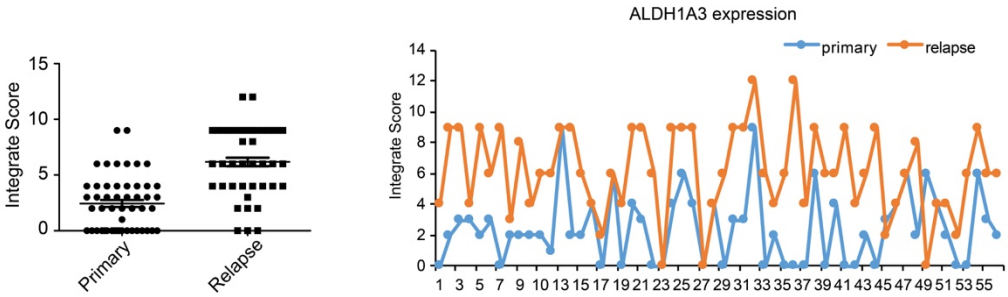

C.

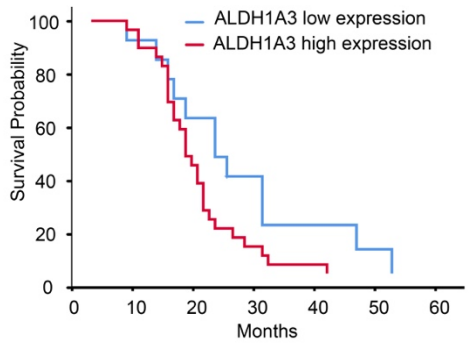

Figure 31. ALDH1A3 expression in the primary and recurrent tumors of GBM patients.

A. Immunohistochemistry results were evaluated by a semi quantitative approach. The score for intensity is 0, 1+, 2+, 3+ . The percentage of cells is scored as Negative (0), ≤10% (1+), ≥11%, ≤30% (2+), ≥31%, ≤50% (3+), ≥51% (4+). The formula for integrate score: the score for the intensity × the score for percentage. B. Specimens from primary GBM showed lower ALDH1A3 expression than the respective

recurrent tumors from the same patients. C. In the specimens of recurrent GBM, patients with ALDH1A3 low-expression (n = 13) have longer survival times than those with ALDH1A3 high-expression (n = 28, *P*<0.05).

To verify this hypothesis, ALDH1A3 expression has been detected in established cell lines and in glioma stem-like cell lines. ALDH1A3 dramatically decreased after 5 days TMZ treatment but recovered to even higher levels after 5 days recovery in fresh medium without TMZ, which indicates that ALDH1A3 positive cells survived the TMZ treatment and formed the resistant subpopulation of the cells. These results demonstrate the key role of ALDH1A3 in the TMZ chemoresistance phenotype of malignant gliomas (Fig. 35).

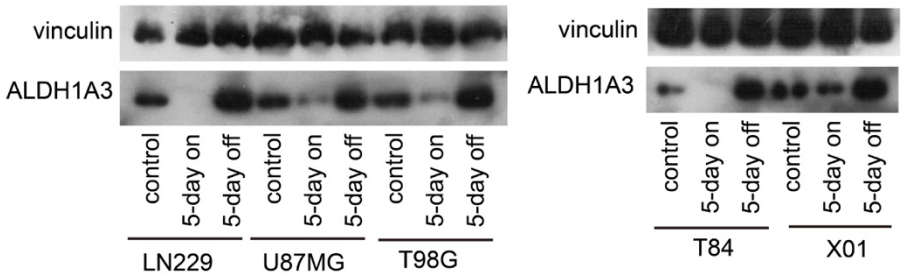

Figure 32. Western blot analysis of ALDH1A3 in LN229, U87MG and T98G cell lines after TMZ treatment.

The established cell lines and glioma stem-like cell lines received 500µM TMZ for 5 consecutive days (5-day on) or further recovered in fresh medium for additional 5 days (5-day off). ALDH1A3 expression diminished after TMZ treatment and recovered to higher levels after 5-day incubation without TMZ.

E. Discussion

Glioblastoma is the most aggressive primary malignant brain tumor (Ostrom et al., 2013). In spite of the advances in multiple treatment approaches, the prognosis of GBMs remains grim and tumor relapse occurs regularly (Davis, 2016). Temozolomide (TMZ) is used as a standard adjuvant chemotherapy for GBM. Many GBM patients with O^6-methylguanine DNA methyltransferase (MGMT) expression show resistance to TMZ treatment. (Thomas et al., 2013, Johannessen and Bjerkvig, 2012). However, some glioblastoma patients with favorable MGMT status don´t respond to therapy, or even those who respond to therapy inevitably relapse (Hegi et al., 2008). Thus, there must be additional mechanisms responsible for TMZ resistance and tumor re-growth of the GBM cells.

The cancer stem cells (CSCs) hypothesis includes an additional mechanism for chemoresistance. The theory suggests that a subset of stem-like cells contributes to tumor initiation and therapeutic resistance (Phi et al., 2018). Aldehyde dehydrogenases (ALDH) have been characterized as markers of cancer stem cells (CSCs), especially the ALDH1 subfamily (Clark and Palle, 2016, Tomita et al., 2016). The subpopulation of tumor cells expressing high ALDH activity appear more resistant to chemo- and radiotherapy (Croker and Allan, 2012, Hu and Fu, 2012). However, it is still illusive how ALDH expression mediates chemoresistance.

The present data shows, that oxidative stress is an important and clinically relevant component of TMZ induced therapeutic effects. Cytotoxicity seems to be mediated by aldehydes resulting from lipid peroxidation, and ALDH1A3 is able to reduce the amount of toxic aldehydes. Therefore, I present a molecular explanation of the role of ALDH1A3 in therapeutic resistance of human GBM cells. These results are corroborated by clinical data showing increased ALDH1A3 levels in GBM operations from recurrent tumors compared to primary patients.

1. ALDH1A3 is a major regulator of ALDH enzyme activity in human GBM cells.

ALDH1A3 is found in the majority of human cancers, and in almost half of gliomas. ALDH1A3 expression also has been identified as a marker for the mesenchymal phenotype in GBM (Mao et al., 2013, Chandran et al., 2015) and associated with poor prognosis of patients with GBM (Zhang et al., 2015).

To investigate the role of ALDH1A3 in chemoresistance of GBM cells, ALDH1A3 has been knockout with CRISPR/Cas9 system. Immunoblotting confirmed the best knockout effect of ALDH1A3 with one of the single-guided RNAs (Fig.8). ALDH enzyme activity was significantly blocked due to the knockout of ALDH1A3 (Fig.9). Aldefluor assay was used to detect ALDH enzyme activity. This assay is based on the conversion of the substrate BAAA (BODIPY-aminoacetaldehyde) by ALDHs into the negatively charged fluorescent reaction product BAA-(BODIPY-aminoacetate). BAAA is a substrate for multiple ALDH isoforms, such as ALDH1A1, ALDH1A3 or ALDH7A1, which demonstrates that ALDH1A3 might be the main isoform regulating ALDH enzyme activity in GBM cells.

The data of Marcato et al. and Croker et al. are in line with my results, they did the knockdown of multiple ALDH isoforms and found that only ALDH1A3 knockdown dramatically down-regulated ALDH activity in breast cancer cells (Marcato et al., 2011, Croker et al., 2017). Shao et al found that ALDH1A3 expression was more important than other isoforms for maintaining non-small cell lung cancer stem cells (Shao et al., 2014). Chen et al. indicated that ALDH1A3 is the main contributor among the 19 ALDH isoforms to ALDH activity in cholangiocarcinoma cells (Chen et al., 2016). ALDH1A3 also revealed 10-fold higher oxidative ability than ALDH1A1 when oxidizing all-trans retinal (Sima et al., 2009, Gagnon et al., 2003).

2. ALDH1A3 expression predicts temozolomide resistance in vitro

Chemoresistance has always been a challenge in cancer therapy and causes treatment failure or tumor relapse. There are two types of resistances: 1. Intrinsic resistance. The resistance is present no matter whether the therapy has been applied or not. Generally, the tumor cells are characterized by a specific DNA repair system, overexpression of certain oncogene or absence of some tumor suppressors. 2. Acquired resistance. It is a response that tumor cells develop to the therapy. Normally it is reflected by certain gene mutation (Lippert et al., 2008).

In my study, the glioblastoma cell lines and primary glioma cells showed more sensitivity to TMZ treatment when ALDH1A3 was inhibited or depleted (Fig.10, 11, 12). Additionally, the change of ALDH1A3 mRNA levels was not significant after TMZ treatment (Fig.18). ALDH1A3 might equip the cells with intrinsic resistance to TMZ treatment since ALDH1A3 is not transcriptionally regulated by TMZ. T98G cells were more resistant to TMZ treatment when compared with the other two cell lines. Chemical inhibition of ALDH1 by DEAB seems more effective than ALDH1A3 KO, which implies that other ALDH isoforms might be involved in the response of T98G to TMZ.

High ALDH1A3 expression has been demonstrated in the resistant subpopulation of various types of cancer. Sullivan et al. illustrated the critical role of ALDH1A3 in maintaining aggressive glioma stem cells via the up-regulation of tissue transglutaminase (Sullivan et al., 2017). Croker et al. suggested that ALDH1A3 deficiency decreased colony formation and metastasis of breast cancer cells (Croker et al., 2017). Chen et al. found that ALDH1A3 is important in enhancing malignancy of cholangiocarcinoma cells and is associated with poor prognosis of patients with intrahepatic cholangiocarcinoma (Chen et al., 2016). These results indicate the potential of ALDH1A3 as a new therapeutic target.

3. TMZ-induced therapeutic effects are partly owing to oxidative stress.

Oxidative stress induced by drug treatment in cancer cells has not been explored comprehensively as a primary aspect of chemotherapy. However, multiple side effects from chemotherapy have been observed in different organs. Doxorubicin (Dox), an established medication for cancer treatment, has been proved that it could induce cardiomyopathy by producing ROS in cardiomyocytes (Zhang et al., 2009). Zidovudine (AZT), the first medication approved for human immunodeficiency virus (HIV) therapy, could lead to skeletal myopathy by releasing dramatic amounts of reactive species (Amatore et al., 2010). Cis-diamminedichloroplatinum (cisplatin), another widely used drug for cancer treatment, also exhibits multiorgan toxicity resulted from redox imbalance (Santos et al., 2007).

Besides DNA damage, Chemotherapy by TMZ also leads to metabolic stress to the cells. MTT assay and PI cell cycle analysis have showed that ALDH1A3 depleted GBM cells are more sensitive to TMZ treatment (Fig.23, 24). N-Acetyl-L-cysteine (NAC), which can effectively increase cellular pools of free radical scavengers, was added together with TMZ to GBM cells. The addition of NAC significantly recovered cell viability and eliminated G2/M cell cycle arrest, suggesting that oxidative stress might play an important role of TMZ-induced cytotoxicity. These data are independent from the MGMT status since it is an universal effect in all three GBM cells, either in MGMT negative cell lines U87 and LN229 or in MGMT positive cell line T98G. Thus, oxidative stress might exert a cytotoxic effect which is independent of the alkylating effect.

Tumors cells are more susceptible to the accumulation of ROS than normal cells, which provides a promising perspective to cancer therapeutic strategies. Hence, elevating ROS in tumor cells until arriving a threshold or targeting the antioxidant system may selectively eliminate tumors cells with limited effect on normal cells (Liu and Wang, 2015). Promyelocytic leukemia protein (PML) tumor suppressor is important for maintaining chronic myeloid

leukemia (CML) stem cells. Arsenic trioxide promotes ROS generation and PML elimination, leading to lethal damage to CML stem cells (Ito et al., 2008). Niclosamide, another potent anti-cancer medication that elevates the ROS production and blocks the NF-κB pathway, is capable to eradicate acute myelogenous leukemia (AML) stem cells without affecting cells from normal bone marrow (Jin et al., 2010). Thus, the ROS production might provide a new vision for developing therapeutic strategies in cancer treatment.

4. The detoxifying effect of ALDH1A3 confers the cells resistance to TMZ

It is widely accepted that cancer stem cells (CSCs) harbor endogenous resistance against chemo- and radiotherapy. This subpopulation of cells rises 2-4 fold after treatment, probably due to a preferential activation of the DNA damage response or inactivation cell cycle checkpoints (Prieto-Vila et al., 2017). ALDHs have been regarded as markers of cancer stem cells. By far, we know that ALDHs mainly exert their function in cytoplasm and seem not to have relations with DNA repair. Thus, there must be other mechanisms responsible for ALDH1A3 mediated chemoresistance.

My study showed that ALDH1A3 inhibition or depletion renders the cells more sensitive to TMZ. However, the differences of cell viability or cell cycle arrest can be eliminated when cells receive the co-treatment with oxidative stress scavenger NAC, indicating that ADH1A3 might be involved in the process of oxidative stress (Fig. 23, 24). So the ROS generation has been investigated in both ALDH1A3 WT and KO cells and found that there were no differences of ROS production no matter ALDH1A3 get depleted or not but a significant higher level of MDA was found in ALDH1A3 KO groups of GBM cells, suggesting that ALDH1A3 plays a critical role in detoxifying end product of lipid peroxidation instead of influencing the process of ROS generation (Fig. 25). These results also indicate that oxidative stress is an upstream factor which triggers the oxidizing effect of ALDH1A3. Additionally, these data are consistent with

immunoblotting with an anti-HNE antibody, in which higher amount of HNE-modified protein was observed when ALDH1A3 enzyme function has been inhibited by ALDH1A3 depletion (Fig. 26).

ALDHs have been regarded as 'aldehyde scavengers' and exert critical influence on chemoresistance phenotype of tumor cells via a detoxifying effect (Pors and Moreb, 2014, Grunblatt and Riederer, 2016). Cojoc et al found that the cells from the xenograft tumors formed by ALDH+ cells have relatively lower expression of ROS and elevated PI3K/AKT signaling (Cojoc et al., 2015). It also has been showed that patients with Parkinson's disease (PD) have substantially down-regulated ALDH and up-regulated toxic aldehydes, like for example MDA, 4-HNE and others (Grunblatt and Riederer, 2016). These data indicate the role of ALDH1A3 in oxidizing the bioactive aldehyde resulted from lipid peroxidation.

5. Autophagy is the main reason for ALDH1A3 degradation.

Our results reveal that ALDH1A3 depletion renders GBM cells more susceptible to TMZ treatment mainly at low dosages ≤ 300µM (Fig. 10). So immunoblotting and aldefluor assay have been conducted to investigate the expression of ALDH1A3. As expected, both ALDH1A3 protein levels and ALDH enzyme activities decreased dramatically at high dosages of TMZ treatment (Fig. 13, 14, 17). Lipid Peroxidation (MDA) Assay also showed that the differences of MDA production between ALDH1A3 WT and KO cells were diminished in 500µM TMZ treated groups (Fig. 25). This could explain the reason why ALDH1A3 WT cells are as sensitive as ALDH1A3 KO cells in high dosages TMZ treated groups.

It is interesting to know the reason of ALDH1A3 elimination when cells receive high concentration TMZ treatment. Interestingly, no significant changes of ALDH1A3 mRNA levels

have been found after different concentrations of TMZ treatment, which suggests that the reduction of ALDH1A3 protein is post-transcriptionally regulated (Fig. 13, 14, 18). Lin et al. proved that TMZ causes ROS/ERK-regulated or mitochondrial damage- and ER stress-dependent autophagy to protect glioma cells (Lin et al., 2012a, Lin et al., 2012b). Thus, the down-regulation of ALDH1A3 might be mediated from a proteolytic aspect and possibly involved in the process of autophagy since TMZ led to an enhancement of autophagy (the up-regulation of LC3-II and down-regulation of p62) and both ALDH1A3 protein expression and enzyme activity have been restored with co-treatment of bafilomycin (Fig. 13, 14). In order to further explore the involvement of ALDH1A3 in autophagy, GBM cells have been treated with autophagy activator rapamycin and autophagy inhibitors bafilomycin and chloroquine. Rapamycin inhibits the mTOR pathway which negatively regulates autophagy (Jung et al., 2010). The reduction of ALDH1A3 has been observed as well as the autophagy substrate p62. Bafilomycin and chloroquine are well-known inhibitors of autophagy, which interrupts the fusion of autophagosomes and lysosomes. The inhibition of autophagy led to ALDH1A3 accumulation (Fig. 19, 20). Thus, ALDH1A3 degradation after TMZ treatment might occur in the process of autophagy.

6. Autophagy has been activated for cleaning up defected proteins from oxidative stress

ALDH1A3 seems to be involved in the process of autophagy, however, the correlation between ALDH1A3 and autophagy is still enigmatic. The molecular mechanisms of ALDH1A3 in autophagy have not been explored in detail. ALDH1A3 knockout cells seem to exhibit stronger autophagic flux reflected by more GFP-LC3 puncta and LC3-II protein expression in ALDH1A3 depleted groups (Fig. 15, 16).

Generally, autophagy is activated to eradicate the damaged organelles or molecules when cells expose to cellular stress. It has been shown that bioactive toxic aldehydes produced by

lipid peroxidation are one of the reasons for autophagy activation. HNE has been proved to enhance autophagy in a JNK-dependent manner in rat aortic smooth muscle cells model (Haberzettl and Hill, 2013). Toxic aldehydes are also found to be accumulated and autophagy has been activated in neurodegenerative diseases, such as Parkinson´s disease (Dias et al., 2013, Lynch-Day et al., 2012). Thus, autophagy is activated by oxidative stress induced by TMZ, since the co-treatment with NAC dramatically decreased the level of autophagy (Fig. 27). Therefore, it is possible that oxidative stress induces lipid peroxidation, which generates numerous toxic aldehydes, leading to the protein modification. The defected proteins trigger the activation of autophagy. ALDH1A3 could be degraded by autophagy as an enzymatic complex with aldehyde or as one of the aldehyde-modified proteins.

The correlation between HNE, ALDH1A3 and autophagy has been investigated further by proximity ligation assay. The proximity of both ALDH1A3 and p62 with HNE-modified proteins, ALDH1A3 and p62 has been observed (Fig. 21, 29). Results of proximity ligation assay are substantiated by the results of co-immunoprecipitation, which also verified the physical interaction between p62 and ALDH1A3 (Fig. 22). Furthermore, immunofluorescence confirmed the co-localization of p62 with HNE-modified proteins (Fig. 30). These results are consistent with the hypothesis that ALDH1A3 is recruited to autophagosomes and degrades in the final stage of autophagy. As the change of ALDH1A3 is not totally in line with p62 expression, a ratio of ALDH1A3 might recruit to the membranes of autophagosome without association with p62 and detaches the autolysosome finally. In line with my observation, Dodson et al. found that low concentrations of 4-HNE treatment induced autophagy and high concentrations resulted in mitochondrial dysfunction. Besides, the blockage of autophagy initiation led to a dramatic decrease of mitochondrial function (Dodson et al., 2017). Hill et al. have the same observation in rat aortic smooth-muscle cells. Unsaturated lipid peroxidation produced 4-HNE, which caused several protein modifications and these defective proteins were moved gradually by autophagy. (Hill et al., 2008). Thus, autophagy plays a survival-promoting role when cells are overload with lipid peroxidation.

7. ALDH1A3 plays an important role in the therapy resistance phenotype of gliomas.

It is well-known that cancer stem cells (CSCs) possess intrinsic resistance to cancer therapy. This small subpopulation of cells increases 2-4 folds after treatment due to self-survival promoting mechanisms. So specimens from neurosurgical resections have been collected from 56 patients with GBM who have both resections of primary and recurrent tumors, and have been investigated for ALDH1A3 expression (Fig. 31). As expected, only a small fraction of cells in the specimens from primary tumors showed the expression of ALDH1A3, but strong ALDH1A3 expression has been observed in the specimens from recurrent tumors, indicating that the cancer stem cells survived the adjuvant therapy after first resection, which verified the role of ALDH1A3 as a stem cell marker. Subsequently, the correlation between ALDH1A3 expression and overall survival of the patients based on samples from recurrent tumors has been analyzed since primary tumors barely express ALDH1A3. Patients with high ALDH1A3 expression exhibited dramatically shorter survival times. These effects seem to be functional also *in vitro*. Three established GBM cell lines and two primary GBM cells were cultured with 500µM TMZ for 5 consecutive days and then replaced with fresh medium and incubated for another 5 days (Fig. 32). ALDH1A3 was significantly down-regulated by lipid peroxidation induced autophagy after 5-day TMZ treatment but recovered to even higher levels in the oxidative stress-free time interval. These results reveal that ALDH1A3 overexpressing cells form the most resistant subpopulation cells within the tumor both *in vitro* and *in vivo.* The presence of ALDH1A3 keeps tumor cells from the cytotoxic effect induced by TMZ and exerts a critical effect on therapy resistance phenotype of gliomas.

8. Conclusion

ALDH1A3 is not only a biomarker for GBM cancer stem cells, but also plays an important role in regulating chemoresistance. ALDH1A3 depletion renders the cells more sensitive to TMZ treatment than ALDH1A3 WT cells. Oxidative stress is a critical and clinically relevant factor of TMZ induced cytotoxicity. Here, it is shown that TMZ treatment induces oxidative stress, which leads to lipid peroxidation, yielding cytotoxic aldehydes including HNE and MDA that are oxidized by ALDH enzymatic activity. The detoxifying effect of ALDH confers tumor cells resistance to TMZ. Autophagy activated by the aldehyde-modified proteins seems then to degrade ALDH as an enzymatic complex bound with an aldehyde or as one of the aldehyde-modified proteins. But ALDH1A3 expression can be restored to even higher levels after oxidative stress-free time interval after TMZ treatment. These data are consistent with *in vivo* results, ALDH1A3 expression is dramatically higher in recurrent specimens than primary ones of GBM from the same patients and patients with higher ALDH1A3 expression show much shorter overall survival rate. These data demonstrate the important role of ALDH1A3 in regulating chemoresistance, which provides a new explanation of the therapeutic resistance of GBM cancer stem cells.

9. Outlook

This study reveals the molecular mechanism of ALDH1A3 as a predictor for TMZ resistance in GBM, which is independent of MGMT expression. Oxidative stress plays an important role in TMZ induced cytotoxicity. Autophagy has been activated to eradicate defected protein resulted from lipid peroxidation and ALDH1A3 could involve in the process of degradation. Further experiments are needed to investigate whether ALDH1A3 degraded by autophagy as an enzymatic complex with aldehyde or as one of the aldehyde-modified proteins. A more precise method to analyze aldehyde modified proteins would be two-dimensional liquid chromatographic tandem mass spectrometry described by Golizeh et al (Golizeh et al., 2016).

Indeed, our *in vitro* study should be verified in an animal model to prove the role of ALDH1A3 in chemoresistance *in vivo*. Recombinant C6 rat GBM cells with or without ALDH1A3 expression could be stereotactically injected into the striatum of the rats and treated with TMZ. The survival time of the rats, the weight of tumor and biological markers could be checked to analyze the effect of ALDH1A3 knockout.

F. Acknowledgement

Upon the completion of this thesis, I am grateful to those who have offered me constant encouragement and support during my study. I am not able to finish my work successfully without their help.

First of all, It is a great pleasure to express my deepest gratitude to Prof. Jürgen Schlegel. I have been benefited a lot from his timely academic advices, enlightened attitude and meticulous supervision. He brought me plenty of inspirations and most importantly, the keen interest in scientific research. It is a great honor to work under his supervision.

I would like to thank profusely Dr. Fabian Schneider, who provided me lots of guidance in my first year of international study. He showed me scientific approaches systematically and enabled me to quickly adjust to the new environment.

I would like to express a deep sense of gratitude to Dr. Martin Schönfelder and Dr. Friederike Liesche, who are not only my mentors but also my good friends. They offered me numerous support no matter in scientific or mental aspects. It is a great pleasure to meet them during my PhD. study.

I am also very grateful to all of my colleagues. I would like to thank especially Sandra Baur for constant technical support and Laura Steingruber and Johannes Schecker for the scientific support and sincere friendship. It is a huge fortune to have them around. I would like to thank our secretary Claudia Walter for her considerate administrative organization. I also would like to thank Charlotte von Rosenstiel, Karoline Mayer, Michael Griessmair, Alicia Gantzkow and Katharina Holzner. I really enjoy the communication with them although our cooperation time is not so long. It is indeed a great team! It is a great pleasure to work here during my 4-year PhD study.

Last but not least, I am extremely thankful to my parents, who always believe in me and give me unconditional love and support. I want to thank sincerely my friends Ziying Jian and Tao Cheng for offering the inspirations in scientific and life aspects. I also want to express my thanks to my best friends Ruoyu Xu, Jing Shang, Lili Zhao, Yamin Zhao, Haokun Bi, Chengyuan Zhai and Kai Zhang for their company and considerate support for all these 4-year international study.

I am so appreciated and I believe that they will be my life-long friends.

Thank you!

G. References

ALAM, M., AHMAD, R., RAJABI, H., KHARBANDA, A. & KUFE, D. 2013. MUC1-C oncoprotein activates ERK-->C/EBPbeta signaling and induction of aldehyde dehydrogenase 1A1 in breast cancer cells. *J Biol Chem,* 288**,** 30892-903.

AMATORE, C., ARBAULT, S., JAOUEN, G., KOH, A. C., LEONG, W. K., TOP, S., VALLERON, M. A. & WOO, C. H. 2010. Pro-oxidant properties of AZT and other thymidine analogues in macrophages: implication of the azido moiety in oxidative stress. *ChemMedChem,* 5**,** 296-301.

BATLLE, E. & CLEVERS, H. 2017. Cancer stem cells revisited. *Nat Med,* 23**,** 1124-1134.

BELIKOV, A. V., SCHRAVEN, B. & SIMEONI, L. 2015. T cells and reactive oxygen species. *J Biomed Sci,* 22**,** 85.

BRAGANZA, M. Z., KITAHARA, C. M., BERRINGTON DE GONZALEZ, A., INSKIP, P. D., JOHNSON, K. J. & RAJARAMAN, P. 2012. Ionizing radiation and the risk of brain and central nervous system tumors: a systematic review. *Neuro Oncol,* 14**,** 1316-24.

CATTANEO, F., GUERRA, G., PARISI, M., DE MARINIS, M., TAFURI, D., CINELLI, M. & AMMENDOLA, R. 2014. Cell-surface receptors transactivation mediated by g protein-coupled receptors. *Int J Mol Sci,* 15**,** 19700-28.

CHANDRAN, U. R., LUTHRA, S., SANTANA-SANTOS, L., MAO, P., KIM, S. H., MINATA, M., LI, J., BENOS, P. V., DEWANG, M., HU, B., CHENG, S. Y., NAKANO, I. & SOBOL, R. W. 2015. Gene expression profiling distinguishes proneural glioma stem cells from mesenchymal glioma stem cells. *Genom Data,* 5**,** 333-336.

CHEN, M. H., WENG, J. J., CHENG, C. T., WU, R. C., HUANG, S. C., WU, C. E., CHUNG, Y. H., LIU, C. Y., CHANG, M. H., CHEN, M. H., CHIANG, K. C., YEH, T. S., SU, Y. & YEH, C. N. 2016. ALDH1A3, the Major Aldehyde Dehydrogenase Isoform in Human Cholangiocarcinoma Cells, Affects Prognosis and Gemcitabine Resistance in Cholangiocarcinoma Patients. *Clin Cancer Res,* 22**,** 4225-35.

CHENG, P., WANG, J., WAGHMARE, I., SARTINI, S., COVIELLO, V., ZHANG, Z., KIM, S. H., MOHYELDIN, A., PAVLYUKOV, M. S., MINATA, M., VALENTIM, C. L., CHHIPA, R. R., BHAT, K. P., DASGUPTA, B., LA MOTTA, C., KANGO-SINGH, M. & NAKANO, I. 2016. FOXD1-ALDH1A3 Signaling Is a Determinant for the Self-Renewal and Tumorigenicity of Mesenchymal Glioma Stem Cells. *Cancer Res,* 76**,** 7219-7230.

CLARK, D. W. & PALLE, K. 2016. Aldehyde dehydrogenases in cancer stem cells: potential as therapeutic targets. *Ann Transl Med,* 4**,** 518.

COBLEY, J. N., FIORELLO, M. L. & BAILEY, D. M. 2018. 13 reasons why the brain is susceptible to oxidative stress. *Redox Biol,* 15**,** 490-503.

COJOC, M., PEITZSCH, C., KURTH, I., TRAUTMANN, F., KUNZ-SCHUGHART, L. A., TELEGEEV, G. D., STAKHOVSKY, E. A., WALKER, J. R., SIMIN, K., LYLE, S., FUESSEL, S., ERDMANN, K., WIRTH, M. P., KRAUSE, M., BAUMANN, M. & DUBROVSKA, A. 2015. Aldehyde Dehydrogenase Is Regulated by beta-Catenin/TCF and Promotes Radioresistance in Prostate Cancer Progenitor Cells. *Cancer Res,* 75**,** 1482-94.

CORREIA-MELO, C., HEWITT, G. & PASSOS, J. F. 2014. Telomeres, oxidative stress and inflammatory factors: partners in cellular senescence? *Longev Healthspan,* 3**,** 1.

CROKER, A. K. & ALLAN, A. L. 2012. Inhibition of aldehyde dehydrogenase (ALDH) activity reduces chemotherapy and radiation resistance of stem-like ALDHhiCD44(+) human breast cancer cells. *Breast Cancer Res Treat,* 133**,** 75-87.

CROKER, A. K., RODRIGUEZ-TORRES, M., XIA, Y., PARDHAN, S., LEONG, H. S., LEWIS, J. D. & ALLAN, A. L. 2017. Differential Functional Roles of ALDH1A1 and ALDH1A3 in Mediating Metastatic Behavior and Therapy Resistance of Human Breast Cancer Cells. *Int J Mol Sci,* 18.

DAVIS, M. E. 2016. Glioblastoma: Overview of Disease and Treatment. *Clin J Oncol Nurs,* 20**,** S2-8.

DI MEO, S., REED, T. T., VENDITTI, P. & VICTOR, V. M. 2016. Role of ROS and RNS Sources in Physiological and Pathological Conditions. *Oxid Med Cell Longev,* 2016**,** 1245049.

DIAS, V., JUNN, E. & MOURADIAN, M. M. 2013. The role of oxidative stress in Parkinson's disease. *J Parkinsons Dis,* 3**,** 461-91.

DODSON, M., WANI, W. Y., REDMANN, M., BENAVIDES, G. A., JOHNSON, M. S., OUYANG, X., COFIELD, S. S., MITRA, K., DARLEY-USMAR, V. & ZHANG, J. 2017. Regulation of autophagy, mitochondrial dynamics, and cellular bioenergetics by 4-hydroxynonenal in primary neurons. *Autophagy,* 13**,** 1828-1840.

DUBROW, R., DAREFSKY, A. S., PARK, Y., MAYNE, S. T., MOORE, S. C., KILFOY, B., CROSS, A. J., SINHA, R., HOLLENBECK, A. R., SCHATZKIN, A. & WARD, M. H. 2010. Dietary components related to N-nitroso compound formation: a prospective study of adult glioma. *Cancer Epidemiol Biomarkers Prev,* 19**,** 1709-22.

FIASCHI, T. & CHIARUGI, P. 2012. Oxidative stress, tumor microenvironment, and metabolic reprogramming: a diabolic liaison. *Int J Cell Biol,* 2012**,** 762825.

GAGNON, I., DUESTER, G. & BHAT, P. V. 2003. Enzymatic characterization of recombinant mouse retinal dehydrogenase type 1. *Biochem Pharmacol,* 65**,** 1685-90.

GAMBINO, V., DE MICHELE, G., VENEZIA, O., MIGLIACCIO, P., DALL'OLIO, V., BERNARD, L., MINARDI, S. P., DELLA FAZIA, M. A., BARTOLI, D., SERVILLO, G., ALCALAY, M., LUZI, L., GIORGIO, M., SCRABLE, H., PELICCI, P. G. & MIGLIACCIO, E. 2013. Oxidative stress activates a specific p53 transcriptional response that regulates cellular senescence and aging. *Aging Cell,* 12**,** 435-45.

GASPAR, N., MARSHALL, L., PERRYMAN, L., BAX, D. A., LITTLE, S. E., VIANA-PEREIRA, M., SHARP, S. Y., VASSAL, G., PEARSON, A. D., REIS, R. M., HARGRAVE, D., WORKMAN, P. & JONES, C. 2010. MGMT-independent temozolomide resistance in pediatric glioblastoma cells associated with a PI3-kinase-mediated HOX/stem cell gene signature. *Cancer Res,* 70**,** 9243-52.

GIANNONI, E., PARRI, M. & CHIARUGI, P. 2012. EMT and oxidative stress: a bidirectional interplay affecting tumor malignancy. *Antioxid Redox Signal,* 16**,** 1248-63.

GLICK, D., BARTH, S. & MACLEOD, K. F. 2010. Autophagy: cellular and molecular mechanisms. *J Pathol,* 221**,** 3-12.

GOLIZEH, M., GEIB, T. & SLENO, L. 2016. Identification of 4-hydroxynonenal protein targets in rat, mouse and human liver microsomes by two-dimensional liquid

chromatography/tandem mass spectrometry. *Rapid Commun Mass Spectrom,* 30**,** 1488-94.

GRUNBLATT, E. & RIEDERER, P. 2016. Aldehyde dehydrogenase (ALDH) in Alzheimer's and Parkinson's disease. *J Neural Transm (Vienna),* 123**,** 83-90.

GUO, J. Y., CHEN, H. Y., MATHEW, R., FAN, J., STROHECKER, A. M., KARSLI-UZUNBAS, G., KAMPHORST, J. J., CHEN, G., LEMONS, J. M., KARANTZA, V., COLLER, H. A., DIPAOLA, R. S., GELINAS, C., RABINOWITZ, J. D. & WHITE, E. 2011. Activated Ras requires autophagy to maintain oxidative metabolism and tumorigenesis. *Genes Dev,* 25**,** 460-70.

GUO, J. Y., XIA, B. & WHITE, E. 2013. Autophagy-mediated tumor promotion. *Cell,* 155**,** 1216-9.

HABERZETTL, P. & HILL, B. G. 2013. Oxidized lipids activate autophagy in a JNK-dependent manner by stimulating the endoplasmic reticulum stress response. *Redox Biol,* 1**,** 56-64.

HANAHAN, D. & WEINBERG, R. A. 2000. The hallmarks of cancer. *Cell,* 100**,** 57-70.

HEGI, M. E., LIU, L., HERMAN, J. G., STUPP, R., WICK, W., WELLER, M., MEHTA, M. P. & GILBERT, M. R. 2008. Correlation of O6-methylguanine methyltransferase (MGMT) promoter methylation with clinical outcomes in glioblastoma and clinical strategies to modulate MGMT activity. *J Clin Oncol,* 26**,** 4189-99.

HILL, B. G., HABERZETTL, P., AHMED, Y., SRIVASTAVA, S. & BHATNAGAR, A. 2008. Unsaturated lipid peroxidation-derived aldehydes activate autophagy in vascular smooth-muscle cells. *Biochem J,* 410**,** 525-34.

HOLZE, C., MICHAUDEL, C., MACKOWIAK, C., HAAS, D. A., BENDA, C., HUBEL, P., PENNEMANN, F. L., SCHNEPF, D., WETTMARSHAUSEN, J., BRAUN, M., LEUNG, D. W., AMARASINGHE, G. K., PEROCCHI, F., STAEHELI, P., RYFFEL, B. & PICHLMAIR, A. 2018. Oxeiptosis, a ROS-induced caspase-independent apoptosis-like cell-death pathway. *Nat Immunol,* 19**,** 130-140.

HONG, S. H., NGO, H. P., NAM, H. K., KIM, K. R., KANG, L. W. & OH, D. K. 2016. Alternative Biotransformation of Retinal to Retinoic Acid or Retinol by an Aldehyde Dehydrogenase from Bacillus cereus. *Appl Environ Microbiol,* 82**,** 3940-3946.

HU, Y. & FU, L. 2012. Targeting cancer stem cells: a new therapy to cure cancer patients. *Am J Cancer Res,* 2**,** 340-56.

ILKANIZADEH, S., LAU, J., HUANG, M., FOSTER, D. J., WONG, R., FRANTZ, A., WANG, S., WEISS, W. A. & PERSSON, A. I. 2014. Glial progenitors as targets for transformation in glioma. *Adv Cancer Res,* 121**,** 1-65.

ITO, K., BERNARDI, R., MOROTTI, A., MATSUOKA, S., SAGLIO, G., IKEDA, Y., ROSENBLATT, J., AVIGAN, D. E., TERUYA-FELDSTEIN, J. & PANDOLFI, P. P. 2008. PML targeting eradicates quiescent leukaemia-initiating cells. *Nature,* 453**,** 1072-8.

JIN, Y., LU, Z., DING, K., LI, J., DU, X., CHEN, C., SUN, X., WU, Y., ZHOU, J. & PAN, J. 2010. Antineoplastic mechanisms of niclosamide in acute myelogenous leukemia stem cells: inactivation of the NF-kappaB pathway and generation of reactive oxygen species. *Cancer Res,* 70**,** 2516-27.

JOHANNESSEN, T. C. & BJERKVIG, R. 2012. Molecular mechanisms of temozolomide resistance in glioblastoma multiforme. *Expert Rev Anticancer Ther,* 12**,** 635-42.

JUNG, C. H., RO, S. H., CAO, J., OTTO, N. M. & KIM, D. H. 2010. mTOR regulation of autophagy. *FEBS Lett,* 584**,** 1287-95.

KAMOGASHIRA, T., FUJIMOTO, C. & YAMASOBA, T. 2015. Reactive oxygen species, apoptosis, and mitochondrial dysfunction in hearing loss. *Biomed Res Int,* 2015**,** 617207.

KATHEDER, N. S., KHEZRI, R., O'FARRELL, F., SCHULTZ, S. W., JAIN, A., RAHMAN, M. M., SCHINK, K. O., THEODOSSIOU, T. A., JOHANSEN, T., JUHASZ, G., BILDER, D., BRECH, A., STENMARK, H. & RUSTEN, T. E. 2017. Microenvironmental autophagy promotes tumour growth. *Nature,* 541**,** 417-420.

KLIONSKY, D. J., ABDELMOHSEN, K., ABE, A., ABEDIN, M. J., ABELIOVICH, H., ACEVEDO AROZENA, A., ADACHI, H., ADAMS, C. M., ADAMS, P. D., ADELI, K., ADHIHETTY, P. J., ADLER, S. G., AGAM, G., AGARWAL, R., AGHI, M. K., AGNELLO, M., AGOSTINIS, P., AGUILAR, P. V., AGUIRRE-GHISO, J., AIROLDI, E. M., AIT-SI-ALI, S., AKEMATSU, T., AKPORIAYE, E. T., AL-RUBEAI, M., ALBAICETA, G. M., ALBANESE, C., ALBANI, D., ALBERT, M. L., ALDUDO, J., ALGUL, H., ALIREZAEI, M., ALLOZA, I., ALMASAN, A., ALMONTE-BECERIL, M., ALNEMRI, E. S., ALONSO, C., ALTAN-BONNET, N., ALTIERI, D. C., ALVAREZ, S., ALVAREZ-ERVITI, L., ALVES, S., AMADORO, G., AMANO, A., AMANTINI, C., AMBROSIO, S., AMELIO, I., AMER, A. O., AMESSOU, M., AMON, A., AN, Z., ANANIA, F. A., ANDERSEN, S. U., ANDLEY, U. P., ANDREADI, C. K., ANDRIEU-ABADIE, N., ANEL, A., ANN, D. K., ANOOPKUMAR-DUKIE, S., ANTONIOLI, M., AOKI, H., APOSTOLOVA, N., AQUILA, S., AQUILANO, K., ARAKI, K., ARAMA, E., ARANDA, A., ARAYA, J., ARCARO, A., ARIAS, E., ARIMOTO, H., ARIOSA, A. R., ARMSTRONG, J. L., ARNOULD, T., ARSOV, I., ASANUMA, K., ASKANAS, V., ASSELIN, E., ATARASHI, R., ATHERTON, S. S., ATKIN, J. D., ATTARDI, L. D., AUBERGER, P., AUBURGER, G., AURELIAN, L., AUTELLI, R., AVAGLIANO, L., AVANTAGGIATI, M. L., AVRAHAMI, L., AWALE, S., AZAD, N., BACHETTI, T., BACKER, J. M., BAE, D. H., BAE, J. S., BAE, O. N., BAE, S. H., BAEHRECKE, E. H., BAEK, S. H., BAGHDIGUIAN, S., BAGNIEWSKA-ZADWORNA, A., et al. 2016. Guidelines for the use and interpretation of assays for monitoring autophagy (3rd edition). *Autophagy,* 12**,** 1-222.

LEE, D. J. & KANG, S. W. 2013. Reactive oxygen species and tumor metastasis. *Mol Cells,* 35**,** 93-8.

LEVY, J. M. M., TOWERS, C. G. & THORBURN, A. 2017. Targeting autophagy in cancer. *Nat Rev Cancer,* 17**,** 528-542.

LI, Y. M., SUKI, D., HESS, K. & SAWAYA, R. 2016. The influence of maximum safe resection of glioblastoma on survival in 1229 patients: Can we do better than gross-total resection? *J Neurosurg,* 124**,** 977-88.

LIEMBURG-APERS, D. C., WILLEMS, P. H., KOOPMAN, W. J. & GREFTE, S. 2015. Interactions between mitochondrial reactive oxygen species and cellular glucose metabolism. *Arch Toxicol,* 89**,** 1209-26.

LIN, C. J., LEE, C. C., SHIH, Y. L., LIN, C. H., WANG, S. H., CHEN, T. H. & SHIH, C. M. 2012a. Inhibition of mitochondria- and endoplasmic reticulum stress-mediated autophagy augments temozolomide-induced apoptosis in glioma cells. *PLoS One,* 7**,** e38706.

LIN, C. J., LEE, C. C., SHIH, Y. L., LIN, T. Y., WANG, S. H., LIN, Y. F. & SHIH, C. M. 2012b. Resveratrol enhances the therapeutic effect of temozolomide against malignant glioma in vitro and in vivo by inhibiting autophagy. *Free Radic Biol Med,* 52**,** 377-91.

LIPPERT, T. H., RUOFF, H. J. & VOLM, M. 2008. Intrinsic and acquired drug resistance in malignant tumors. The main reason for therapeutic failure. *Arzneimittelforschung,* 58**,** 261-4.

LIU, J. & WANG, Z. 2015. Increased Oxidative Stress as a Selective Anticancer Therapy. *Oxid Med Cell Longev,* 2015**,** 294303.

LOCK, R., ROY, S., KENIFIC, C. M., SU, J. S., SALAS, E., RONEN, S. M. & DEBNATH, J. 2011. Autophagy facilitates glycolysis during Ras-mediated oncogenic transformation. *Mol Biol Cell,* 22**,** 165-78.

LOUIS, D. N., PERRY, A., REIFENBERGER, G., VON DEIMLING, A., FIGARELLA-BRANGER, D., CAVENEE, W. K., OHGAKI, H., WIESTLER, O. D., KLEIHUES, P. & ELLISON, D. W. 2016. The 2016 World Health Organization Classification of Tumors of the Central Nervous System: a summary. *Acta Neuropathol,* 131**,** 803-20.

LYNCH-DAY, M. A., MAO, K., WANG, K., ZHAO, M. & KLIONSKY, D. J. 2012. The role of autophagy in Parkinson's disease. *Cold Spring Harb Perspect Med,* 2**,** a009357.

MALMSTROM, A., POULSEN, H. S., GRONBERG, B. H., STRAGLIOTTO, G., HANSEN, S., ASKLUND, T., HOLMLUND, B., LYSIAK, M., DOWSETT, J., KRISTENSEN, B. W., SODERKVIST, P., ROSELL, J., HENRIKSSON, R. & NORDIC CLINICAL BRAIN TUMOR STUDY, G. 2017. Postoperative neoadjuvant temozolomide before radiotherapy versus standard radiotherapy in patients 60 years or younger with anaplastic astrocytoma or glioblastoma: a randomized trial. *Acta Oncol,* 56**,** 1776-1785.

MALTA, T. M., DE SOUZA, C. F., SABEDOT, T. S., SILVA, T. C., MOSELLA, M. S., KALKANIS, S. N., SNYDER, J., CASTRO, A. V. B. & NOUSHMEHR, H. 2018. Glioma CpG island methylator phenotype (G-CIMP): biological and clinical implications. *Neuro Oncol,* 20**,** 608-620.

MAO, P., JOSHI, K., LI, J., KIM, S. H., LI, P., SANTANA-SANTOS, L., LUTHRA, S., CHANDRAN, U. R., BENOS, P. V., SMITH, L., WANG, M., HU, B., CHENG, S. Y., SOBOL, R. W. & NAKANO, I. 2013. Mesenchymal glioma stem cells are maintained by activated glycolytic metabolism involving aldehyde dehydrogenase 1A3. *Proc Natl Acad Sci U S A,* 110**,** 8644-9.

MARCATO, P., DEAN, C. A., PAN, D., ARASLANOVA, R., GILLIS, M., JOSHI, M., HELYER, L., PAN, L., LEIDAL, A., GUJAR, S., GIACOMANTONIO, C. A. & LEE, P. W. 2011. Aldehyde dehydrogenase activity of breast cancer stem cells is primarily due to isoform ALDH1A3 and its expression is predictive of metastasis. *Stem Cells,* 29**,** 32-45.

MARINO, G., SALVADOR-MONTOLIU, N., FUEYO, A., KNECHT, E., MIZUSHIMA, N. & LOPEZ-OTIN, C. 2007. Tissue-specific autophagy alterations and increased tumorigenesis in mice deficient in Atg4C/autophagin-3. *J Biol Chem,* 282**,** 18573-83.

MATHEW, R., KARANTZA-WADSWORTH, V. & WHITE, E. 2007a. Role of autophagy in cancer. *Nat Rev Cancer,* 7**,** 961-7.

MATHEW, R., KONGARA, S., BEAUDOIN, B., KARP, C. M., BRAY, K., DEGENHARDT, K., CHEN, G., JIN, S. & WHITE, E. 2007b. Autophagy suppresses tumor progression by limiting chromosomal instability. *Genes Dev,* 21**,** 1367-81.

MAUGERI-SACCA, M., DI MARTINO, S. & DE MARIA, R. 2013. Biological and clinical implications of cancer stem cells in primary brain tumors. *Front Oncol,* 3**,** 6.

MCFALINE-FIGUEROA, J. L., BRAUN, C. J., STANCIU, M., NAGEL, Z. D., MAZZUCATO, P., SANGARAJU, D., CERNIAUSKAS, E., BARFORD, K., VARGAS, A., CHEN, Y., TRETYAKOVA, N., LEES, J. A., HEMANN, M. T., WHITE, F. M. & SAMSON, L. D. 2015. Minor Changes in Expression of the Mismatch Repair Protein MSH2 Exert a Major Impact on Glioblastoma Response to Temozolomide. *Cancer Res,* 75**,** 3127-38.

MIZUSHIMA, N., YOSHIMORI, T. & LEVINE, B. 2010. Methods in mammalian autophagy research. *Cell,* 140**,** 313-26.

MUNOZ, J. L., RODRIGUEZ-CRUZ, V., GRECO, S. J., RAMKISSOON, S. H., LIGON, K. L. & RAMESHWAR, P. 2014. Temozolomide resistance in glioblastoma cells occurs partly through epidermal growth factor receptor-mediated induction of connexin 43. *Cell Death Dis,* 5**,** e1145.

OSTROM, Q. T., GITTLEMAN, H., FARAH, P., ONDRACEK, A., CHEN, Y., WOLINSKY, Y., STROUP, N. E., KRUCHKO, C. & BARNHOLTZ-SLOAN, J. S. 2013. CBTRUS statistical report: Primary brain and central nervous system tumors diagnosed in the United States in 2006-2010. *Neuro Oncol,* 15 Suppl 2**,** ii1-56.

OSUKA, S. & VAN MEIR, E. G. 2017. Overcoming therapeutic resistance in glioblastoma: the way forward. *J Clin Invest,* 127**,** 415-426.

PANIERI, E. & SANTORO, M. M. 2016. ROS homeostasis and metabolism: a dangerous liason in cancer cells. *Cell Death Dis,* 7**,** e2253.

PEARSON, J. R. D. & REGAD, T. 2017. Targeting cellular pathways in glioblastoma multiforme. *Signal Transduct Target Ther,* 2**,** 17040.

PHI, L. T. H., SARI, I. N., YANG, Y. G., LEE, S. H., JUN, N., KIM, K. S., LEE, Y. K. & KWON, H. Y. 2018. Cancer Stem Cells (CSCs) in Drug Resistance and their Therapeutic Implications in Cancer Treatment. *Stem Cells Int,* 2018**,** 5416923.

PORS, K. & MOREB, J. S. 2014. Aldehyde dehydrogenases in cancer: an opportunity for biomarker and drug development? *Drug Discov Today,* 19**,** 1953-63.

PRIETO-VILA, M., TAKAHASHI, R. U., USUBA, W., KOHAMA, I. & OCHIYA, T. 2017. Drug Resistance Driven by Cancer Stem Cells and Their Niche. *Int J Mol Sci,* 18.

QIU, Y., PU, T., GUO, P., WEI, B., ZHANG, Z., ZHANG, H., ZHONG, X., ZHENG, H., CHEN, L., BU, H. & YE, F. 2016. ALDH(+)/CD44(+) cells in breast cancer are associated with worse prognosis and poor clinical outcome. *Exp Mol Pathol,* 100**,** 145-50.

RAMIREZ, Y. P., WEATHERBEE, J. L., WHEELHOUSE, R. T. & ROSS, A. H. 2013. Glioblastoma multiforme therapy and mechanisms of resistance. *Pharmaceuticals (Basel),* 6**,** 1475-506.

RICH, J. N. 2016. Cancer stem cells: understanding tumor hierarchy and heterogeneity. *Medicine (Baltimore),* 95**,** S2-7.

RINALDI, M., CAFFO, M., MINUTOLI, L., MARINI, H., ABBRITTI, R. V., SQUADRITO, F., TRICHILO, V., VALENTI, A., BARRESI, V., ALTAVILLA, D., PASSALACQUA, M. & CARUSO, G. 2016. ROS and Brain Gliomas: An Overview of Potential and Innovative Therapeutic Strategies. *Int J Mol Sci,* 17.

RINGEL, F., PAPE, H., SABEL, M., KREX, D., BOCK, H. C., MISCH, M., WEYERBROCK, A., WESTERMAIER, T., SENFT, C., SCHUCHT, P., MEYER, B., SIMON, M. & GROUP, S. N. S. 2016. Clinical benefit from resection of recurrent glioblastomas: results of a multicenter study including 503 patients with recurrent glioblastomas undergoing surgical resection. *Neuro Oncol,* 18**,** 96-104.

SALAZAR-RAMIRO, A., RAMIREZ-ORTEGA, D., PEREZ DE LA CRUZ, V., HERNANDEZ-PEDRO, N. Y., GONZALEZ-ESQUIVEL, D. F., SOTELO, J. & PINEDA, B. 2016. Role of Redox Status in Development of Glioblastoma. *Front Immunol,* 7**,** 156.

SANTOS, N. A., CATAO, C. S., MARTINS, N. M., CURTI, C., BIANCHI, M. L. & SANTOS, A. C. 2007. Cisplatin-induced nephrotoxicity is associated with oxidative stress, redox state unbalance, impairment of energetic metabolism and apoptosis in rat kidney mitochondria. *Arch Toxicol,* 81**,** 495-504.

SHAO, C., SULLIVAN, J. P., GIRARD, L., AUGUSTYN, A., YENERALL, P., RODRIGUEZ-CANALES, J., LIU, H., BEHRENS, C., SHAY, J. W., WISTUBA, II & MINNA, J. D. 2014. Essential role of aldehyde dehydrogenase 1A3 for the maintenance of non-small cell lung cancer stem cells is associated with the STAT3 pathway. *Clin Cancer Res,* 20**,** 4154-66.

SIMA, A., PARISOTTO, M., MADER, S. & BHAT, P. V. 2009. Kinetic characterization of recombinant mouse retinal dehydrogenase types 3 and 4 for retinal substrates. *Biochim Biophys Acta,* 1790**,** 1660-4.

SINGH, S., BROCKER, C., KOPPAKA, V., CHEN, Y., JACKSON, B. C., MATSUMOTO, A., THOMPSON, D. C. & VASILIOU, V. 2013. Aldehyde dehydrogenases in cellular responses to oxidative/electrophilic stress. *Free Radic Biol Med,* 56**,** 89-101.

STROHECKER, A. M., GUO, J. Y., KARSLI-UZUNBAS, G., PRICE, S. M., CHEN, G. J., MATHEW, R., MCMAHON, M. & WHITE, E. 2013. Autophagy sustains mitochondrial glutamine metabolism and growth of BrafV600E-driven lung tumors. *Cancer Discov,* 3**,** 1272-85.

STUPP, R., MASON, W. P., VAN DEN BENT, M. J., WELLER, M., FISHER, B., TAPHOORN, M. J., BELANGER, K., BRANDES, A. A., MAROSI, C., BOGDAHN, U., CURSCHMANN, J., JANZER, R. C., LUDWIN, S. K., GORLIA, T., ALLGEIER, A., LACOMBE, D., CAIRNCROSS, J. G., EISENHAUER, E., MIRIMANOFF, R. O., EUROPEAN ORGANISATION FOR, R., TREATMENT OF CANCER BRAIN, T., RADIOTHERAPY, G. & NATIONAL CANCER INSTITUTE OF CANADA CLINICAL TRIALS, G. 2005. Radiotherapy plus concomitant and adjuvant temozolomide for glioblastoma. *N Engl J Med,* 352**,** 987-96.

STURM, D., BENDER, S., JONES, D. T., LICHTER, P., GRILL, J., BECHER, O., HAWKINS, C., MAJEWSKI, J., JONES, C., COSTELLO, J. F., IAVARONE, A., ALDAPE, K., BRENNAN, C. W., JABADO, N. & PFISTER, S. M. 2014. Paediatric and adult glioblastoma: multiform (epi)genomic culprits emerge. *Nat Rev Cancer,* 14**,** 92-107.

SULLIVAN, K. E., ROJAS, K., CERIONE, R. A., NAKANO, I. & WILSON, K. F. 2017. The stem cell/cancer stem cell marker ALDH1A3 regulates the expression of the survival factor tissue transglutaminase, in mesenchymal glioma stem cells. *Oncotarget,* 8**,** 22325-22343.

TAKAMURA, A., KOMATSU, M., HARA, T., SAKAMOTO, A., KISHI, C., WAGURI, S., EISHI, Y., HINO, O., TANAKA, K. & MIZUSHIMA, N. 2011. Autophagy-deficient mice develop multiple liver tumors. *Genes Dev,* 25**,** 795-800.

THOMAS, R. P., RECHT, L. & NAGPAL, S. 2013. Advances in the management of glioblastoma: the role of temozolomide and MGMT testing. *Clin Pharmacol,* 5**,** 1-9.

THON, N., KRETH, S. & KRETH, F. W. 2013. Personalized treatment strategies in glioblastoma: MGMT promoter methylation status. *Onco Targets Ther,* 6**,** 1363-72.

TOMITA, H., TANAKA, K., TANAKA, T. & HARA, A. 2016. Aldehyde dehydrogenase 1A1 in stem cells and cancer. *Oncotarget,* 7**,** 11018-32.

VERHAAK, R. G., HOADLEY, K. A., PURDOM, E., WANG, V., QI, Y., WILKERSON, M. D., MILLER, C. R., DING, L., GOLUB, T., MESIROV, J. P., ALEXE, G., LAWRENCE, M., O'KELLY, M., TAMAYO, P., WEIR, B. A., GABRIEL, S., WINCKLER, W., GUPTA, S., JAKKULA, L., FEILER, H. S., HODGSON, J. G., JAMES, C. D., SARKARIA, J. N., BRENNAN, C., KAHN, A., SPELLMAN, P. T., WILSON, R. K., SPEED, T. P., GRAY, J. W., MEYERSON, M., GETZ, G., PEROU, C. M., HAYES, D. N. & CANCER GENOME ATLAS RESEARCH, N. 2010. Integrated genomic analysis identifies clinically relevant subtypes of glioblastoma characterized by abnormalities in PDGFRA, IDH1, EGFR, and NF1. *Cancer Cell,* 17**,** 98-110.

WANG, Q., HU, B., HU, X., KIM, H., SQUATRITO, M., SCARPACE, L., DECARVALHO, A. C., LYU, S., LI, P., LI, Y., BARTHEL, F., CHO, H. J., LIN, Y. H., SATANI, N., MARTINEZ-LEDESMA, E., ZHENG, S., CHANG, E., SAUVE, C. G., OLAR, A., LAN, Z. D., FINOCCHIARO, G., PHILLIPS, J. J., BERGER, M. S., GABRUSIEWICZ, K. R., WANG, G., ESKILSSON, E., HU, J., MIKKELSEN, T., DEPINHO, R. A., MULLER, F., HEIMBERGER, A. B., SULMAN, E. P., NAM, D. H. & VERHAAK, R. G. W. 2017. Tumor Evolution of Glioma-Intrinsic Gene Expression Subtypes Associates with Immunological Changes in the Microenvironment. *Cancer Cell,* 32**,** 42-56 e6.

WELLER, M. 2013. Assessing the MGMT status in glioblastoma: one step forward, two steps back? *Neuro Oncol,* 15**,** 253-4.

WELLER, M., NABORS, L. B., GORLIA, T., LESKE, H., RUSHING, E., BADY, P., HICKING, C., PERRY, J., HONG, Y. K., ROTH, P., WICK, W., GOODMAN, S. L., HEGI, M. E., PICARD, M., MOCH, H., STRAUB, J. & STUPP, R. 2016. Cilengitide in newly diagnosed glioblastoma: biomarker expression and outcome. *Oncotarget,* 7**,** 15018-32.

WENGER, K. J., WAGNER, M., YOU, S. J., FRANZ, K., HARTER, P. N., BURGER, M. C., VOSS, M., RONELLENFITSCH, M. W., FOKAS, E., STEINBACH, J. P. & BAHR, O. 2017. Bevacizumab as a last-line treatment for glioblastoma following failure of radiotherapy, temozolomide and lomustine. *Oncol Lett,* 14**,** 1141-1146.

WHITE, E. 2015. The role for autophagy in cancer. *J Clin Invest,* 125**,** 42-6.

WICK, A., KESSLER, T., ELIA, A. E. H., WINKLER, F., BATCHELOR, T. T., PLATTEN, M. & WICK, W. 2018. Glioblastoma in elderly patients: solid conclusions built on shifting sand? *Neuro Oncol,* 20**,** 174-183.

XU, S. L., LIU, S., CUI, W., SHI, Y., LIU, Q., DUAN, J. J., YU, S. C., ZHANG, X., CUI, Y. H., KUNG, H. F. & BIAN, X. W. 2015. Aldehyde dehydrogenase 1A1 circumscribes high invasive glioma cells and predicts poor prognosis. *Am J Cancer Res,* 5**,** 1471-83.

YABROFF, K. R., HARLAN, L., ZERUTO, C., ABRAMS, J. & MANN, B. 2012. Patterns of care and survival for patients with glioblastoma multiforme diagnosed during 2006. *Neuro Oncol,* 14**,** 351-9.

YANG, S., WANG, X., CONTINO, G., LIESA, M., SAHIN, E., YING, H., BAUSE, A., LI, Y., STOMMEL, J. M., DELL'ANTONIO, G., MAUTNER, J., TONON, G., HAIGIS, M., SHIRIHAI, O. S., DOGLIONI, C., BARDEESY, N. & KIMMELMAN, A. C. 2011. Pancreatic cancers require autophagy for tumor growth. *Genes Dev,* 25**,** 717-29.

ZHANG, B. & ZEHNDER, J. L. 2013. Oxidative stress and immune thrombocytopenia. *Semin Hematol,* 50**,** e1-4.

ZHANG, J., STEVENS, M. F. & BRADSHAW, T. D. 2012. Temozolomide: mechanisms of action, repair and resistance. *Curr Mol Pharmacol,* 5**,** 102-14.

ZHANG, K., WANG, X. Q., ZHOU, B. & ZHANG, L. 2013. The prognostic value of MGMT promoter methylation in Glioblastoma multiforme: a meta-analysis. *Fam Cancer,* 12**,** 449-58.

ZHANG, W., LIU, Y., HU, H., HUANG, H., BAO, Z., YANG, P., WANG, Y., YOU, G., YAN, W., JIANG, T., WANG, J. & ZHANG, W. 2015. ALDH1A3: A Marker of Mesenchymal Phenotype in Gliomas Associated with Cell Invasion. *PLoS One,* 10**,** e0142856.

ZHANG, Y. W., SHI, J., LI, Y. J. & WEI, L. 2009. Cardiomyocyte death in doxorubicin-induced cardiotoxicity. *Arch Immunol Ther Exp (Warsz),* 57**,** 435-45.

ZHOU, Y., YAN, H., GUO, M., ZHU, J., XIAO, Q. & ZHANG, L. 2013. Reactive oxygen species in vascular formation and development. *Oxid Med Cell Longev,* 2013**,** 374963.

ZONG, H., VERHAAK, R. G. & CANOLL, P. 2012. The cellular origin for malignant glioma and prospects for clinical advancements. *Expert Rev Mol Diagn,* 12**,** 383-94.

H. Abbreviations

ALDH	Aldehyde dehydrogenase
AML	Acute myeloid leukemia
APS	Ammonium persulfate
ATG4	Autophagy Related 4
BAAA	BODIPY-aminoacetaldehyde
BHT	Butylated hydroxytoluene
BSA	Bovine serum albumin
CML	Chronic myelogenous leukemia
CNS	Central nervous system
Co-IP	Co-immunoprecipitation
CRISPR	Clustered Regularly Interspaced Short Palindromic Repeats
CSC	Cancer stem cell
DAPI	4’,6-diamidino-2-phenylindole
DCFH	Dichloro-dihydro-fluorescein
DEAB	N,N-diethylaminobenzaldehyde
DMEM	Dulbecco Modified Eagle Medium
DMSO	Dimethyl sulfoxide
DNA	Deoxyribonucleic acid
DSB	Double-strand break
DTT	Dithiothreitol
EDTA	Ethylenediaminetetraacetic acid
EGF	Epidermal growth factor
FBS	Fetal Bovine Serum
FGF	Fibroblast Growth Factor
GBM	Glioblasoma
GFP	Green fuorescent protein
H_2O_2	Hydrogen peroxide
HCl	Hydrochloric acid
HEPES	4-(2-hydroxyethyl)-1-piperazineethanesulfonic acid
HNE	4-Hydroxynonenal
IDH1/2	Isocitrate dehydrogenase 1 and 2
ICH	Immunohistochemistry
IRS	Immunoreactive score
KO	Knockout
LC3	Light chain 3
MDA	Malondialdehyde
MEM	Minimum Essential Medium
$MgCl_2$	Magnesium Chloride
Min	Minute
MGMT	O-6-methylguanine-DNA methyltransferase
mTOR	mammalian target of rapamycin

MTT	3-(4,5-Dimethylthiazol-2-yl)-2,5-diphenyltetrazolium bromide
NAC	N-acetylcysteine
NaCl	Sodium chloride
NaOH	Sodium hydroxide
NEAA	Non-Essential Amino Acid
PBS	Phosphate buffered saline
PCR	Polymerase chain reaction
PI	Propidium iodide
PI3K	Phosphoinositide 3-kinase
PLA	Proximity ligation assay
PML	Progressive multifocal leukoencephalopathy
RIPA	Radioimmunoprecipitation assay
RNA	Ribonucleic acid
ROS	Reactive oxygen species
RT	Room temperature
S	Second
SD	Standard deviation
SDS	Sodium dodecyl sulfate
SDS-PAGE	Sodium dodecyl sulfate polyacrylamide gel electrophoresis
sgRNA	Single-guided RNA
TBA	Thiobarbituric acid
TBARS	Thiobarbituric Acid Reactive Substances
TBST	Tris-buffered saline
TMZ	Temozolomide
WT	Wildtype

I. Publications

1. Wei Wu, Karoline Mayer, Charlotte von Rosenstiel, Johannes Schecker, Sandra Baur, Friederike Liesche, Sylvia Würstle, Jens Gempt and Jürgen Schlegel. Aldehyde Dehydrogenase 1A3 confers chemoresistance by detoxification of aldehydes from lipid peroxidation in human glioblastoma (submitted to ***Oncogene***)

2. Wei Wu, Johannes Schecker, Sylvia Würstle, Fabian Schneider, Martin Schönfelder and Jürgen Schlegel. Aldehyde Dehydrogenase 1A3 (ALDH1A3) is Regulated by Autophagy in Human Chemotherapy Resistant Glioblastoma Cells. ***Cancer Lett***. 2018 Jan 3;417:112-123.

3. Silvia Würstle, Fabian Schneider, Florian Ringel, Jens Gempt, Friederike Lämmer, Claire Delbridge, Wei Wu and Jürgen Schlegel. Temozolomide induces autophagy in primary and established glioblastoma cells in an EGFR independent manner. ***Oncol Lett,*** 2017;14(1):322-328.